The Role of the Mucin-Like Glycoprotein Podoplanin in the Progression of Cutaneous Squamous Cell Carcinoma

Dissertation

Faculty of Biosciences
Ruperto Carola University Heidelberg

Melanie Schwab
2019

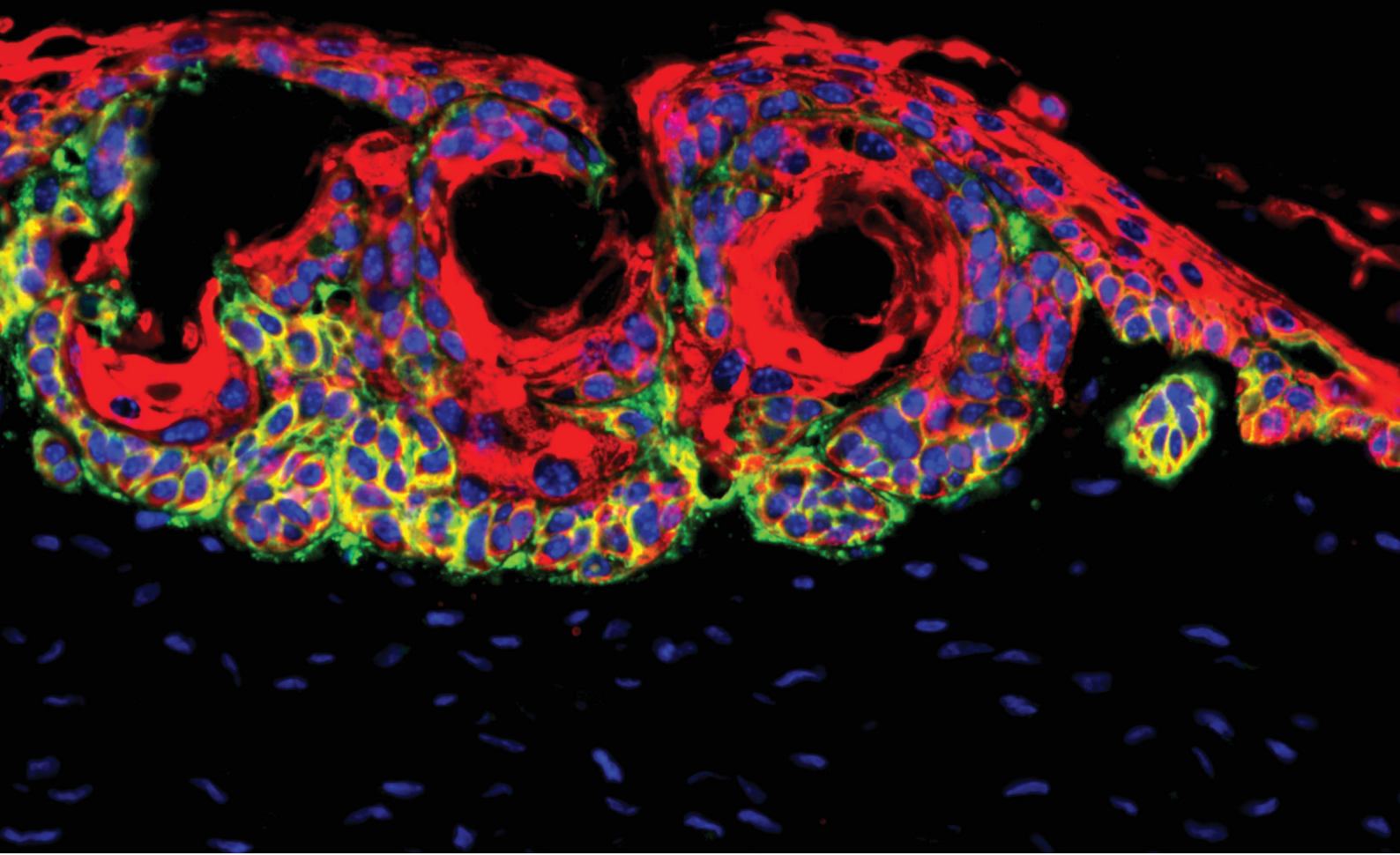

Dissertation

submitted to the

Combined Faculty of Natural Sciences and Mathematics

of the Ruperto Carola University Heidelberg, Germany

for the degree of

Doctor of Natural Sciences

Presented by

Melanie Schwab, M.Sc.

born in: Pforzheim, Germany

Oral examination: 07th November, 2019

The Role of the Mucin-Like Glycoprotein Podoplanin

in the Progression of

Cutaneous Squamous Cell Carcinoma

Referees: Prof. Dr. Peter Angel

Prof. Dr. Michael Boutros

SUMMARY

The incidence of cutaneous squamous cell carcinoma (cSCC) is increasing each year. Although early stages of cSCC can still be treated successfully, late stage tumors invade into the surrounding tissue and metastasize to distant body sites, which is associated with a poor prognosis. Strong upregulation of the transmembrane glycoprotein Podoplanin (PDPN) has been demonstrated in various tumor entities including cSCC. Enhanced PDPN expression was correlated to poor cSCC patients' outcome, but its function in skin cancer progression is still unknown. Therefore, my study aimed to define the impact of PDPN on cSCC carcinogenesis. The descriptive analysis of differentiated cSCC patients' material showed PDPN overexpression in tumor cells and increased expression in activated fibroblasts, particularly at the invasive front of the tumor. To functionally examine the importance of PDPN in cSCC tumor cells, *PDPN* was deleted in human and murine cSCC cell lines by the CRISPR/Cas9 technology followed by functional *in vitro* assays. Human and murine cells harboring a *PDPN* knockout (KO) genotype showed similar morphology and proliferative behavior as control cells in monolayer culture system. Performing both the Boyden Chamber assay and the most advanced three-dimensional organoid skin cancer model demonstrated that the loss of *PDPN* in human cells neither affected transmigration nor invasion. Strikingly, murine *Pdpn* KO cells transmigrated and invaded with less efficiency in both approaches. The invasive phenotype of murine tumor cells was further characterized to be independent of epithelial-mesenchymal transition (EMT). An initial examination of one previously described PDPN downstream pathway revealed that ezrin recruitment and cytoskeletal remodeling were not impaired upon *Pdpn* KO in 2D culture. Complementing these *in vitro* approaches, labeled murine control and *Pdpn* KO cells were injected orthotopically into the dermis of nude mice, to define the role of PDPN in tumor progression *in vivo*. Formed tumors derived from control and *Pdpn* KO cells displayed a well-differentiated morphology with a PDPN-positive reaction in fibroblasts in the tumor stroma recapitulating human cSCC. Smaller tumors as well as delayed tumor outgrowth were observed upon *Pdpn* loss, which was due to reduced tumor cell proliferation *in vivo*. Moreover, abrogation of *Pdpn* resulted in diminished EMT-independent tumor cell invasion. In conclusion, this study underscores the crucial impact of PDPN in cSCC progression. Future studies are required in order to characterize underlying molecular mechanisms that could propose potential therapeutic strategies targeting PDPN-dependent tumor cell invasion especially in late-stage cSCC patients.

ZUSAMMENFASSUNG

Die Inzidenz des kutanen Plattenepithelkarzinoms (cSCC) nimmt jährlich zu. Obwohl frühe Stadien des cSCCs noch erfolgreich behandelt werden können, wachsen fortgeschrittene Tumore invasiv in das umliegende Gewebe ein und metastasieren zu entfernten Organen, was mit einer schlechten Prognose verbunden ist. Eine starke Hochregulierung des transmembranen Glykoproteins Podoplanin (PDPN) wurde in verschiedenen Krebsarten, einschließlich cSCC, gezeigt. Die erhöhte PDPN Expression korreliert mit einem schlechten Krankheitsausgang für cSCC Patienten. Allerdings ist seine Funktion in der cSCC Entwicklung noch immer unbekannt. Deshalb zielte meine Studie darauf ab, den Einfluss von PDPN in der cSCC Karzinogenese zu bestimmen. Die deskriptive Analyse von differenziertem cSCC Patientenmaterial zeigte eine PDPN Überexpression in Tumorzellen und in aktivierten Fibroblasten, insbesondere an der invasiven Tumorfront. Um die Bedeutung von PDPN in cSCC Krebszellen zu untersuchen, wurde *PDPN* mithilfe der CRISPR/Cas9-Technologie in humanen und murinen cSCC Zelllinien deletiert und anschließend diese Zellen *in vitro* funktionell analysiert. Humane und murine Zellen, die einen *PDPN* knockout (KO) Genotyp tragen, zeigten eine ähnliche Morphologie sowie ein ähnliches Wachstumsverhalten wie die Kontrollzellen im Einzelzellschicht-Kultursystem. Die Durchführung des Boyden-Kammer-Experiments und des drei-dimensionalen organoiden Hautkrebsmodells zeigten, dass der Verlust von *PDPN* in humanen Zellen weder die Transmigration noch die Invasion beeinträchtigte. Murine *Pdpn* KO Zellen hingegen transmigrierten und wuchsen weniger invasiv in beiden Ansätzen. Der invasive Phänotyp der murinen Tumorzellen war unabhängig von einer epithelial-mesenchymalen Transition (EMT). Eine erste Untersuchung einer bereits beschriebenen PDPN-nachfolgenden Signaltransduktion zeigte, dass die Rekrutierung von Ezrin und die Modulation des Zytoskeletts nicht durch den *Pdpn* KO in der 2D Kultur beeinflusst waren. Zur Vervollständigung dieser *in vitro* Experimente, wurden markierte murine Kontroll- und *Pdpn* KO-Zellen orthotop in die Dermis von Nacktmäusen injiziert, um die Rolle von PDPN in der Tumorentwicklung *in vivo* zu definieren. Gewachsene Tumore, die von Kontroll- oder *Pdpn* KO-Zellen stammten, wiesen eine gut differenzierte Morphologie auf; darüber hinaus zeigten Fibroblasten im Tumorstroma eine PDPN-positive Reaktion, was insgesamt humane cSCCs rekapituliert. Durch den Verlust von *Pdpn* traten kleinere Tumore sowie verzögertes Tumorwachstum auf. Beide Beobachtungen waren auf ein vermindertes Krebszellwachstum *in vivo* zurückzuführen. Des Weiteren führte das Fehlen von *Pdpn* zu einer verringerter EMT-unabhängigen Tumorzellinvasion. Zusammenfassend unterstreicht diese Studie die entscheidende Bedeutung von PDPN in der cSCC

Entwicklung. Zukünftige Untersuchungen sind erforderlich, um die zugrunde liegenden molekularen Mechanismen zu charakterisieren und um mögliche therapeutische Strategien zu empfehlen, die auf die PDPN-abhängige Krebszellinvasion insbesondere in Patienten mit späten cSCC Stadien zielen.

TABLE OF CONTENT

LIST OF FIGURES

LIST OF TABLES

LIST OF EQUATIONS

LIST OF ABBREVIATIONS

2D	two-dimensional
3D	three-dimensional
ABC	avidin biotin complex
AK	actinic keratosis
AP-1	activator protein-1
APC	allophycocyanin
ATF	activating transcription factor
BCC	basal cell carcinoma
BCM	Boyden chamber matrigel
BDVII	murine cSCC cell line
BM	basement membrane
BrdU	bromofroxyuridine
BSA	bovine serum albumin
CAF	cancer-associated fibroblast
CAR	chimeric antigen receptor
Cas	CRISPR-associated
CDM	chemically defined medium
CIS	carcinoma *in situ*
CLEC-2	C-type lectin-like receptor 2
CMV	cytomegalovirus
CO_2	carbon dioxide
CRISPR	clustered regularly interspaced short palindromic repeats
cSCC	cutaneous squamous cell carcinoma
ctrl	control
D10	Dulbecco's modified Eagle's medium including supplementation
DAB	3'-diaminobenzidine
DC	dendritic cell
dd	double-distilled
DiD	4-chlorobenzenesulfonate salt
DKFZ	German Cancer Research Center
DMBA	7,12-dimethylbenz(a)anthracene
DMEM	Dulbecco's modified Eagle's medium
DMSO	dimethylsulfoxide
DNA	desoxyribonucleic acid

DPBS	Dulbecco’s phosphate-buffered saline
DTT	1,4-dithiothreitol
DWAT	dermal white adipose tissue
ECL	enhanced chemiluminescence
ECM	extracellular matrix
ED	ectodomain
EDTA	ethylenediaminetetraacetic acid
EGF	epidermal growth factor
EGFR	epidermal growth factor receptor
ELISA	enzyme-linked immunosorbent assay
EMT	epithelial-mesenchymal transition
ERM	eosin, radixin, moesin
ERMAD	esosin, radixin, moesin associated domain
EtOH	ethanol
F12	Ham’s F-12 medium
FACS	fluorescence-activated cell sorting
FACSort	fluorescence-activated cell sort
FBS	fetal bovine serum
fdm	fibroblast-derived matrix
FFPE	formalin-fixed paraffin-embedded
FGF	fibroblast growth factor
FSC	forward scatter
G	gauge
GEMM	genetic engineered mouse model
GOF	gain-of-function
gRNA	guide ribonucleic acid
GSK-3β	glycogen synthase kinase 3 beta
H	height
H_2O	water
H_2O_2	hydrogen peroxide
Ha	Harvey
HaCaT	human adult low calcium high temperature keratinocytes
HCl	hydrochloric acid
HDAC2	histone deacetylase 2
hDF	human dermal fibroblast
HE	hematoxylin and eosin
HEK	human embryonic kidney

HRP	horseradish peroxidase
hSOS	human Son of Sevenless
IC	intracellular
i.d.	intradermal
IF	immunofluorescence
IFN-γ	interferon gamma
IgG	immunoglobulin G
IHC	immunohistochemistry
IL-6	interleukin 6
i.p.	intraperitoneal
K	keratin
KCl	potassium chloride
KD	knockdown
kDa	kilo Dalton
KH_2PO_4	monopotasium phosphate
KO	knockout
L	maximal tumor length
LEC	lymphatic endothelial cells
LOF	loss-of-function
LV	lymphatic vessel
M	molar
mA	milliampere
MAPK	mitogen-activated protein kinase
mCh	mCherry
MDCK	Madin-Darby canine kidney
MEM	minimum essential medium
MetOH	methanol
MLC2	myosin light chain 2
µm	micrometer
mm	millimeter
mM	millimolar
mm^2	square millimeter
MP	myosin phosphatase
N	normal concentration
n	number
NaCl	sodium chloride
$NaH_2PO_4.2H_2O$	sodium dihydrogen phosphate

NaOH	sodium hydroxide
neg	negative
NhEK	normal human embryonic keratinocytes
NMRI	Naval Medical Research Institute
NMSC	non-melanoma skin cancer
NP-40	Nonidet P40
n.s.	not significant
O_2	oxygen
o/n	overnight
OSCC	oral squamous cell carcinoma
OTC	organotypic culture
p	probability value
P/S	penicillin streptomycin
P/S/A	penicillin streptomycin amphotericin
PAGE	polyacrylamide gel electrophoresis
PAM	protospacer adjacent motif
PAP	papilloma
PBS	phosphate-buffered saline
pCK	pan cytokeratin
PD-1	programmed death 1
Pdpn	podoplanin (murine gene)
PDPN	podoplanin (human gene)
PDPN	podoplanin (human and murine protein)
PEI	polyethylenimin
PFA	paraformaldehyde
pH	potential of hydrogen
PI	propidium iodide
PI3K	phosphoinositide 3-kinase
PLAG	platelet activating domain
PLCγ2	phospholipase C gamma 2
P-MLC2	phospho-myosin light chain 2
pos	positive
Q	quadrant
R	hair root
RAS	rat sarcoma
rh	recombinant human
Rho	Ras homologue

RIPA	radioimmunoprecipitation assay
RNA	ribonucleic acid
ROCK	Rho-associated kinase
RT	room temperature
Sb	sebaceous gland
s.c.	subcutaneous
SCC	squamous cell carcinoma
SCM	skin cancer model
SD	standard deviation
SDS	sodium dodecyl sulfate
Ser	serine
sh	short hairpin
si	small interfering
SSC	side scatter
St	stroma
T	tumor
Thr	threonine
TBS	tris-buffered saline
TBST	tris-buffered saline + Tween 20
TGF-β	transforming growth factor beta
TM	transmembrane
TME	tumor microenvionment
TPA	12-O-tetradecanoylphorbol 13-acetate
TRE	12-O-tetradecanoylphorbol 13-acetate-responsive element
UV	ultraviolet
V	volt
v/v	volume percent
V5	V5-Firefly-luciferase-mCherry
w	week
W	tumor width orthogonally to maximal tumor length
WT	wild-type
Z	amount of counted cells

1 INTRODUCTION

1 INTRODUCTION

1.1 Physiology and Pathology of the Skin

1.1.1 The Structure of the Skin

The skin is the largest organ of the human body and comprises several layers (Watt 2014). Starting from outside, these layers are composed of the epidermis including several appendages like hair roots, sebaceous and sweat glands. Below the epidermis is the dermis as the underlying connective tissue consisting mostly of fibroblasts and extracellular matrix (ECM). The deepest layer is the dermal white adipose tissue (DWAT; Figure 1).

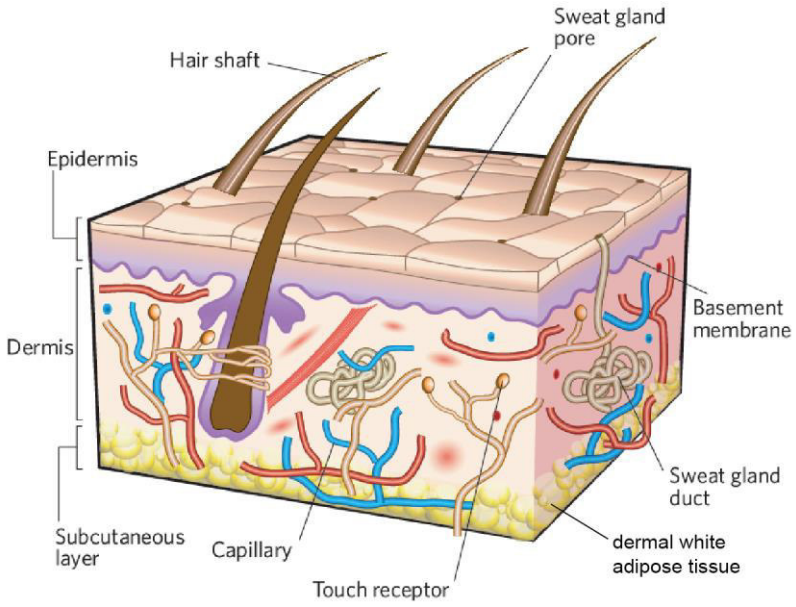

Figure 1 The human skin architecture.
The skin is composed of multiple layers. The outermost layer is the stratified epithelium with several appendages like sebaceous and sweat glands as well as hair follicles. The epidermis is separated from the subjacent dermis by the BM. The dermis consists of ECM produced by fibroblasts and harbors touch receptors and blood as well as lymphatic vessels. The lowest layer is the DWAT. Terminal differentiation of epidermal keratinocytes results in a barrier layer protecting the body from different kind of traumas (e.g. bacterial infection, UV radiation, loss of fluid). Adapted from MacNeil (2007).

The epidermis is separated from the underlying dermis by the basement membrane (BM) which is a thin layer of ECM components like type IV collagen and laminin secreted by keratinocytes and fibroblasts (Fuchs and Raghavan 2002, Simpson et al. 2011, Watt 2014). The skin forms a barrier protecting the body from the environment against physical (e.g. mechanical stress or ultraviolet (UV) radiation), chemical (e.g. irritants) or microbial (e.g. bacteria or viruses) traumas (Fuchs and Raghavan 2002, Simpson et al. 2011). Moreover, the skin also prevents dehydration of the body by retaining body fluids and is involved in thermoregulation (Fuchs and Raghavan 2002, Simpson et al. 2011, Watt 2014).

1.1.1.1 The Epidermis

The epidermis is composed of multilayered keratinocytes which are the most abundant cell type of this skin layer (MacNeil 2007). Additional epidermal cells are melanocytes, Langerhans and Merkel cells (MacNeil 2007). Keratinocytes which are positioned in the innermost layer are named basal keratinocytes and are anchored to the BM (Alonso and Fuchs 2003, Watt and Fujiwara 2011). Keratinocytes located in this so-called basal layer (*stratum basale*) are able to proliferate asymmetrically, referred as transiently amplifying cells, thus, resulting in keratinocytes which on the one side stay at the BM and on the other side upon a trigger leave the basal layer to undergo a process of terminal differentiation (Fuchs and Raghavan 2002, Alonso and Fuchs 2003). During this process which is also named keratinization or stratification, keratinocytes go through specific morphological changes until they reach the surface of the skin. Thereby, the different epidermal layers can be identified: the basal layer, the spinous layer (*stratum spinosum*), the granular layer (*stratum granulosum*) and the cornified layer (*stratum corneum*; Figure 2, Simpson et al. (2011)). The skin is a constantly renewing tissue as cells in the cornified layer are continuously replaced by newly differentiated cells (Boukamp 2005b).

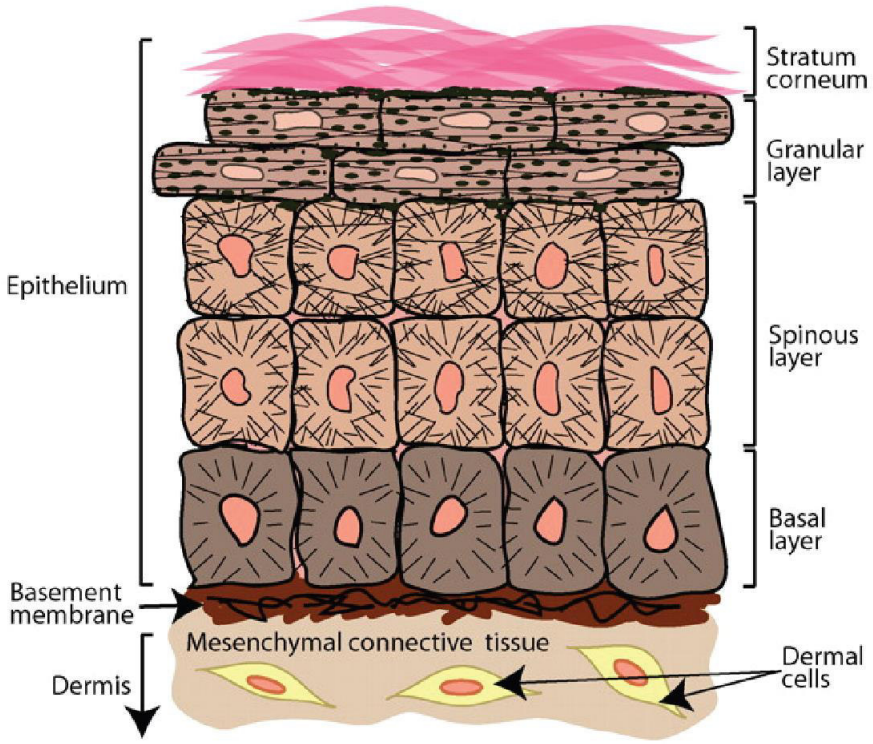

Figure 2 Schematic illustration of the epidermis.
The epidermis is made up of several distinct layers: basal (*stratum basale*), spinous (*stratum spinosum*), granular (*stratum granulosum*) and cornified layer (*stratum corneum*). Keratinocytes in the basal layer, so-called basal cells, are anchored to the BM which divides the epidermis and underlying dermis from each other. The ECM in the dermis is produced by fibroblasts. Basal cells can enter the process of terminal differentiation undergoing specific morphological changes until corneocytes in the top layer are shed. Alonso and Fuchs (2003).

Basal keratinocytes express specific keratin (K) filaments K5 and K14 and are connected to the BM through hemidesmosomes and integrin-based adhesion molecules (Candi et al. 2005, Simpson et al. 2011). After leaving the basal layer, cells maintain their metabolic activity while the keratin expression profile is changed (Fuchs 2008). Suprabasal cells stop the expression of K5 and K14 and start expressing K1 and K10 (Fuchs and Green 1980, Candi et al. 2005). Spinous keratinocytes start to strengthen their cell-cell junctions, the so-called desmosomes, by enhancing the intermediate filament network (Alonso and Fuchs 2003). Granular cells generate lipid-rich granules and produce filaggrin which links keratin filaments into tight bundles (Candi et al. 2005, Fuchs 2008). Moreover, suprabasal keratinocytes activate several transglutaminases that are important to interconnect structural filaments like filaggrin, loricrin and involucrin to build the cornified envelope (Candi et al. 2005). The aggregation of these structural proteins leads to the flattening of the keratinocytes resulting in squames within the cornified layer, which are dead-cell enucleated remnants (Candi et al. 2005). This outermost layer comprised of corneocytes

creates a mechanical barrier for the skin which is shed off by proteolytic cleavage of the cornified envelope, the so-called desquamation (Candi et al. 2005, Watt 2014).

1.1.1.2 The Dermis

The main cell type within the dermis is the fibroblast (Watt 2014, Watt and Fujiwara 2011). Other cellular components are immune cells, blood and lymphatic vessels as well as nerves and the arrector pili muscle (Watt and Fujiwara 2011). Like in the epidermis, the dermis can be dissected into multiple layers: (i) the papillary dermis, which is directly below the BM and contains the highest density of fibroblasts; (ii) the reticular dermis, which is dense of collagen fibers; (iii) the hypodermis or DWAT, which mainly consists of white adipocytes (Watt 2014, Watt and Fujiwara 2011). Fibroblasts are responsible for the secretion of ECM components as well as nutrient supply of the avascular epidermis (Watt and Fujiwara 2011). Cellular debris within the skin is cleared by skin-resident macrophages (Davies et al. 2013).

1.1.2 Cutaneous Squamous Cell Carcinoma

As the outermost layer protecting the body from various environmental stress, the skin is prone for cancer development which can originate from various cell types of the multiple cutaneous layers. The most aggressive skin cancer is the malignant melanoma originating from epidermal and dermal melanocytes (reviewed in Bastian (2014)). However, the most frequent cancer worldwide in the Caucasian population are the non-melanoma skin cancers (NMSC; Leiter et al. (2017), Waldman and Schmults (2019)). NMSC is subclassified as basal cell carcinoma (BCC) and cutaneous squamous cell carcinoma (cSCC) as well as other tumor entities including Merkel cell carcinoma and fibrosarcoma (reviewed in Boukamp (2005b), Augsburger et al. (2017), Waldman and Schmults (2019)). The majority of NMSC are the keratinocyte-derived tumors BCC which accounts for around 80 % and cSCC with roughly 20 % of all skin cancers (Leiter et al. 2017, Nagarajan et al. 2018, Waldman and Schmults 2019).

The incidence of cSCC was ranged from 15 to 35 per 100,000 people in the United States of America (Burton et al. 2016). However, the accurate numbers are difficult to determine and often underestimated as many cancers are not registered or only the first tumor is recorded (Leiter et al. 2017). The incidence is increasing each year with an expected rate of 2-4 % due to the aging population, environmental impacts as a result to certain lifestyle

behavior (e.g. sunbathing) and higher detections rates due to more frequent screenings (Alam and Ratner 2001, Burton et al. 2016, Leiter et al. 2017). In comparison to BCC, which grows locally invasive but hardly metastasizes, the metastatic risk of cSCC is only 5 % but can reach 50 % in defined clinical settings associated with poor long-term survival (Alam and Ratner 2001, Boukamp 2005b, Huang and Balmain 2014).

The development of cSCC is a multistep process with distinct stages (Figure 3, Boukamp (2005b), Ackerman and Mones (2006)). Originating from epidermal keratinocytes, actinic keratosis (AK) is associated with hyperplasia and considered to be a precursor lesion (Ackerman and Mones 2006, Fernandez Figueras 2017). It can persist at the same stage for many years but left untreated, it may progress to cSCC *in situ* (CIS) with increased genetic instability (Ackerman and Mones 2006, Ratushny et al. 2012, Fernandez Figueras 2017). The differentiation program is partially disrupted in AK, whereas it progresses to a complete malfunction becoming a CIS (Ratushny et al. 2012). Additional mutations in oncogenes result finally in an invasively growing or even metastatic cSCC (Ratushny et al. 2012).

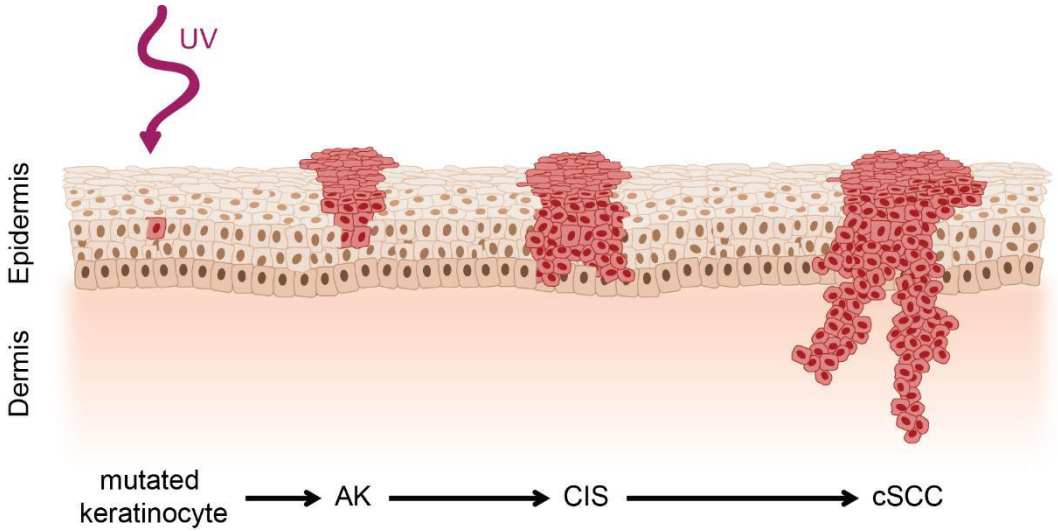

Figure 3 Schematic representation of cSCC development.
cSCC carcinogenesis is a multistep process. UV radiation causes DNA alteration in epidermal keratinocytes. If these mutated cells do not undergo apoptosis, they start to grow uncontrolled resulting in AK. Left untreated, AK can progress to a CIS and to invasively growing cSCC which breaks through the BM. During this multistage carcinogenesis genetic instability is increasing as well as additional oncogenes are mutated. Adapted and modified from Alam and Ratner (2001).

The initiation and progression of cSCC are primarily due to sunlight exposure mediated by UV radiation (Boukamp 2005b, Huang and Balmain 2014, Leiter et al. 2017). Other factors

such as older age, fair skin, exposure to chemicals (e.g. arsenic) and immunosuppression are also associated with cSCC development (Leiter et al. 2017, Nagarajan et al. 2018, Waldman and Schmults 2019). Exposure to UV light causes DNA alterations in multiple genes. The most frequent aberration, which appears early in cSCC development, is the mutation in the *TRP53* tumor suppressor gene in around 50 % of the cases (Popp et al. 2002, Boukamp 2005a). The typical UVB signature mutation is manifested as C to T transition at CC sites (Lomas et al. 2012, Nagarajan et al. 2018). In around 20 %, the rat sarcoma (*RAS*) proto-oncogene is mutational locked in its activated state (Boukamp 2005a). In particular, UV-sensitive CC sites are preferentially affected within the *Harvey* (*Ha*)-*RAS* gene in comparison to *Kirsten*- and *N-RAS*. Failure to repair these DNA mutations normally results in keratinocyte apoptosis; however, some cells survive generating e.g. mutated p53 patches leading to an abnormal cell population and may be the beginning of an AK which then can further progress to cSCC (Alam and Ratner 2001, Boukamp 2005b).

cSCC is clinically presented as red scaly plaque and typically on sun-exposed areas in older-aged individuals (Popp et al. 2002, Ackerman and Mones 2006, Waldman and Schmults 2019). The histopathological examination ranges from well to poorly differentiated morphology (Waldman and Schmults 2019). Depending on the stage and location, different therapeutic strategies are pursued. Well-defined small tumors can be treated by non-surgical destructive options for instance cryosurgery and curettage (Alam and Ratner 2001, Jennings and Schmults 2010, Nagarajan et al. 2018). These techniques are inexpensive and easy to perform. Nevertheless, the primary treatment option is surgical removal leading to lowered recurrence and metastasis rates despite higher costs (Alam and Ratner 2001). Standard surgical excision is performed for low-risk and micrographic surgery for high-risk cSCC or tumors at cosmetically sensitive areas (Jennings and Schmults 2010, Nagarajan et al. 2018, Waldman and Schmults 2019). Moreover, the disease risk is highly linked to immunosuppression, thus, newer therapy options like checkpoint inhibition are currently under review. Migden and colleagues treated patients with locally advanced and metastatic cSCC with Cemiplimab, an antibody directed against programmed death 1 (PD-1), showing that approximately half of the patients responded to this monoclonal antibody therapy (Migden et al. 2018). Even though the majority of cSCC has an excellent prognosis, the survival rate of metastatic or unresectable tumors drops to 20 % (Alam and Ratner 2001). These late-stage tumors can be treated with radiation and/or chemotherapy as palliative care or additional possibility prior to surgery (Jennings and Schmults 2010, Waldman and Schmults 2019).

1.2 *In Vitro* Systems to Investigate Cutaneous Squamous Cell Carcinoma Tumorigenesis

In order to gain better insights into the development of cSCC, different model systems ranging from monolayer cell culture via three-dimensional (3D) organotypic systems to animal models have been established.

1.2.1 Cell Lines

Monolayer cultures represent the simplest system to reveal underlying molecular mechanisms by performing functional tests. For *in vitro* as well as *in vivo* analysis of epithelial skin tumors, several cell lines representing different tumor stages have been established. Based on their diverse genetic alterations (Table 1), these cell lines are used to investigate different functional aspects of cSCC.

The MET cell lines represent a sequential series of poorly differentiated cSCCs as all lines were derived from a single immunosuppressed renal transplant patient (Popp et al. 2000, Proby et al. 2000): MET-1 cells were isolated from a primary cSCC which developed on the back of the left hand; MET-2 and -3 from two recurrences at the same site as the primary tumor; and MET-4 cells from an axillary lymph node metastasis. The SCL-I and the SCL-II cell lines were established from two patients suffering facial cSCCs derived from an untreated differentiated and a locally radiated undifferentiated cSCC, respectively (Tilgen et al. 1983). SCC-12 and SCC-13 cells were isolated from cSCCs of the facial epidermis from two different patients who received immunosuppressive drugs upon kidney transplantation or radiation therapy, respectively (Rheinwald and Beckett 1981). Both tumors presented a well-organized differentiated histology.

Table 1 Overview of established cell lines and their genetic alterations and histology.
Murine cell line is indicated by *.

Cell line	Origin	Genetic alterations, histology	Reference
MET-1	primary cSCC, hand	p53 WT, poorly differentiated	Popp et al. (2000), Proby et al. (2000)
MET-2	recurrence of primary cSCC, hand	p53 WT, poorly differentiated	Popp et al. (2000), Proby et al. (2000)
MET-3	recurrence of primary cSCC, hand	p53 WT, poorly differentiated	Popp et al. (2000), Proby et al. (2000)
MET-4	cSCC metastasis, lymph node	p53 WT, poorly differentiated	Popp et al. (2000), Proby et al. (2000)
SCL-I	primary cSCC, face	p53 mutant, differentiated	Tilgen et al. (1983)
SCL-II	primary cSCC, face	p53 mutant, poorly differentiated	Tilgen et al. (1983)
SCC-12	primary cSCC, face	p53 mutant, differentiated	Rheinwald and Beckett (1981)
SCC-13	primary cSCC, face	p53 mutant, differentiated	Rheinwald and Beckett (1981)
HaCaT	keratinocyte cell line	p53 mutant, non-tumorigenic	Boukamp et al. (1988)
HaCaT A5	oncogenic *Ha-RAS* keratinocyte cell line	benign growth *in vivo*, differentiated	Boukamp et al. (1990)
HaCaT II-4	oncogenic *Ha-RAS* keratinocyte cell line	invasive growth *in vivo*, differentiated	Boukamp et al. (1990)
BDVII*	DMBA-induced cSCC	*Ha-Ras* mutant, differentiated	Fusenig et al. (1978)

To establish a human keratinocyte cell culture, cells of a not extensively sun-exposed area were isolated from a melanoma patient (Boukamp et al. 1988). This keratinocyte cell line was generated under specific culture conditions designating “human adult low calcium high temperature keratinocytes” (HaCaT). During the process of establishing this cell line, HaCaT cells spontaneously immortalized *in vitro*, while they still maintained their highly differentiated morphology (Boukamp et al. 1988, Micallef et al. 2009). Originated from these HaCaT cells, additional cell lines were established via transfecting the mutant *Ha-Ras* gene (Boukamp et al. 1990). Hence, several clones were generated which were able to form benign or malignant tumors *in vivo*. For instance, HaCaT A5 was slowly growing with highly differentiated benign tumors, whereas injection of HaCaT II-4 cells resulted in highly differentiated but locally invasive cSCCs. Thus, HaCaT cells represent another model system which can be used for the analysis of the multistep skin cancer development.

Besides several human cell lines, only one murine cSCC line was established, namely BDVII. This cell line was generated by chemical induction of cSCC in C57BL/6 mice allowing syngeneic injection into this mouse strain (Fusenig et al. 1978). Employing graft models in the backskin of mice which comprise of tumor cell suspension alone or tumor cell cultures on top of a collagen matrix, BDVII cells grew invasively into the host tissue and formed stratified structures (Fusenig et al. 1978). Furthermore, subcutaneous (s.c.) inoculation into mice verified invasively growing tumors with differentiated cornified tissue (Lederle et al. 2010, Meides et al. 2014). Thus, this murine cSCC cell line offers a great model system to investigate skin cancer development in immunocompetent C57BL/6 mice.

1.2.2 Three-Dimensional Skin Models

For the functional analysis examining keratinocytes or cutaneous tumor cell characteristics such as migration and invasion, different 3D *in vitro* model systems have been established. In comparison, monolayer-based cultures lack physiological context as superior properties of 3D culture conditions are the addition of fibroblasts as feeder layer which can be embedded in a certain type of matrix. This scaffold enables keratinocytes or skin tumor cells to grow on top of the dermal equivalent recapitulating skin or tumor features, respectively.

In the traditional 3D system composed of epithelial cells (either keratinocytes or tumor cells) and murine fibroblasts or collagen-embedded human fibroblasts (e.g. hydrogel-based model), ECM lacks mechanical stability resulting in contraction of the culture (Muffler et al. 2008, Wolf et al. 2009). Thus, this results in limiting cultivation time (only up to 3-4 weeks). Moreover, ECM composition in hydrogel-based models is insufficiently reflected (Wolf et al. 2009). However, these characteristics play a decisive role to investigate migration and invasion of cSCC tumor cells. Hence, the 3D organotypic skin cancer model (SCM) established by Berning and colleagues represents the most advanced system (Figure 4; Berning et al. (2015)). In this model system primary human dermal fibroblasts (hDFs) serve as a feeder layer and produce ECM components themselves over four weeks of cultivation. This fibroblast-derived matrix (fdm) reflects the ECM composition and geometry of human papillary dermis. Human cSCC tumor cells cultivated on top of this dermal compartment form a well-established multilayered epithelium. All in all, the SCM system closely mimics the epidermal-dermal environment *in vitro* as tumor cells grow air-exposed on top of a thick fibroblast feeder layer allowing invasive growth of tumor cells (Berning et al. 2015).

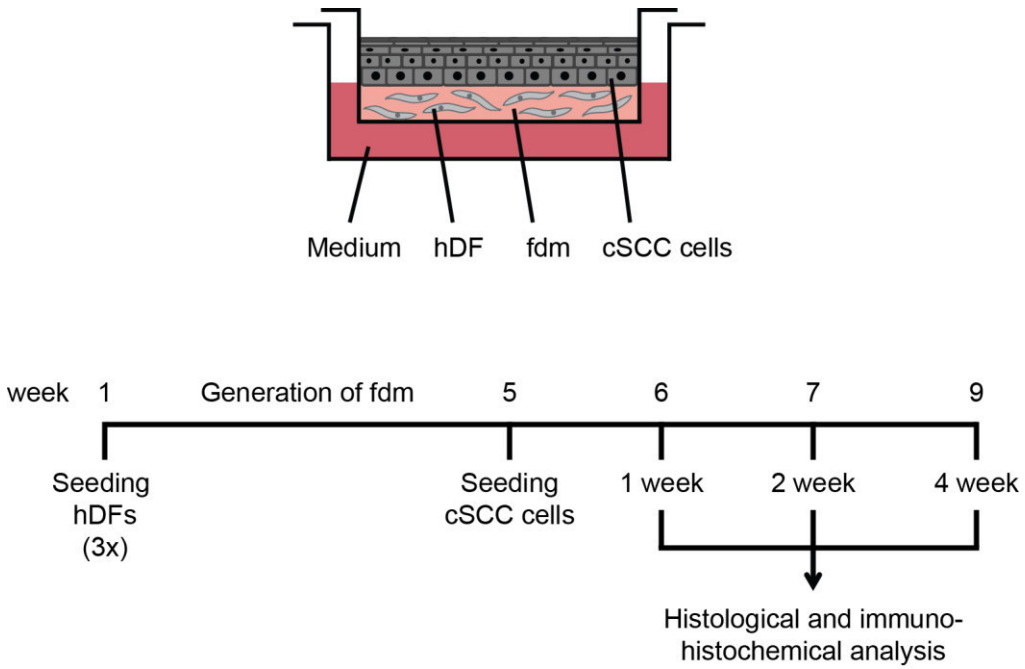

Figure 4 The three-dimensional *in vitro* skin and skin cancer model.
Scheme and timeline of the SCM according to Berning et al. (2015). hDFs are provided by three seeding steps and cultured for four weeks to generate fdm. cSCC cells are seeded on top of the dermal equivalent and cultured air-exposed resulting in a multilayered epidermal compartment. Cultures can be harvested at different time points allowing histological and immunohistochemical analyses.

1.3 Mouse Models to Study Cutaneous Squamous Cell Carcinoma

The mouse is the preferred model as this complex system can be used to mimic human pathologies incorporating all factors of a living organism such as tumor growth, interaction of tumor with stromal cells, immune response and tumor angiogenesis. Different model systems are utilized to examine the multistep process of cSCC development *in vivo*. Importantly, it has to be kept in mind that the murine skin is structured differently in several aspects from the human skin. The epidermal layers as well as the dermis in mice are much thinner than in humans and moreover, the murine skin has a much higher density of hair follicles (Watt and Fujiwara 2011). So it is contentious whether obtained results can be transferred in regard to the human situation. However, the mouse represents still the best model to recapitulate tumor growth and characteristics in a mammalian organism.

1.3.1 UV Radiation

cSCC develops at sun-exposed body sites which can be explained by chronic UV damage. Therefore, it is self-explaining to use UV light to induce cSCC in mice. Several groups used immunocompetent hairless mice (e.g. *SKH-1*) which lack the expression of the *Hairless* gene. These studies showed that UV exposure resulted in typical human cancer characteristic for instance, frequent *Trp53* mutation and only a low mutation rate in the *Ha-Ras* oncogene (reviewed in van Kranen et al. (1995), van Kranen and de Gruijl (1999)). Nevertheless, it was already demonstrated that the *Hairless* gene plays a role in skin metabolism which might influence skin cancer development (Kumpf et al. 2012).

1.3.2 Chemically Induced Skin Tumors

The malignant transition of human epidermal cells in cSCC was found to be a multistep process, in which numerous genetic and epigenetic events result in the transformation of normal to malignant cellular stages. Several mouse models based on chemical cancer induction have been established (reviewed in Abel et al. (2009)). One of the best-established mouse skin carcinogenesis models applying 7,12-Dimethylbenz-[a]-anthracene (DMBA) and the most active constituent of croton oil 12-O-tetradecanoylphorbol-13-acetate (TPA) has been an important tool to investigate epithelial hyperplasia and multistep processes of tumor development and progression (Berenblum and Shubik 1947, Boutwell 1964).

In this model system, tumor formation is chemically induced in the backskin of mice upon a single subcarcinogenic dose of DMBA resulting in point mutations including nucleotide exchanges in the proto-oncogene *Ha-Ras* (initiation; Kemp (2005), Schwarz et al. (2013)). Upon initiation, the skin is continuously treated several times a week with the tumor promoting agent TPA (Boutwell 1964). In this second step, the so-called promotion, TPA causes an inflammatory reaction which is associated with epidermal hyperplasia (Stanley et al. 1991). Due to induced cell proliferation, *Ha-Ras* mutated keratinocytes expand clonally leading to the generation of benign tumor, so-called papilloma (PAP; (Finch et al. 1996). TPA treatment is stopped after 20 weeks and consequently, the majority of PAP regresses. However, some PAP progress further in the observation period (up to 52 weeks) resulting in invasively growing cSCC (Kemp 2005, Abel et al. 2009, Schwarz et al. 2013). This model system recapitulates human cSCC carcinogenesis as tumors develop in multiple steps and the morphology is similar to human tumors (Benjamin and Ananthaswamy 2007, Abel et al. 2009). However, there are also some limitations of this

mouse model. Treated mice primarily develop PAP which does not represent human equivalent as human PAP form rather due to human papilloma virus infections (Schwarz et al. 2013). In human tumor initiation the *Trp53* gene is the main target of chronic UV damage, but in this model, *Ha-Ras* is primarily targeted by topical DMBA treatment (Benjamin and Ananthaswamy 2007). Furthermore, the conversion from benign PAP to invasively growing cSCC strongly depends on the chemical dosage and background of the used mouse strain (Reiners and Singh 1997, Yamakage et al. 2000, Gebhardt et al. 2008, Abel et al. 2009).

1.3.3 Genetic Engineered Mouse Models

A variety of genetic engineered mouse models (GEMMs) has been established including global or skin-specific inactivation of tumor suppressor or activation of oncogenes (reviewed in Eferl and Casanova (2015)).

Mice with a deficiency of the tumor suppressor gene p53 do not develop skin tumors spontaneously (Harvey et al. 1993). Additional application of the chemical skin carcinogenesis protocol by topical DMBA/TPA treatment allowed addressing the question of p53 contribution in skin tumorigenesis. This example demonstrates that if the gene of interest is not a driver mutation, additional tumor initiating and/or promoting is required (e.g. DMBA/TPA-induction; Kemp (2005)). Employing this model, Kemp and colleagues were able to show that the malignant progression from PAP to cSCC depends on this tumor suppressor as PAP progressed more rapidly to cSCCs.

In the *K5-hSOS-F* mouse model the human Ras activator *Son of Sevenless* (*hSOS-F*) is activated under the basal cell-specific promoter K5 (Sibilia et al. 2000). These transgenic mice showed an increased epidermal proliferation and develop PAP within weeks. These PAPs grew so quickly, that mice needed to be sacrificed before malignant transformation of arisen PAP could be investigated.

These two examples show that GEMMs are a powerful tool to study skin diseases as well as tumorigenesis and to test the ability of specific genes in tumor initiation and progression. GEMMs develop *de novo* tumors over a longer time period compared to injection models (Kersten et al. 2017). Nevertheless, this is the preferred model system closely recapitulating human tumor characteristics also due to more realistic slow tumor development.

1.3.3 Orthotopic Tumor Cell Injection

Besides inducing skin carcinogenesis by exogenous factors like chemicals or UV radiation, or by altered gene expression, tumor cells can also be injected orthotopically. Two different inoculation sites are commonly used: (i) while injecting tumor cells s.c., the tumor develops below the skin and (ii) performing intradermal (i.d.) injections, tumor cells grow within the dermis. Depending on the cell line and cell number either injection site results in fast-growing tumors within weeks. While s.c. administration is rather easy to perform, i.d. injection requires some experience to administer cells just under the superficial layer of the epidermis. However, depending on the scientific question which is addressed, it is important to keep in mind that the microenvironment differs on the injection site. Within the dermis, tumor cells get into closer contact with fibroblast and other stromal cells than cancer cells which have been injected s.c. (Bonnotte et al. 2003). Thus, i.d. inoculation represents the more conclusive model to address the relation of tumor and stromal cell during epidermal tumor cell invasion.

The underlying genetic program in cSCC development and progression is only partly understood. Thus, the described *in vitro* and *in vivo* model systems are still used to clarify important signaling pathways and involved genes. One candidate which has been associated with poor long-term survival especially in late-stage cSCC patients is the transmembrane protein podoplanin (PDPN; Vinicius de et al. (2011). Further information on this protein as well as data indicating its role in cSCC progression is presented in the following chapter.

1.4 The Glycosylated Transmembrane Protein Podoplanin

1.4.1 Podoplanin Function in Physiology

The mucin-like glycoprotein PDPN was named due to its function in flattening podocytes in the kidney (Breiteneder-Geleff et al. 1999). The protein was independently described in different biological contexts and therefore, it is also known by several designations. The clone OTS-8 was isolated from mouse lung tissue treated with TPA (Nose et al. 1990). Farr and colleagues found a glycoprotein 38 in mouse peripheral lymphoid tissue (Farr et al. 1992). The rat homolog T1α was described in rat type I lung alveolar cells (Rishi et al. 1995). Furthermore, E11 was reported to be expressed in osteoblasts, lung and lymphatic

endothelial cells (LECs; Wetterwald et al. (1996)). PDPN expression in LECs is commonly used as a valid marker for lymphatic vessels (Breiteneder-Geleff et al. 1999). Furthermore, PA2.26 was reported in mouse skin keratinocytes upon wound healing and chemical carcinogenesis (Gandarillas et al. 1997). Aggrus/gp44 was identified as a platelet-aggregation factor (Kato et al. 2003).

Although PDPN is expressed in a variety of different tissues, the physiological function is mostly unknown. Several studies using *Pdpn* knockout (KO) mice have demonstrated its crucial role in the development of different tissues. Type I alveolar cells lacking *Pdpn* have deregulated proliferation and differentiation resulting in impaired inflation of the lung and thus, in respiratory failure and perinatal death of these animals (Ramirez et al. 2003). Schacht and colleagues showed that the development of lymphatic endothelium is impaired upon *Pdpn* loss and these defects are leading to reduced lymphatic transport and hence, to lymphedema (Schacht et al. 2003). The lack of *Pdpn* in the heart results in dysregulation of epithelial-mesenchymal transition (EMT) and thus, to hypoplasia in *Pdpn*-deficient animals (Gittenberger-de Groot et al. 2007, Douglas et al. 2009). Moreover, constitutive *Pdpn* ablation induces hemorrhages in the embryonic brain (Lowe et al. 2015). Focusing on the skin, basal cells of sebaceous glands, hair follicles and lymphatic vessels express PDPN (Honma et al. 2012, Wojciechowska-Zdrojowy et al. 2016). However, it is expressed neither by basal keratinocytes of the interfollicular epidermis nor by dermal fibroblasts (Gandarillas et al. 1997, Honma et al. 2012). Employing an *in vivo* loss-of-function (LOF) approach, keratinocytes lacking *Pdpn* resulted in normal mouse development and showed no signs of skin abnormalities (Baars et al. 2015).

Despite performing these studies, the biological function remains unclear. Although PDPN lacks a catalytical domain, it mainly functions through protein-protein interactions.

1.4.2 Podoplanin Protein Structure and Its Interaction Partners

The type I transmembrane protein PDPN consists of 162 amino acids in humans and the murine homolog is 172 amino acids long (Martin-Villar et al. 2005). The protein-protein interactions are mediated by the different domains of PDPN including an ectodomain (ED), a single transmembrane (TM) domain and a short intracellular (IC) tail (Figure 5).

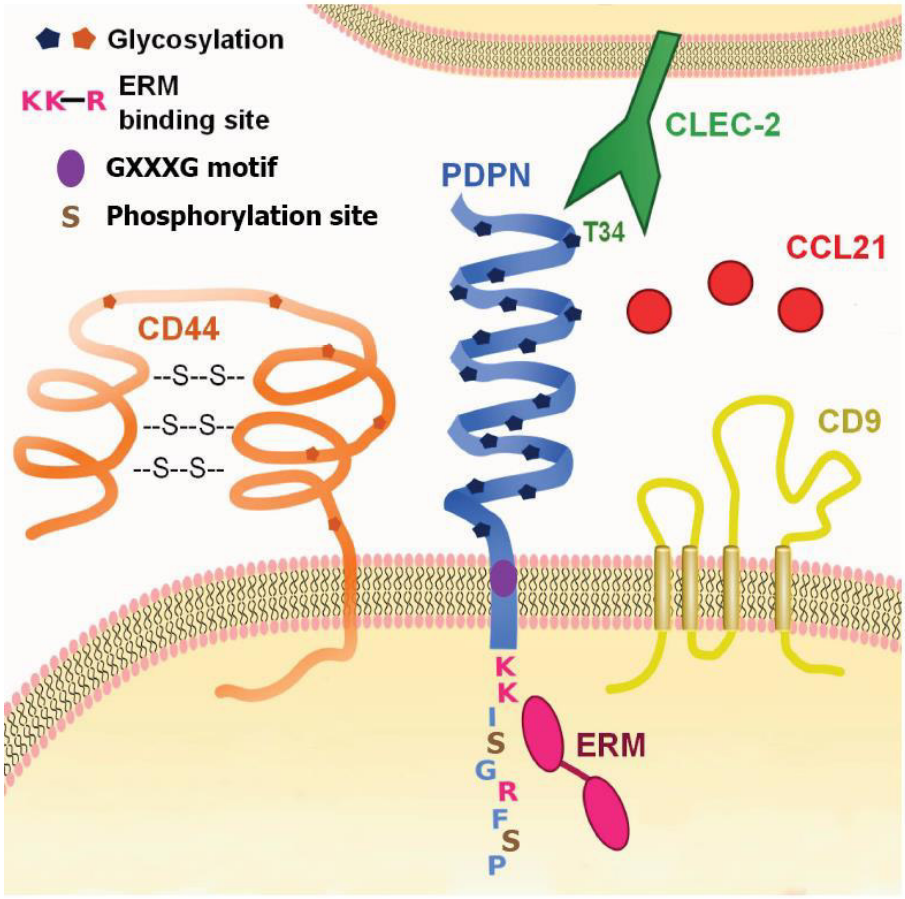

Figure 5 Schematic representation of PDPN and its interaction partners.
The extracellular and intracellular domains of PDPN have been shown to interact with various proteins including CD44, CLEC-2, CCL21, CD9 and the ERM protein family. Adapted from Astarita et al. (2012).

The ED is heavily O-glycosylated with sialic acid α-2,3 linked to galactose at serine (Ser) and threonine (Thr) residues (Scholl et al. 1999). Scholl and colleagues demonstrated that these sugar residues account mainly for the molecular weight of PDPN (Scholl et al. 1999). Moreover, they isolated protein extracts from different organs and revealed that it had a different molecular mass. These results as well as the data of the simultaneous PDPN discovery suggest that this glycoprotein is modified differently resulting in varying molecular weight ranging from 36 to 43 kDa (Gandarillas et al. 1997, Farr et al. 1992, Kato et al. 2003). Nevertheless, whether these modifications are organ- or even tumor-specific has not been explored yet. So far, Kato and Kaneko gave the only evidence by developing an antibody targeting cancer-specific PDPN (Kato and Kaneko 2014). Epitope mapping was performed using an enzyme-linked immunosorbent assay (ELISA). The established antibody detected only an aberrant glycosylated PDPN (Thr54 and probably Ser56) which was expressed by brain and oral SCC (OSCC) tumor cells and not in lymphatic vessels.

Whether this antibody represents a new possibility to treat patients with PDPN-positive tumors is still under observation. The glycosylation of PDPN is responsible for the main protein function. The importance of this posttranslational modification was shown *in vivo* when the glycosylation was abrogated. Mice lacking the T-synthase which is responsible for O-glycosylation suffered from the same phenotypic defects similar to global *Pdpn* KO mice (Ju and Cummings 2002, Fu et al. 2008). Three tandemly repeated motifs (EDXXXVTPG) in the ED were identified and named platelet aggregation-stimulating domains (PLAG1-3; (Kato et al. 2003, Sekiguchi et al. 2015). The glycosylation in these domains is essential for the interaction with the C-type lectin-like receptor 2 (CLEC-2; Suzuki-Inoue et al. (2007)). Kaneko and colleagues reported that the glycosylation of Thr at position 52 within the PLAG3 domain in human PDPN and Thr34 in the PLAG1 domain in the murine homolog is responsible for the interaction with CLEC-2 (Kaneko et al. 2007, Bianchi et al. 2014). CLEC-2 is expressed by platelets and immune cells resulting in platelet aggregation and increased motility of immune cells and is so far the only known receptor for PDPN (Astarita et al. 2012, Suzuki-Inoue et al. 2007). The CLEC-2-PDPN-interaction is critical for the process of lymphatic vessel maintenance as platelet aggregation is induced by PDPN expressing LECs (Suzuki Inoue et al. 2010). Upon PDPN binding, CLEC-2 dimerizes and is phosphorylated in the IC domain by the kinase Syk (Suzuki-Inoue et al. 2007). Consequently, phospholipase C gamma 2 (PLCγ2) is activated resulting in platelet aggregation (Navarro-Nunez et al. 2013). Moreover, Acton and colleagues described a functional role of CLEC-2 in dendritic cell (DC) motility (Acton et al. 2014). CLEC-2 is expressed by skin as well as lymph node DCs. Upon PDPN binding, CLEC-2 dimerizes and the downstream signaling via Syk and PLCγ2 is activated as in platelets. The Vav protein gets activated additionally, reducing Ras homologe (Rho) A activity. Based on the abolished contractility of the actomyosin skeleton, the actin cytoskeleton is remodeled and DCs can spread along stromal scaffold, extend protrusions and migrate.

The standard isoform of CD44 is expressed in various cell types in physiology and pathology and interacts with the carbohydrate moieties of the PDPN ED (Martin-Villar et al. 2010). Performing *in vitro* studies as well as using an experimental skin carcinogenesis model, they reported that both glycoproteins cooperate leading to enhanced cell migration and tumor progression. However, further investigations are required to unravel the exact interaction mechanism between these glycoproteins.

The chemokine CCL21 is another partner interacting with PDPN. It was described that PDPN builds complexes with CCL21 on the basal cell membrane of LECs in a glycosylation-dependent manner (Kerjaschki et al. 2004). These complexes are shed into the perivascular stroma forming a CCL21 gradient for the attraction of CCR7-positive

immune cells resulting in the rejection of kidney transplants in humans. However, the underlying mechanism of PDPN shedding was not described. The proteolytic cleavage of potential sites within the ED is masked due to the posttranslational addition of glycans (Pan et al. 2014).

Yurrita and colleagues reported that instead of degrading PDPN via cleavage of the ED, the TM domain is cleaved mediated by metalloproteases (Yurrita et al. 2014). Besides degradation, the homodimerization and localization of PDPN to the plasma membrane within lipid rafts rely on the GXXXG motif, which is highly conserved in all species (Russ and Engelman 2000, Fernandez-Munoz et al. 2011),
Moreover, PDPN associates with CD9, a tetraspanin protein, via its TM (Nakazawa et al. 2008). The interaction of PDPN with CD9 showed that exogenous expression of CD9 in PDPN-positive HT1080 fibrosarcoma cells resulted in decreased formation of pulmonary metastases in an experimental metastasis model (Nakazawa et al. 2008). Moreover, they reported that the reduction of metastasis formation is most likely due to decreased platelet aggregation. Although the PDPN-CLEC-2-interaction is not affected by CD9, CD9 suppresses CLEC-2 multimerization and hence, decreased platelet aggregation.

The nine amino acids short IC domain is required for PDPN activity as well as for the localization to the cell membrane (Fernandez-Munoz et al. 2011, Martin-Villar et al. 2015). Besides other proteins, PDPN recruits the members of the ezrin, radixin and moesin (ERM) protein family (Scholl et al. 1999, Martin-Villar et al. 2005). This recruitment can lead to EMT (Martin-Villar et al. 2006, Fernandez-Munoz et al. 2011). Moreover, the localization of PDPN to the plasma membrane is crucial for invadopodia functionality (Martin-Villar et al. 2015).
Members of the ERM protein family consist of an N-terminal ERM associated domain (N-ERMAD) and a C-terminal ERMAD (C-ERMAD) which are linked by flexible α-helices (Gary and Bretscher 1995). The N-ERMAD interacts with numerous proteins, whereas the C-ERMAD binds to F-actin, thus, building a regulated linkage between membrane proteins to the actin cytoskeleton (Bretscher et al. 2002). The N- and C-terminal domains are binding to each other with high affinity resulting in a closed conformation (Gary and Bretscher 1995). A two-step process is needed for ERM activation. First, ERM proteins are recruited to phosphatidyl-inositol 4,5-bisphosphate regions at the cell membrane (Fehon et al. 2010). Second, various kinases including Rho GTPases phosphorylate ERM proteins at Thr residues in the C-ERMAD (reviewed in Gary and Bretscher (1995), Bretscher et al. (2002)). In the context of PDPN, ERM proteins are binding to the cluster of three basic amino acids within the IC domain (human: **RK**MSG**R**YSP, mouse: **KK**ISG**R**FSP (Scholl et al. 1999, Martin-Villar et al. 2006)). Hence, Rho GTPases are

locally increased and activated. Subsequently, Rho-associated kinase (ROCK) is stimulated leading to phosphorylation and stabilization of PDPN-attached ERM proteins. ERM proteins remodel the actin cytoskeleton linked to membrane-bound PDPN setting the cell for migration. In functional *in vitro* studies performing exogenous overexpression of PDPN in human immortalized keratinocytes, mouse carcinoma as well as breast cancer cell lines, it was shown mechanistically that single or collective cell migration and invasion were mediated by PDPN in an EMT-independent and -dependent manner (Scholl et al. 1999, Wicki et al. 2006, Martin-Villar et al. 2015).

Furthermore, the IC domain can be phosphorylated at the two conserved Ser sites by protein kinase A and by cyclin-dependent kinase 5 (Krishnan et al. 2013, Krishnan et al. 2015)). The phosphorylation needs to occur on both sites in order to diminish cell motility. Whether this modification interferes with ERM protein binding or another mechanism resulting in reduced migration has not been addressed yet.

The degradation of the ECM is a critical process for tumor cell invasion. Increased PDPN expression in epidermal tumor cells suggests a decisive role in tissue remodeling (Vinicius de et al. 2011, Martin-Villar et al. 2015). Martín-Villar and colleagues reported that ERM proteins mediate and stabilize PDPN in invadopodia (Martin-Villar et al. 2015). Invadopodia are actin-rich protrusions of the plasma membrane which are important for tumor cell invasion. Although the location of PDPN in these structures is dispensable for the formation, PDPN is required for invadopodia maturation (Martin-Villar et al. 2015). This process is regulated by the RhoC GTPase phosphorylates LIM kinases and subsequent cofilin dephosphorylation and activation (reviewed in Kanellos and Frame (2016)). The cofilin-mediated actin polymerization leads then to invadopodia stabilization.

1.4.3 Transcriptional Regulation of Podoplanin

PDPN is expressed in a variety of tissues and interacts with multiple partners in different context, hence, it could be expected that the *PDPN* promoter region is controlled by multiple context-specific signaling pathways and transcription factors.

The transcription of PDPN was found in *in vitro* studies to be controlled by several growth factors (e.g. transforming growth factor beta (TGF-β) and epidermal growth factor (EGF)) as well as cytokines (interferon gamma (IFN-γ) and interleukin 6 (IL-6); reviewed in Renart et al. (2015), Quintanilla et al. (2019)).

Besides others, the transcription factor activating protein 1 (AP-1) family can result in PDPN expression (Durchdewald et al. 2008). AP-1 members are comprised of homo- or heterodimers formed by Jun, Fos and activating transcription factor (ATF) proteins

mediating gene regulation in development and pathology as response to extracellular stimuli like cytokines, growth factors and chemical carcinogens (Angel et al. 2001, Eferl and Wagner 2003). AP-1 target genes are involved in cell differentiation, proliferation as well as cell-cell and cell-matrix interactions, respectively (reviewed in Angel et al. (2001)). Several *in vivo* studies highlight the important role of AP-1 transcription factors in the skin. Saez and colleagues reported that c-Fos is dispensable for physiological epidermal differentiation and first steps of tumor development, however, it is required for malignant tumor conversion (Saez et al. 1995). Regulating AP-1 activity during chemically induced skin tumorigenesis by a dominant negative Fos mutant revealed that AP-1 activity interferes with the development of benign or malignant squamous cell lesions (Gerdes et al. 2006). Durchdewald and colleagues used the *K5-hSOS-F* transgenic mouse model in combination with epidermal *Fos* deletion to screen for Fos-regulated genes in skin tumor development (Durchdewald et al. 2008). Using isolated RNA from generated PAP, *Pdpn* was detected as the highest differentially expressed gene in the performed global gene expression analysis indicating that PDPN is a direct Fos target. Moreover, protein expression analysis on tissue sections pf TPA-treated wild-type (WT) animals confirmed PDPN upregulation in tumor cells at the invasive front.

The absence of PDPN in keratinocytes in healthy skin but its upregulation in transformed epidermal cells at the invasive tumor front implies a relevant involvement in cSCC progression.

1.4.4 The Role of Podoplanin in Pathology

In contrast to healthy skin, its expression is strongly induced under pathological conditions. In the process of wound healing, PDPN is upregulated in keratinocytes and fibroblasts (Honma et al. 2012, Baars et al. 2015). Despite the upregulation in the re-epithelizing wounded epidermis, *in vitro* and *in vivo* analysis showed that the loss of *Pdpn* in keratinocytes is not essential for wound healing and most likely, is compensated by yet to define mechanisms (Baars et al. 2015). Furthermore, in psoriatic hyperproliferative epidermis PDPN expression can be upregulated in basal cells (Honma et al. 2012). Diverse PDPN protein levels were observed in patients suffering from NMSC and CIS. PDPN was detected in around 30 % of BCC tumor cells, whereas PDPN expression was strongly increased in AK (~70 %) and cSCC (up to 90 %; Wicki and Christofori (2007), Wojciechowska-Zdrojowy et al. (2016)). In addition, stromal cells showed also a PDPN-positive reaction: ~45 % in BCC, ~20 % in AK and ~80 % in cSCC (Wojciechowska-

Zdrojowy et al. 2016). Notably, cSCC tumor cells and fibroblasts at the invasive front strongly upregulated PDPN (Figure 6 A; Gandarillas et al. (1997), Wicki and Christofori (2007), Vinicius de et al. (2011), Wojciechowska-Zdrojowy et al. (2016)). Clinical studies demonstrated that a strong expression of PDPN is associated with lymph node metastasis and consequently with poor prognosis in cSCC among other tumor types (Figure 6 B; Vinicius de et al. (2011), Wojciechowska-Zdrojowy et al. (2016)). In functional *in vitro* studies using human immortalized keratinocytes, mouse carcinoma as well as breast cancer cell lines, it was demonstrated that exogenous overexpression of PDPN results in enhanced migration and invasion (Scholl et al. 1999, Wicki et al. 2006). These data indicate a functional role of this glycoprotein in tumor cell migration and invasion.

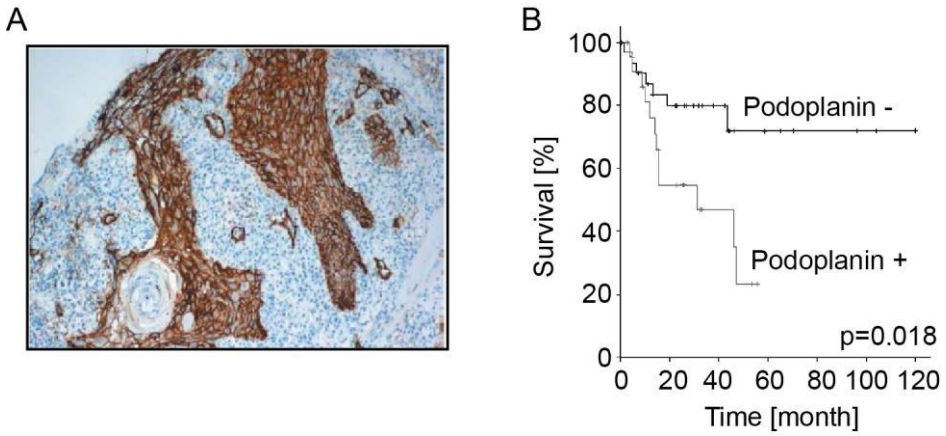

Figure 6 PDPN protein expression is associated with invasive growth and worse patient outcome.
A) PDPN expression is strongly increased in cSCC tumor cells (brown signal). B) High PDPN expression in tumor cells of locally advanced cSCC is correlated with poor long-term survival. Adapted from Vinicius de et al. (2011) and Wojciechowska-Zdrojowy et al. (2016).

In conclusion, as an AP-1 target gene the function of PDPN in cSCC has not been clarified yet, although *in vitro* and *in vivo* studies investigating its role in other SCC entities suggest increased tumor cell invasion, the causality of PDPN in keratinocyte tumors as well as the clinical suitability is still missing.

1.5 Aim

Even though the cure rate of early-stage cSCC is high, there is still an immense amount of patients suffering from late-stage non-curable tumors. Moreover, certain lifestyle behaviors like sun tanning are still attractive, life expectancy is increasing and as this NMSC is a disease of the older-aged population, there will be a vast increase of cSCC patients in the next decades (Leiter et al. 2017, Nagarajan et al. 2018). Therefore, investigations are needed to identify possible therapeutic targets for novel therapies treating patients with cSCC.

Experiments using exogenous overexpression of PDPN resulted in enhanced invasion and migration (Scholl et al. 1999, Martin-Villar et al. 2006, Wicki et al. 2006). Furthermore, PDPN is strongly expressed in cSCC, especially at the invasive front, and clinical data of advanced tumor stages has shown that high PDPN expression in cancer cells correlates with poor survival (Vinicius de et al. 2011, Wojciechowska-Zdrojowy et al. 2016). Although these studies suggest that PDPN expression in tumor cells can cause more aggressive and life-threatening cSCCs, these studies lack mechanistically the causality of PDPN expression and skin cancer cell migration and invasion and thus, worse clinical outcome.

Therefore, I aimed to study the decisive impact of PDPN in the process of cSCC carcinogenesis, since its fundamental role during this process is still unknown. For this purpose an orthotopic *in vivo* mouse model as well as different functional *in vitro* assays were performed. These analyses addressed the functional consequences of CRISPR/Cas9-mediated *PDPN* deletion in human and murine cancer cells on tumor cell proliferation, migration and invasion to gain more understanding on the role of PDPN in skin carcinoma progression.

2 MATERIAL AND METHODS

2 MATERIAL AND METHODS

2.1 Materials

2.1.1 Technical Equipment

Animal Trimmer Aesculap® Isis	Braun, Suhl
Axio Scan.Z1 Slidescanner	Zeiss, Oberkochen
BD FACSAria I	Becton Dickinson, Heidelberg
BD FACSAria Fusion II	Becton Dickinson, Heidelberg
BD FACSCalibur™	Becton Dickinson, Heidelberg
BD LSR Fortessa HTS	Becton Dickinson, Heidelberg
Cell incubator Heraeus HERA cell 240	Heraeus Instruments, Hanau
Cell incubator Heraeus HERA cell 240i	Thermo Scientific, USA
Cell incubator	Binder, Tuttlingen
Centrifuge Biofuge Fresco	Heraeus Instruments, Hanau
Centrifuge Biofuge 13	Thermo Scientific, USA
Centrifuge Heraeus Megafuge 16	Thermo Scientific, USA
Centrifuge Varifuge 3.0 R	Heraeus Sepatech, USA
Centrifuge Heraeus Fresco17	Thermo Scientific, USA
Cryo freezing container	Nalgene; Thermo Scientific, USA
Cryotome CM3050S	Leica, Wetzlar
Developer Classic E.O.S.	Agfa, USA
Digital Caliper	RS Pro, Mörfelden-Walldorf
Drying Cabinet	Heraeus Instruments, Hanau
Electrophoresis chamber for SDS-PAGE	Bio-Rad Laboratories, Munich
Embedding machine Tissue-Tek TEC	Sakura, USA
Fine scale XS205 DualRange	Mettler Toledo, Gießen
Heating mat	Conrad Electronic, Mannheim
Heat plate Top Line 2000	Rommelsbacher, Dinkelsbühl
Isoflurane gas vaporizer Vapor 19.3	Dräger, Lübeck
Magnetic stirrer/heat plate IKA® BH basic 2	IKA, Staufen
Magnetic stirrer/heat plate MR 2000	Heideloph, Schwabach
Microliter syringe 705LT 50 µl	Hamilton Robotics, USA
Microplate reader Clariostar	BMG Labtech, Ortenberg
Microscope AX10	Zeiss, Oberkochen
Microscope Leica DMLB	Leica, Wetzlar

Microscope Nikon Eclipse Ti	Nikon, Düsseldorf
Microscope Olympus IX51	Olympus, Japan
Microscope Zeiss LSM 700	Zeiss, Oberkochen
Microtome RM2155	Leica, Bensheim
Mircotome SM2010 R	Leica, Bensheim
Mixing Block MB-102	Bioer, China
Needle, 27 gauge beveled	World Precision Instruments, Berlin
Orbital shaker, Minishaker MS1	IKA, Staufen
pH meter 765 Calimatric	Knick, Berlin
Pipettes (Pipetman)	Gilson, USA
Pipettor accu-jet® pro	Brand, Wertheim
Pipettor Pipetboy acu	Integra Biosciences, Switzerland
Platform shaker Polymax 2040	Heidolph, Schwabach
Power supply Power Pac 300/3000	Bio-Rad Laboratories, München
Rotator/Shaker Rotoshake Genie	Scientific Industries, USA
Scale BP4100	Sartorius, Göttingen
Scale KERN® 440-47N	Kern & Sohn, Balingen
Shaker	Multitron Infors, Schweiz
Shaker SD5D	CAT Laboratories, Staufen
Slide Staining Tray	Pyramid Innovation, UK
Sterile GARD® Hood VBM600	Baker Company Inc., USA
Surgical tools	Fine Science Tools, Heidelberg
Thermomixer 5437	Eppendorf, Hamburg
Vacuboy	Integra, USA
Vortex IKA® MS 3 digital	IKA, Staufen
Water bath	GFL, Burgwedel
Water bath Ecoline 19	LAUDA Scientific, Lauda-Königshofen
Water bath HI 1210	Leica, Wetzlar
Wet blot transfer system	Bio-Rad Laboratories, USA
Z2 Coulter Particle Count and Size Analyzer	Beckman Coulter, USA

2.1.2 Consumables

Cell culture plates (35 mm, 60 mm, 100 mm, 150 mm)	Sigma-Aldrich, Steinheim; Corning, The Netherlands
Cell scraper	Corning, The Netherlands
Conical centrifuge tubes (15ml, 50ml)	Corning, USA
Cover glasses	Menzel-Gläser, Braunschweig
Coverslips	Thermo Scientific, USA
Cryo Tube™	Fisher Scientific, Schwerte
Disposable pipettes (5 ml, 10 ml, 25 ml, 50 ml)	Corning, The Netherlands
Disposable scalpel	Feather, Japan
Easystrainer™ Cell Sieves	Greiner Bio-One, Frickenhausen
ELISA Microlon™ 96-well plate clear	Greiner Bio-One, Frickenhausen
FACS tubes round-bottom with cell-strainer	Corning, The Netherlands
Filter pipette tips (10 µl, 20 µl, 200 µl)	Krisker, Steinfurt
Filter pipette tips (1250 µl)	Nerbe Plus, Winsen
HTS FluoroBlok Permeable Supports	Fisher Scientific, Schwerte
ImmEdge Pen™	Vector Laboratories, USA
Multiwell plates (48-well)	Greiner Bio-One, Frickenhausen
Multiwell plates (6-well, 12-well, 24-well, 96-well)	Corning, The Netherlands
Object slides Superfrost® Plus	NeoLab Migge, Heidelberg
Parafilm PM996	Bemis, USA
Pasteur capillary pipettes	WU, Mainz
Pipette tips (10 µl, 20 µl, 200 µl, 1000 µl)	Steinbrenner, Wiesenbach
Reaction tubes (1.5 ml, 2 ml)	Eppendorf, Hamburg; Sarstedt, Nürnberg
RunBlue SDS Gel 10 %	Expedeon, UK
Syringe filters 0.22 µm, 0.45 µm	Merck, Darmstadt
ThinCert™ cell culture inserts	Greiner Bio-One, Frickenhausen
ThinCert™ plate	Greiner Bio-One, Frickenhausen
Tissue embedding medium Histo-Comp®	Vogel, Fernwald
Tissue-Tek® Cryomold®	Sakura Finetek, Stauffen
Whatman™ Opitran BA-S83 nitrocellulose membrane	GE Helthcare, Munich
Whatman™ 3 MM paper	Whatman, Dassel
Fuji Medical X-ray films	Fuji, Japan

2.1.3 Chemicals and Reagents

Acetic acid	Merck, Darmstadt
AEC+ High Sensitivity Substrate Chromogen Ready-to-use	Agilent Technologies, Waldbronn
ATX Ponceau S Red Staining solution	Fluka, Buchs
BD Matrigel™ Basement Membrane Matrix	BD Biosciences, Heidelberg
Bovine serum albumin (BSA)	Sigma-Aldrich, Steinheim
Bradford MX	Expedeon, UK
Bromodeoxyuridine (BrdU)	BD Biosciences, Heidelberg
Citric acid	AppliChem, Darmstadt
Dimethylsulfoxide (DMSO)	Biomol, Hamburg
Dispase II	Sigma-Aldrich, Steinheim
Dithiothreitol (DTT)	AppliChem, Darmstadt
Eosin B	Sigma-Aldrich, Steinheim
Ethanol (EtOH)	VWR, France
Ethylenediamine tetraacetate (EDTA)	Roth, Karlsruhe
Eukitt®	Kindler, Freiburg
FACS-Clean	BD Biosciences, Heidelberg
FACS-Flow	BD Biosciences, Heidelberg
FACS-Rinse	BD Biosciences, Heidelberg
Fluorescence Mounting Medium	Agilent Technologies, Waldbronn
Glycerol	AppliChem, Darmstadt
Glycine	GERBU Biotechnik, Heidelberg
Hematoxylin	Fluka, Buchs
Hydrochloric acid (HCl)	Fisher Chemical, UK
Hydrogen peroxide (H_2O_2)	AppliChem, Darmstadt
Isopropanol (2-Propanol)	Fisher Chemical, UK
Methanol (MetOH)	Fisher Chemical, UK
Milk powder	Roth, Karlsruhe
Monopotasium phosphate (KH_2PO_4)	Roth, Karlsruhe
Mowiol 4-88	Roth, Karlsruhe
Normal Goat Serum	Vector Laboratories, USA
Nonidet P40 (NP-40)	Fluka, Buchs
Nuclease-free water	Invitrogen, Kalsruhe; Qiagen, Hilden
PageRuler™ Prestained Protein Ladder	Thermo Scientific, USA
Paraffin	Vogel, Giessen

Paraformaldehyde (PFA)	Roth, Karlsruhe
Phosphatase Inhibitor Cocktail II	Sigma-Aldrich, Steinheim
Pierce Bovine Serum Albumin Standard Pre-Diluted Set	Life Technologies, Darmstadt
Polyethylenimin (PEI), linear, MW 25.000	Alfa Aesar, USA
Polybrene	Merck, Darmstadt
Potassium chloride (KCl)	Roth, Karlsruhe
Protease Inhibitor Cocktail I	Sigma-Aldrich, Steinheim
Proteinase K	Sigma-Aldrich, Steinheim
Puromycin dihydrochloride	Life Technologies, Darmstadt
RunBlue LDS Sample Buffer (4x)	Expedeon, UK
RunBlue SDS Run Buffer TEO-Tricine	Expedeon, UK
Sodium chloride (NaCl)	Fisher Chemical, UK
Sodium citrate	Fluka, Buchs
Sodium dihydrogen phosphate ($NaH_2PO_4.2H_2O$)	Fluka, Buchs
Sodium dodecylsulfate (SDS)	GERBU Biotechnik, Heidelberg
Sodium deoxycholate	Sigma-Aldrich, Steinheim
Sodium hydroxide (NaOH) solution	Fluka, Buchs
Tissue-Tek® O.T.C.™ Compound	Sakura Finetek, Staufen
Tris-base	Sigma-Aldrich, Steinheim
Tris-hydrochloride (Tris-HCl)	Roth, Karlsruhe
Triton-X-100	AppliChem, Darmstadt
Tween-20	AppliChem, Darmstadt
Xylene	VWR, France

2.1.4 Buffers and Solutions

Table 2 Composition of buffers and solutions.

Buffer	Composition
Blocking buffer I	5 % (v/v) normal goat serum 2 % (v/v) BSA PBS, 1x
Blocking buffer II	10 % (v/v) normal goat serum 1 % (v/v) BSA PBS, 1x
Blocking buffer III	5 % (w/v) milk powder TBST, 1x

Buffer	Composition
Blocking buffer IV	10 % (v/v) normal goat serum 3 % (v/v) BSA PBS, 1x
Citrate buffer, pH 6	1.8 mM citric acid 8.2 mM sodium citrate
FACS buffer	1 % (v/v) BSA PBS, 1x
HCl, 2 N	0.17 % (v/v) HCl, 37 %
Mowiol mounting medium	6 g Mowiol 4-88 6 g glycerol 6 ml H_2O
PBS, 10x pH 7.2	1.5 M NaCl 27 mM KCl 82 mM $Na_2HPO_4.2H_2O$ 17 mM KH_2PO_4
Permeabilization buffer	10 % (v/v) normal goat serum 2% (v/v) BSA 0.1 % (v/v) Triton-X-100 PBS, 1x
PFA, 4 % pH 7.4	5 N NaOH 20 g PFA 1 l PBS, 1x
RIPA buffer	50 mM Tris-HCl, pH 8 150 mM NaCl 0.1 % (v/v) SDS 0.5 % (v/v) sodium deoxycholate 1 % (v/v) NP-40
TBS, 10x pH 7.6	0.2 M Tris-base 1.37 M NaCl
TBST, 1x	0.5 % (v/v) Tween-20 10 % (v/v) TBS, 10x
Triton/PBS, 0.3 %	0.3 % (v/v) Triton-X-100 10 % (v/v PBS, 10x)
Western blot transfer buffer, 10x	0.25 M Tris-base 1.9 M glycine
Western blot transfer buffer, 1x	20 % (v/v) MetOH 10 % (v/v) Western blot transfer buffer, 10x

2.1.5 Oligonucleotides

Table 3 Sequences of guide RNAs.

Target	Sequence 5'-3'
Renilla luciferase	CACCGGGTATAATACACCGCGCTAC
PDPN exon 1 (KO2)	CACCGGCCTGGAGGAGCGCGACGGT
PDPN exon 2 (KO1)	CACCGAGACTTATAGCGGTCTTCGC
Pdpn exon 1	CACCGCTCCCGAGCTCTTCCCGGCT

2.1.6 Plasmids

Table 4 List of plasmids.

Name	Company
lentiCRISPRv2	Addgene #52961
pCMV-VSV-G	Addgene #8454
psPAX2	Addgene #12260
pUltra-hot (mCherry)	Addgene #24130
pUltra-hot-V5-Firefly-luciferase-mCherry (V5)	Addgene #24130 + V5-tagged luciferase excised from #19166 using XbaI and NheI

2.1.7 Primary Antibodies

Table 5 Antibodies used for flow cytometry.

Antigen	Clone	Conjugate	Concentration	Company/catalogue number
PDPN	NC-08	Alexa 647	4 µl/1x10^6 cells	BioLegend® #337008
PDPN	8.1.1	APC	0.024 µg/5x10^5 cells	BioLegend® #127409

Table 6 Antibodies utilized for immunohistochemistry and immunofluorescence.

Antigen	Clone	Host species	Dilution	Antigen retrieval	Company/ catalogue number
BrdU	Ab-3	mouse	1:100	Citrate buffer pH 6	Merck, #NA61
Cleaved caspase 3	D175	rabbit	1:200	Citrate buffer pH 6	Cell Signaling #9661
Cytokeratin pan	polyclonal	rabbit	1:150	Citrate buffer pH 6	Progen #10550
E-cadherin	36	mouse	1:100	Citrate buffer pH 6	BD Biosciences #610181
Ezrin	monoclonal	mouse	1:100	Citrate buffer pH 6	Santa Cruz #sc-32759
Keratin 5	polyclonal	rabbit	1:100	Citrate buffer pH 6	Biolegend #905501
Keratin 14	LL002	mouse	1:500	Citrate buffer pH 6 EDTA pH 8	Abcam #7800
Ki67	polyclonal	rabbit	1:500	Citrate buffer pH 6	Abcam #15580
mCherry	polyclonal	rabbit	1:300	Proteinase K	Abcam #167453
Laminin	polyclonal	rabbit	1:200	EDTA pH 8	Abcam #11575
PDPN	D2-40	mouse	1:100	Citrate buffer pH 6	BioLegend® #916002
PDPN	8.1.1	Syrian hamster	1:100	Citrate buffer pH 6	Hybridoma Bank
Vimentin	ERP3776	rabbit	1:500	Citrate buffer pH 6	Abcam #92547
V5	poly29038	rabbit	1:100	Citrate buffer pH 6	BioLegend® #903801

Table 7 Primary antibodies utilized for Western blotting.

Antigen	Clone	Host species	Dilution	Company/catalogue number
Cas9	7A9.3A3	mouse	1:2000	Cell Signaling #14697
Cyclophilin A	polyclonal	rabbit	1:1000	Cell Signaling #2175S
HDAC2	C-8	mouse	1:2000	Santa-Cruz #sc-9959
mCherry	polyclonal	rabbit	1:100	Abcam #167453
PDPN	D2-40	mouse	1:1000	BioLegend® #916602
PDPN	8.1.1	Syrian hamster	1:2000	Hybridoma Bank
V5	monoclonal	mouse	1:5000	Thermo Scientific #R960-25

2.1.8 Secondary Antibodies

Table 8 Secondary antibodies used for immunohistochemistry and immunofluorescence.

Antigen	Host species	Dilution	Conjugate	Company/catalogue number
Mouse IgG	goat	1:200	biotin	Vector Laboratories #BA-2000
Mouse IgG	goat	1:500	Alexa 488	Invitrogen #A11001
Mouse IgG	goat	1:500	Alexa 647	Invitrogen #A21235
Rabbit IgG	goat	1:200	biotin	Vector Laboratories #BA-1000
Rabbit IgG	donkey	1:500	Alexa 488	Invitrogen #A21206
Rabbit IgG	goat	1:500	Alexa 546	Invitrogen #A11010
Rabbit IgG	goat	1:500	Alexa 647	Invitrogen #A21244
Syrian hamster IgG	goat	1:200	biotin	Jackson ImmunoResearch #107-065-142
Syrian hamster IgG	goat	1:500	Alexa 488	Dianova #107-547-142
Syrian hamster IgG	goat	1:200	Cy3	Jackson ImmunoResearch #107-165-142
Syrian hamster IgG	goat	1:200	Cy5	Dianova #705-176-147

Table 9 Secondary antibodies used for Western blotting.

Antigen	Host species	Dilution	Conjugate	Company/catalogue number
Mouse IgG	horse	1:2000	HRP	Cell Signaling #7076S
Rabbit IgG	goat	1:2000	HRP	Cell Signaling #7074S
Syrian hamster IgG	goat	1:2000	HRP	Jackson ImmunoResearch #107-065-142

2.1.9 Reagents for Immunofluorescence and Flow Cytometry

Table 10 Substances used for immunofluorescence and flow cytometry.

Compound	Dilution	Company/catalogue number
4-chlorobenzenesulfonate salt (DiD)	4 µl/million cells	Biotium #60014
Hoechst 33342	1:1000	Chemodex #CDX-B0030
Propidium iodide (PI)	1:1000	BioLegend® #421301

2.1.10 Commercially Available Kits

Cell Proliferation Kit XTT	AppliChem, Darmstadt
DAB Peroxidase Substrate Kit	Vector Laboratories, USA
Enhanced Chemiluminescence (ECL) Substrate	PerkinElmer, USA
VECTASTAIN® Elite® ABC HRP Kit	Vector Laboratories, USA
Venor® GeM Classic Kit	Minerva biolabs®, Berlin

2.1.11 Human Skin Samples

Human skin samples of healthy and diseased skin were kindly provided by Dr. Doris Helbig (University Clinic for Dermatology and Venerology, Cologne).

2.1.12 Cells and Cell Lines

Table 11 Primary cells.

Name	Species	Description	Provenience
hDF	human	normal human dermal fibroblasts, female donor, 23 years old	Petra Boukamp lab, DKFZ Heidelberg

Table 12 Established human and murine cell lines.

Name	Species	Description	Reference
BDVII	mouse	DMBA-induced cSCC	Fusenig et al. (1978)
HEK-293T	human	embryonic kidney	-
MET-4	human	cSCC metastasis, lymph node, p53 WT	Popp et al. (2000), Proby et al. (2000)
SCL-II	human	primary cSCC, face, p53 mutant	Tilgen et al. (1983)

2.1.13 Cell Culture Media and Supplements

Table 13 Cell culture conditions.

Cells	Condition	Medium	Medium composition	Company/catalogue number
hDF	37 °C, 5 %CO2	D10	DMEM 10 % FBS 1 % L-glutamine	Sigma-Aldrich #D5671 Sigma-Aldrich #F7524 Sigma-Aldrich #G7513
BDVII	37 °C, 5 %CO2	D10+2	DMEM 10 % FBS 2 % L-glutamine	Sigma-Aldrich #D5671 Sigma-Aldrich #F7524 Sigma-Aldrich #G7513
HEK-293T MET-4 SCL-II	37 °C, 8 %CO2	D10	DMEM 10 % FBS 1 % L-glutamine	Sigma-Aldrich #D5671 Sigma-Aldrich #F7524 Sigma-Aldrich #G7513

Table 14 Cell culture reagents.

Name	Company/catalogue number
Opti-MEM® Reduced Serum Medium	Life Technologies #31985
Poly-L-lysine solution	Sigma-Aldrich #P4707
Penicillin/Streptomycin (P/S)	Sigma-Aldrich #P4333
Trypan Blue	Sigma-Aldrich #93595

Table 15 Culture media and solutions.

Medium	Composition	Company/catalogue number
CDM	DMEM, DMEM:F12 (1:1) 10 % FBS 1 % P/S/A 200 µg/ml 2-phospho-L-ascorbic acid 1 ng/ml rh TGF-β1 2.5 ng/ml rh EGF 5 ng/ml rh FGF-2 5 µg/ml rh insulin	Lonza #BE12-604F, #BE12-719F Sigma-Aldrich #F7524 Lonza #17-745E Sigma-Aldrich #49752 Life Technologies #PHG9214 PromoCell #C-60170 PromoCell #C-60240 Sigma-Aldrich #91077C
Freezing Medium	DMEM 20 % FBS 1 % L-glutamine 10 % glycerol	Sigma-Aldrich #D5671 Sigma-Aldrich #F7524 Sigma-Aldrich #G7513 AppliChem #A3092
DPBS/EDTA	DPBS EDTA 0.5 M	PAN Biotech #P04-36500, Sigma-Aldrich #D8537 self-made

Medium	Composition	Company/catalogue number
rFAD	DMEM, DMEM:F12 (1:1)	Lonza #BE12-604F, #BE12-719F
	10 % FBS	Sigma-Aldrich #F7524
	1 % P/S/A	Lonza #17-745E
	200 µg/ml 2-phospho-L-ascorbic acid	Sigma-Aldrich #49752
	0.4 µg/ml hydrocortisone	Sigma-Aldrich #H4001
	10^{-10} M Cholera toxin	Sigma-Aldrich #C8052
Trypsin/EDTA	DPBS	PAN Biotech #P04-36500, Sigma-Aldrich # D8537
	EDTA 0.5 M	self-made
	Trypsin	Pan-Biotech #P10-822100

2.1.14 Mice

Female NMRI nude mice (Rj:NMRI-Foxn1$^{nu/nu}$) were purchased from Janvier Laboratories (Saint Berthevin Cedex, France).

2.1.15 Software

Adobe Illustrator	Adobe System, USA
BD FACSDiva™	BD Biosciences, Heidelberg
EndNote v.X7	Adept Scientific GmbH, Frankfurt am Main
FlowJo V10	Tree Star, Inc., USA
GIMP 2.10.8	Das GIMP-Team
GraphPad Prism 7.05	GraphPad Software, Inc., USA
ImageJ	National Institute of Health, USA
Inkscape 0.92.3	Inkscape Project, USA
NIS Element AR 4.13.04	Nikon, Darmstadt
Office 2013	Microsoft, USA
StepOne™ Software v2.2.2	Life Technologies, USA
Zen 2.3 (Blue edition)	Zeiss, Oberkochen

2.2 Methods

2.2.1 Animal Experiments

2.2.1.1 Housing of Mice

All experiments were reviewed and approved by the local government authority for animal experimentation (Regierungspräsidium Karlsruhe, Germany). Mice were housed in a specific pathogen-free environment in the animal facility at controlled temperature of 21 °C, 50-60 % humidity and 12 h time-controlled light cycles (DKFZ, Heidelberg, Germany). Food and drinking water was supplied *ad libitum*.

2.2.1.2 Orthotopic Injection of Tumor Cells

Female 6-8 weeks old NMRI nude mice (Rj:NMRI-*Foxn1*$^{nu/nu}$) were used for intradermal (i.d.) injection of labeled murine BDVII cSCC cells with or without specific *Pdpn* deletion under the approved license #G-75/17. The BDVII cell line was generated from DMBA-induced mouse skin carcinomas in C57BL/6 mice (Fusenig et al. 1978). Mice were anesthetized using isoflurane (O_2 flow 2 l/min, 1.5-2 Vol% isoflurane). A heating mat ensured maintenance of mouse body temperature during the procedure. To prevent eyes from dehydration, they were covered with eye ointment. Single cell suspension of labeled BDVII WT, Cas9 control or *Pdpn* KO cells (2x 10^6 diluted in 20 µl sterile DPBS) were i.d. injected into the right flank of the animals using a 27 G Hamilton syringe.
Tumor growth was checked by measuring tumor length (L) and width (W) with a digital caliper at least three times per week starting from seven days after tumor cell injection until mice were sacrificed. Tumor volume was calculated according to the formula given below (Equation 1). For final tumor measurement all three dimensions were determined (Equation 2).

Equation 1 Formula for calculation of tumor volume during observation period.
L = maximum tumor length, W = tumor width orthogonally to maximum tumor length.

$$\text{tumor volume} = 0.5 \times \text{L} \times \text{W}^2$$

Equation 2 Formula for final tumor volume calculation.
L = maximum tumor length, W = tumor width orthogonally to maximum tumor length, H = tumor height.

$$\text{tumor volume (final)} = \text{L} \times \text{W} \times \text{H}$$

CO_2 inhalation was used to sacrifice mice at indicated time points after tumor cell injection or when termination criteria were reached. Death of mice was determined by lacking reflexes (eyes and toes). To assess proliferating tumor cells, BrdU was intraperitoneally injected (100 µg/g body weight) into mice four hours prior to euthanization. Developed tumors were resected with surrounding tissue, fixed and embedded for further analysis (paragraph 2.2.3).

2.2.2 Cell culture

2.2.2.1 Thawing and Cryopreserving Cells

All cell stocks were stored in cryovials in -80 °C freezer. Cell stocks were thawed at 37 °C in a water bath, gently mixed and added to pre-warmed cell type-specific medium in 10 cm cell culture dishes. Cells were cultured according to section 2.2.2.2 and 2.2.2.3.
For cryopreservation, cells were harvested and dissociated (paragraph 2.2.2.2 and 2.2.2.3). Cells were counted with a Z2 Coulter Particle Count and Size Analyzer and centrifuged at 1300 rpm for 3 min. After aspirating the supernatant, the cell pellet was resuspended in freezing medium at 2x 10^6 cells in 1.8 ml (1.1x 10^6 cells/ml). Aliquoted cryovials were cryopreserved using a Cryo Freezing Container o/n at -80 °C. Frozen cell stocks were stored long-term in -80 °C freezer.

2.2.2.2 Culture and Passaging of Primary Fibroblasts

Normal human dermal fibroblasts (hDFs) were cultured in D10 medium at 37 °C, 5 % CO_2, 20 % O_2 in humid incubators (Table 13). Culture medium was refreshed every other day. Reaching confluence, hDFs were washed with DPBS/EDTA and detached with Trypsin/EDTA by 5 min incubation at 37 °C. By adding D10 medium hDFs were gently detached, singularized and counted using Z2 Coulter Particle Count and Size Analyzer. hDFs were subcultured in D10 medium with 3-5x 10^5 cells per 15 cm cell culture dish.

2.2.2.3 Culture and Passaging of Established Cell Lines

Details of used human and murine cell lines are listed in table 13. The murine cSCC cell line BDVII and generated subclones were cultured in D10+2 medium at 37 °C, 5 % CO_2, 20 % O_2 in humid incubators. Human cell lines HEK-293T, SCL-II, MET-4 and all

corresponding generated sublines were cultured in D10 medium at 37 °C, 8 % CO_2, 20 % O_2 in humid incubators. Medium was changed every other day.
For cultivating, HEK-293T cells were washed with DPBS/EDTA followed by detaching using Trypsin/EDTA for 2 min incubation at 37 °C. The reaction was stopped by adding D10 medium. Cells were gently detached, singularized and subcultured. All other cell lines were initially washed with DPBS, followed by treatment with DPBS/EDTA for cell type-specific incubation times (5-20 min at 37 °C). Trypsin/EDTA solution was added for incubation up to 5 min at 37 °C. Dissociation was stopped by adding cell type-specific medium. Cells were singularized and subcultured. All cells were subcultured at subconfluence.

All experiments were performed using cell passage between two and ten after thawing.

2.2.2.4 Contamination Control

Cell lines were tested regularly for mycoplasma contaminations. Therefore, medium which had been on cultured cells for at least two days was used and processed according to the Venor® GeM Classic Kit. Tests were performed by Melanie Sator-Schmitt.

2.2.2.5 Cell Culture Microscopy

All monolayer cultures were routinely checked for cell morphology and cellular growth as well as for bacterial or fungal contaminations using an Olympus IX51 microscope.

2.2.2.6 Lentivirus Production

For the stable transfer of desired CIRSPR/Cas9 construct or maker (Table 4), established cSCC cell lines were lentivirally transduced (Table 13). Therefore, HEK-293T cells were subcultured (section 2.2.2.3) and seeded in D10 medium on one 10 cm cell culture dish with a density of 2.5x 10^6 cells per one transfection condition. Cells grew 50 % confluence after o/n incubation; culture medium was refreshed 2 h prior to transfection. Every transfection mixture was prepared as the following: 3x transfection reagent polyethylenimin (PEI) was added to Opti-MEM® Reduced Serum Medium followed by adding DNA (Table 16).

Table 16 Composition of transfection mixture for lentivirus production.

Opti-MEM®	PEI [1 mg/ml]	pCMV-VSV-G	psPAX2	Plasmid of interest
200 µl	21 µl	2 µg	1 µg	4 µg

After 15 min incubation at room temperature (RT), the transfection mixture was added drop-wise to cells. Transfected HEK-293T cells were subsequently transferred to an S2 laboratory for o/n incubation at 37 °C, 5 % CO_2, 20 % O_2. Culture medium was changed the following morning. 24 and 48 h later, virus-containing medium was harvested and filtered through a 0.4 µm strainer. Virus-containing medium was stored at 4 °C for maximum one week.

2.2.2.7 Lentiviral Transduction of Cutaneous Squamous Cell Carcinoma Cells

For lentiviral transduction, human and murine cSCC cells were seeded onto 10 cm cell culture dishes after cells were harvested (section 2.2.2.3). Following steps were performed in a S2 laboratory. After 24 h incubation cSCC cells reached 50 % confluency and culture medium was exchanged by virus-containing medium supplemented with polybrene (1:1000) and incubated o/n. Virus-containing medium was exchanged by cell type-specific medium the next morning and cells were left for additional 24 h for resting. After intensive washing with DPBS transduced cells were transferred to an S1 laboratory and subcultured.

2.2.2.8 Transient Transfection of Cutaneous Squamous Cell Carcinoma Cells

To delete *Pdpn* in murine cSCC cells using the CRISPR/Cas9 technology without continuous Cas9 expression, BDVII cells were transfected. Thus, for every transfection condition, 2x 10^5 BDVII cells were seeded onto one 10 cm cell culture dish. Transfection was performed on the next day as described (section 2.2.2.6). Table 17 is displaying the composition of used transfection mixture, whereas plasmid of interest in table 4. After transfection tumor cells were cultivated in an S1 laboratory.

Table 17 Mixture used for cSCC cell transfection.

Opti-MEM®	PEI [1 mg/ml]	Plasmid of interest
200 µl	24 µl	8 µg

2.2.3 Histological Methods

2.2.3.1 Fixation, Paraffin or Cryo Embedding and Sectioning

Tumor with surrounding tissue isolated from mice as well as samples of the 3D SCM were fixed in 4 % PFA solution o/n at 4 °C (tumor samples) or RT (3D culture samples), respectively, followed by o/n incubation in 70 % ethanol at 4 °C. Samples were transferred into tissue cassettes and processed for paraffin embedding using the Tissue-Tek® VIP™ 5 Jr. Vacuum Infiltration Processor with an automated program protocol (Table 18). For embedding in paraffin, samples were taken out of plastic cassettes and transferred into metal molds filled with liquid paraffin using a Tissue-Tek® TEC™ Tissue Embedding Console. Solidified paraffin blocks were stored at 4 °C until sectioning. 4-6 µm sections were cut by Sabrina Lohr, Angela Funk, Angelika Kritschke or by myself using sliding microtomes SM2010R or RM2155. Sections were smoothened in a 42 °C water bath and transferred to SuperFrost® slides followed by a drying incubation at 42 °C o/n. Sections were stored at RT until staining.

Table 18 Processing of tissue before paraffin embedding.
Automated program of Tissue-Tek® VIP 5 Jr. Vaccuum Infiltration Processor.

Step	Temperature [°C]	Cycles	Time [min]
70 % EtOH	35	1	45
80 % EtOH	35	1	90
90 % EtOH	35	2	90
96 % EtOH	35	2	90
Isopropanol	35	2	90
Xylene	40	2	150
Paraffin	60	4	45

Depending on used antibody, murine material needed to be embedded into Tissue-Tek® O.C.T.™ Compound into Cryomolds®. Embedded samples were frozen using dry ice and stored at -80 °C until usage. Cryo-embedded samples were pre-warmed to -20 °C and cut into 6 µm section using the Cryotome CM3050S.

2.2.3.2 Tissue Preparation for Stainings

Paraffin was removed from paraffin-embedded sections by washing twice with xylene (8 and 5 min) followed by rehydration using an ethanol series of 2 min incubation steps each (96 %, 80 %, 70 %, 60 % in water) and 2 min incubation with distilled water.
Frozen sections were thawed at RT for 20 min followed by fixation with 4 % PFA for 15 min at RT.

2.2.3.3 Hematoxylin and Eosin Staining

Hematoxylin staining of paraffin-embedded as well as frozen sections was performed for 6 min followed by washing in running water for 8 min. Sections were stained in eosin for 6 min and washed in running water for 6 min. Sections were dehydrated in 2 min 80 % ethanol, 2 min 90 % ethanol followed by 2 min isopropanol and 2x 5 min xylene. Finally, sections were mounted in Eukitt®.

2.2.3.4 Immunohistochemistry of Paraffin-Embedded Sections

For immunohistochemical (IHC) staining antigen retrieval was performed on rehydrated sections corresponding to used antibodies listed in table 6.

(i) Citrate buffer or EDTA: 500 ml citrate buffer or 1 mM EDTA solution was boiled in a glass beaker on a heating plate. Deparaffinized and rehydrated sections were incubated in sub-boiling retrieval solution for 15 min or 8 min, respectively. Glass beaker was removed from the heating plate and left at RT for cooling down for 15 min.

(ii) Protease K: sections were incubated with 20 µg/ml protease K for 20 min at 37 °C.

After antigen retrieval, sections were washed in PBS and encircled with a hydrophobic barrier ImmEdge Pen™ followed by another washing in PBS. For all following incubation steps, sections were placed into a humid chamber and sections were washed in PBS between incubations. Sections were incubated light-protected with 3 % H_2O_2 solution for 10 min at RT to block endogenous peroxidase. Subsequently, sections were blocked in blocking buffer II for 30 min at RT. Primary antibodies were diluted in blocking buffer II and sections were incubated o/n at 4 °C (Table 6). One section per experiment was left in blocking buffer II without primary antibody and served as staining control. Biotin-linked secondary antibody staining was performed light-protected with secondary antibody

(Table 8) diluted in blocking buffer II 1 h at RT. Meanwhile, avidin/horseradish peroxidase (HRP) was prepared according to manufacturer's instructions (VECTASTAIN® ABC-Elite reagent) and used for the next incubation for 30 min at RT. Further, the signal was developed using 3'-diaminobenzidine (DAB) reagent, which was prepared as designated in the manufacturer's protocol. The reaction of DAB staining was monitored using the Leica DMLB microscope and stopped with tap water when the signal was sufficiently visible. Cell nuclei were counterstained with hematoxylin for 30 s to 2 min, dehydrated and mounted as described in paragraph 2.2.3.3. Sections were stored at RT until imaging.

Sections were additionally treated for BrdU staining. After H_2O_2 incubation, 0.3 % Triton/PBS was applied to sections for 10 min at RT followed by 20 min incubation at 37 °C with 2 N HCl. Blocking and antibody staining were performed as described. Instead of the DAB reagent, staining was developed utilizing AEC substrate and after hematoxylin staining sections were mounted using fluorescent mounting medium.

2.2.3.5 Immunofluorescent Staining of Tissue and 3D Culture Samples

Rehydration and antigen-retrieval of paraffin-embedded sections were performed as described (section 2.2.3.2 and 2.2.3.4). Sections were placed in a humid chamber for all incubation steps of the immunofluorescence (IF) staining and washed in between with PBS. After blocking sections with blocking buffer II for 30 min at RT, o/n incubation at 4 °C was performed applying primary antibody dilutions in blocking buffer II (Table 6). One section per experiment was left in blocking buffer II without primary antibody and served as staining control. On the following day, sections were stained light-protected with fluorophore-labeled secondary antibodies diluted in blocking buffer II for 1 h at RT (Table 8). Additionally, cell nuclei were stained light-protected with Hoechst 33342 solution (1:1000) for 5 min at RT. Finally, sections were mounted in fluorescent mounting medium and stored light-protected at 4 °C until imaging.

Sections were differently treated for Laminin-K14 co-staining. After antigen retrieval sections were washed twice in TBST (0.1 % Tween 20) followed by 15 min incubation in 0.2 % Tritin-X-100 in TBS. Sections were blocked in blocking buffer IV for 1 h at RT and primary antibodies were diluted in blocking buffer II and incubated o/n at 4 °C (Table 6). One section per experiment was left in blocking buffer II without primary antibody and served as staining control. All following washing steps were performed in three-times for 10 min in TBS. Incubation with secondary antibodies was performed in blocking buffer II for 1 h at RT light-protected (Table 8). Cell nuclei were stained light-protected with

Hoechst 33342 solution (1:1000) for 5 min at RT. Finally, sections were mounted in fluorescent mounting medium and stored light-protected at 4 °C until imaging.

2.2.4 Protein Biochemistry Methods

2.2.4.1 Immunofluorescence Staining of Cultured Cells

Cells were seeded on poly-L-lysine-mounted coverslips placed into 48-well plates and cultured in cell type-specific medium until cells reached desired density (section 2.2.2.3). For fixation, medium was removed and cells were fixed with 4 % PFA for 20 min at RT. After washing with PBS, coverslips were placed in a humid chamber for all incubation steps and washed in between with PBS. Cells were permeabilized and blocked in parallel with permeabilization buffer for 30 min at RT. Incubation with primary antibody dilutions in blocking buffer I (Table 6) was performed o/n at 4 °C. One coverslip per experiment was left in blocking buffer I without primary antibody and served as staining control. On the following day, cells were stained light-protected with fluorophore-labeled secondary antibodies diluted in blocking buffer I for 1 h at RT (Table 8). Additionally, cell nuclei were stained light-protected with Hoechst 33342 solution (1:1000) for 5 min at RT. Finally, coverslips were mounted face-down on microscope slides in Mowiol solution and stored light-protected at 4 °C until imaging.

2.2.4.2 Preparation of Protein Extracts

Confluent grown cells were washed once with cold PBS. Cells were lysed in cell lysis buffer (Table 18) and transferred into a 1.5 ml reaction tube. After centrifugation (20 min, 13 000 rpm, 4 °C), supernatant containing isolated whole cell protein extracts were transferred to a new reaction tube and stored at -80 °C.

Table 19 Composition of cell lysis buffer for protein extraction.

Reagent	Amount
RIPA buffer	979 µl
Protease Inhibitor Cocktail I	10 µl
Phosphatase Inhibitor Cocktail II	10 µl
DTT	1 µl

2.2.4.3 Determination of Protein Concentration

Protein concentration of cellular extracts was quantified according to the Bradford assay. Lysates were diluted 1:5 in water. To define the standard curve a Pierce™ Bovine Serum Albumin (BSA) Standard Pre-Diluted Set was used. Water was used as blank. Duplicates of each sample and standard were prepared in a transparent 96-well plate and Bradford MX™ solution was added. Absorbance was detected with a microplate reader at 595 nm wavelength. Final protein concentrations were calculated by the BSA standard curve.

2.2.4.4 Protein Separation with SDS-PAGE

The concentration of protein extracts was equally set to either 20 or 30 µg and supplemented with 4x RunBlue LDS Sample Buffer followed by denaturation for 10 min at 95 °C. Samples were cooled down to 4 °C and loaded onto a pre-casted 10 % RunBlue SDS gel. The PageRuler™ Prestained Protein Ladder was additionally loaded for size comparison. SDS gel was placed into an SDS-PAGE chamber filled with 1x RunBlue SDS Run Buffer. Electrophoretic separation of proteins was achieved by applying a current of 80 V for the first 10 min followed by 120 V for full separation.

2.2.4.5 Western Blotting

Separated proteins were transferred from separation gel onto nitrocellulose membranes using a wet blotting system. Therefore, the gel and Whatman™ nitrocellulose membrane were embedded between two pre-moistened sheets of Whatman™ 3MM paper on each side. Proteins were transferred at 400 mA for 2 h at 4 °C. Successful protein transfer to the nitrocellulose membrane was confirmed by Ponceau staining followed by washing with tap water. To avoid unspecific protein binding, the membrane was blocked with blocking buffer III for 1 h at RT followed by o/n incubation at 4 °C with primary antibody diluted in blocking buffer III (Table 7). On the next day, the membrane was washed with 1x TBST buffer and membrane was stained with HRP-linked secondary antibody diluted in blocking buffer III at RT for 1 h (Table 9). Membrane was washed with 1x TBST. Enhanced chemiluminescence (ECL) solution was prepared according to the manufacturer's protocol and distributed equally over the membrane. Protein signals were detected using x-ray films and the Developer Classic E.O.S machine.

2.2.5. Flow Cytometry and Fluorescence Activated Cell Sorting

2.2.5.1 Flow Cytometric Analysis

2D-cultured cells were harvested and single cell suspensions were counted using the Z2 Coulter Particle Count and Size Analyzer. For flow cytometric analysis, 5x 10^5 cells were resuspended in FACS buffer and incubated for 20 min at 4 °C light-protected with appropriate antibody (Table 5). Cells were washed and resuspended in 250 µl FACS buffer. Protein expression was analyzed using BD FACSCalibur™ or LSR Fortessa HTS. Analysis was performed using the FlowJoV10 Program or BD FACSDiva™ Software.

2.2.5.2 Fluorescence Activated Cell Sorting

For the generation of polyclonal *PDPN* KO cultures derived from the *PDPN* KO-transduced cells, *PDPN* KO and WT cells (*PDPN*-positive control) were expanded and singularized (section 2.2.2.3). Cells were counted using the Z2 Coulter Particle Count and Size Analyzer, resuspended in FACS buffer and stained with the species-specific fluorophore-labeled anti-PDPN antibody at 4 °C for 20 min in the dark (Table 5). Afterwards, cells were washed with DPBS, resuspended in FACS buffer and dead cells were stained with PI (1 µl/ml cell suspension). Cell suspensions were transferred to FACS tubes by filtering through 0.35 µm sieves. Cells were transported to the Flow Cytometry Facility (DKFZ, Heidelberg, Germany), who performed the bulk sort to establish *PDPN*-negative cell population using the BD FACSDiva™ Software. After sorting, cells were centrifuged (1300 rpm, 3 min) and cultured in D10 supplemented with 1 % P/S. After one week, medium was exchanged to D10 and cells were expanded and cryopreserved (paragraph 2.2.2.1).

In order to establish BDVII WT, Cas9 control and *Pdpn* KO cultures expressing either V5-Firefly-luciferase-mCherry or mCherry marker, these cell lines were FACSorted for mCherry after lentiviral transduction (paragraph 2.2.2.7). Cells were prepared and sorted as described with one exception: no PI staining was performed. mCherry-positive cells were cultivated in medium supplemented with 1 % P/S for one week and expanded for cryopreservation (section 2.2.2.1).

2.2.6 Functional Analyses

2.2.6.1 Proliferation Assay

Control and *PDPN* KO human and murine cSCC cell lines were seeded as triplicates for each time point onto 12-well plates and incubated as described (section 2.2.2.3). Cells were harvested 24, 48 and 72 h after seeding. Single-cell suspensions of triplicates were used to assess proliferation by counting. Cells were counted manually using the Neubauer chamber and trypan blue to identify dead cells (Equation 3). Experiments were run three times in triplicates. Two-tailed Welch's t test was used to determine potential differences in proliferation. Significant differences were considered with $p < 0.05$.

Equation 3 Formula for determination of total cell amount.
Cell number was calculated using the Neubauer Chamber. Z = amount of counted cells.

$$\text{total cell amount} = \text{Z} \times 10^4$$

2.2.6.2 Viability Test

To assess metabolically active cells the Cell Proliferation Kit XTT was performed according to the manufacturer's protocol. Therefore, human and murine control and *PDPN* KO cell lines were seeded onto transparent flat-bottomed 96-well plates in cell type-specific medium. Wells only containing medium were used as blank displaying background control. Viability was detected 24, 48 and 72 h after cell seeding. To this end, XTT reaction solution was prepared just prior to use and added to cultured cells. After 2 h incubation time in a humid incubator, the absorbance of samples (460 nm) against background control (660 nm) was detected. Experiments were run three times in triplicates. Two-tailed Welch's t test was used to determine potential differences in metabolic activity. Significant differences were considered with $p < 0.05$.

2.2.6.3 Boyden Chamber Transmigration Assay

Human and murine cSCC *PDPN* KO cells and corresponding Cas9 controls were seeded as triplicates onto 6-well plates under cell type-specific culture conditions (section 2.2.2.3). After o/n culture, cells with ~50 % density were starved using starvation medium (culture medium without FBS) and incubated for another 24 h. On the following day 24-well HTS FluoroBlok cell culture inserts with an 8 µm filter were coated with 0.2 mg/ml BD Matrigel™ and incubated 1 h at RT. Meanwhile, cSCC cells were harvested, singularized in starvation

medium and labeled with the hydrophobic marker DiD (Table 10). Therefore, cells were counted using the Z2 Coulter Particle Count and Size Analyzer and incubated with DiD in starvation medium for 20 min at 37 °C followed by washing with DPBS. Cells were resuspended in starvation medium with 2.5x 10^5 cells/ml. Cell culture inserts were transferred to a 24-well plate prepared with 500 µl/well cell line-specific medium supplemented with FBS and 200 µl cSCC cell suspension was added drop-wise on matrigel-coated inserts. Cells were incubated with cell line-specific conditions in humid incubators. Transmigration was monitored regularly by DiD stained cells which reached the bottom of the filter inserts using the Nikon Eclipse Ti microscope. Optimal cell line-specific incubation time was determined according to transmigrated control cells during the first performance of the experiment.

After cell line-specific incubation, cells were fixed light-protected with 4 % PFA for 20 min at RT followed by washing with PBS. Non-transmigrated cells on top of the filter were removed with a Q-tip. Filters were cut out of inserts and placed bottom-to-top into a humid chamber for IF staining which was performed as described (section 2.2.4.1). Instead of permeabilization buffer, blocking buffer I was used for the blocking step. After the staining procedure filters were transferred to a microscope slide and mounted using Mowiol solution and 12 mm coverslips. Transmigrated cells were detected using the Nikon Eclipse Ti microscope. Transmigrated cells were automatically quantified by Hoechst staining using an ImageJ macro written by myself. Experiments were run three times in technical triplicates. To see whether transmigratory capacity was affected by the loss of *PDPN*, two-tailed Welch's t test was performed. Differences in transmigration were considered significant with $p < 0.05$.

2.2.6.4 Organotypic Skin Cancer Model

The organotypic skin cancer model (SCM) is a 3D culture system based on fibroblast-derived matrix (fdm) with keratinocytes or cSCC cells growing air-exposed on top of hDFs within a deep-well system (Figure 4). This experiment was performed as published by Berning et al. (2015).

For the generation of fdm, low-passage hDFs were expanded until a sufficient number of cells were grown (paragraph 2.2.2.2). hDFs were seeded step-wise within the first week. In detail, 5x 10^5 hDFs were seeded three times in CDM medium onto one 12-well ThinCert™ cell culture insert with a density of 0.4 µm pores. The filter inserts were placed into deep-well plates prepared with CDM medium and cultured at 37 °C, 5 % CO_2, 20 % O_2.

CDM medium was changed in the deep-well and in the filter insert every other day for four weeks.
After four weeks murine or human cSCC cells were added on top of the generated fdm. Therefore, medium in deep-well was changed to rFAD medium and medium on top of hDFs was removed. cSCC cells were harvested and single-cell suspensions were provided after cells were strained through a 70 µl cell sieve. 2.5x 10^5 tumor cells were seeded onto hDFs and incubated at 37 °C, 5 % CO_2, 20 % O_2. Medium was refreshed every other day until defined time points were reached. After the first five days, medium on top of the cells was completely removed, so that cSCC cells were growing air-exposed. Experiments were run once with one to three technical replicates for human cell lines for each time point. For each time point the experiment was performed three times with technical triplicates for murine cSCC cells.
For the harvest, organotypic co-culture samples on filters were removed from inserts and cut in half. One half was fixed in 4 % PFA and embedded in paraffin, the filter membrane of the bottom side of the other half was removed and the sample was embedded into Tissue-Tek® O.C.T.™ Compound and stored at -80 °C until usage (section 2.2.3.1).

2.2.7 Image Acquisition and Analysis

Images were captured using the Nikon Eclipse Ti microscope, confocal Zeiss LSM 700 microscope or the Axio Scan.Z1. ImageJ or Zen Blue software were used for image processing adjusting brightness, contrast and gamma. Images were quantified using macros for ImageJ software written by myself together with Dr. Damir Krunic, Light Microscopy Facility (DKFZ, Heidelberg, Germany).

2.2.8 Statistical Analysis

To determine potential differences of tumor volumes between two groups (control and *Pdpn* KO group), tumor volumes were plotted and statistically compared by the implementation of the one-tailed Mann-Whitney test. For the identification of the significant difference between the means of two groups (control and *Pdpn* KO group), the two-tailed Welch's t test was performed.
Analyses were done using GraphPad Prism 7.05 Software. Dr. Tim Holland-Letz was consulted for the definition of group sizes for the animal license and Thomas Hielscher aided the statistical analysis of performed functional *in vitro* and *in vivo* experiments.

3 RESULTS

3 RESULTS

3.1 Varying Podoplanin Protein Expression in Different Cell Types of Patients Suffering from Different Skin Diseases

As podoplanin (PDPN) has been proposed as a major driver in the progression of different cancer entities including cutaneous squamous cell carcinoma (cSCC), this study aimed to define this proposed function in cSCC progression. Moreover, previous publications had shown that PDPN is expressed in varying intensities by different cell types in healthy and diseased skin (section 1.4.1 and 1.4.4). Thus, to validate and further extend our knowledge the location and expression levels of PDPN in physiology and pathology, immunohistochemistry (IHC) staining of human tissue sections of healthy skin as well as of multiple pathological diseases was performed.

Confirming published data, PDPN was weakly expressed in healthy skin by some basal keratinocytes, whereas dermal fibroblasts were negative for PDPN (Figure 7 A; Gandarillas et al. (1997)). Moreover, lymphatic vessels, hair roots and sebaceous glands showed a PDPN-positive reaction. Staining of the inflammatory skin diseases Lichen Planus Ruber and eczema showed an increased PDPN expression in basal keratinocytes as well as in fibroblasts suggesting that fibroblasts were in an activated state (Figure 7 B and C). PDPN-positive fibroblasts were also detected in skin affected by the auto-immune disease psoriasis (Figure 7 D; Honma et al. (2012)). Particularly, in psoriasis PDPN was strongly upregulated in basal keratinocytes compared to healthy skin. The potential precancerous stage of cSCC can be actinic keratosis (AK), which showed a prominent PDPN expression in basal keratinocytes of the hyperactive epidermis (Figure 7 E). In descriptive cSCC analysis, PDPN expression was only described in poor- to moderate-differentiated tumors (Schacht et al. 2005, Vinicius de et al. 2011). In contrast, I found that tumor cells of six moderate (n=1) to well-differentiated cSCC (n=5) highly expressed PDPN at the invasive front suggesting that PDPN is involved in differentiated tumors as well (Figure 7 F). Interestingly, a PDPN-positive reaction with varying intensities was also detected in CAFs in six out of six analyzed tumor samples.

In conclusion, PDPN protein expression levels as well as location differed in health and disease conditions and among analyzed diseases. In comparison to other skin diseases, cSCC tumor cells showed constantly strong PDPN expression, especially at the invasive front. This observation suggested a crucial role of this glycoprotein in differentiated cSCC. Moreover, a PDPN-positive reaction was detected in the tumor stroma as well. These

results indicated that PDPN might act as a driver in the process of tumor cell invasion in differentiated cSCC.

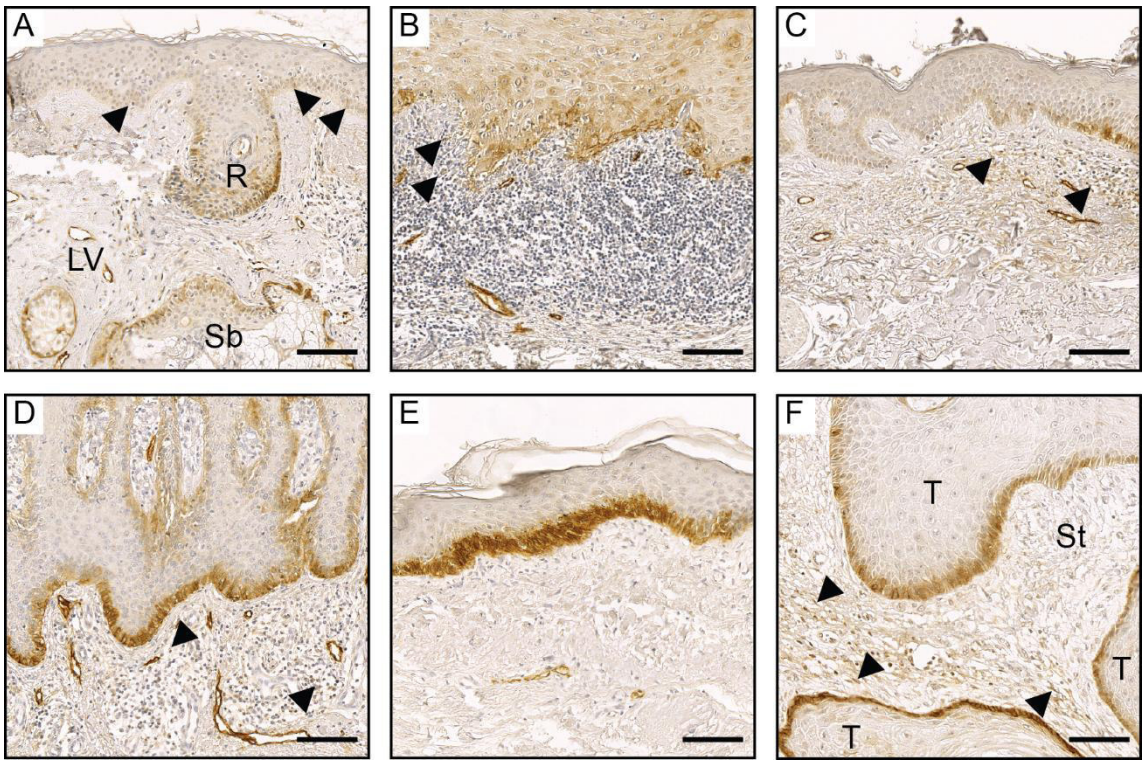

Figure 7 Differential PDPN protein expression in healthy and diseased skin.
Human PDPN expression was determined by IHC staining. A) In healthy skin PDPN was focally expressed in basal keratinocytes (arrowheads) and showed stronger expression in lymphatic vasculature (LV), hair root (R) and sebaceous glands (Sb). B) and C) Lichen Planus Ruber and escema displayed stronger PDPN expression in basal keratinocytes and fibroblasts (arrowheads). D) Expression of PDPN in psoriasis was strongly increased in basal keratinocytes and showed a weak positive staining in fibroblasts (arrowheads). E) In AK enhanced PDPN expression was detected in basal keratinocytes of the hyperactive epidermis. F) PDPN was highly expressed in tumor cells (T) at the invasive front of cSCC. CAFs showed weak PDPN staining (arrowheads) in the stroma (St). Representative images are shown. N=6 cSCC. Nuclei were stained with hematoxylin. Scale bar 200 µm, image quality was optimized by adjustment of brightness, contrast and gamma.

3.2 Podoplanin Acts as a Driver in Cutaneous Squamous Cell Carcinoma *in Vitro*

The descriptive analysis of PDPN protein expression in well-differentiated cSCC patients' material implied a critical role of PDPN in tumor cell invasion. However, functional experiments were necessary to conclude on the causality of PDPN expression and cSCC progression. So far it has only been shown that PDPN upregulation by exogenous

overexpression increases cell migration in immortalized mouse keratinocytes as well as in breast cancer cell lines (Scholl et al. 1999, Wicki et al. 2006). To investigate the importance of PDPN loss in cSCC cancer cells on the invasive capacity in functional *in vitro* and *in vivo* experiments, a loss-of-function (LOF) approach was used by applying the CRISPR/Cas9 technology on human and murine cSCC cell lines.

3.2.1 Selection of Human and Murine Cell Lines

Several cell lines displaying different cSCC stages have been established which can be used in *in vitro* and *in vivo* approaches (section 1.2.1). For the establishment of *PDPN*-deficient cSCC tumor cells, the CRISPR/Cas9 technology with subsequent bulk fluorescent activated cell sort (FACSort) was chosen. As PDPN is a transmembrane protein a *PDPN*-negative polyclonal cell culture can be generated with this approach while avoiding single cell clones and potential related clonal artifacts. For this procedure, PDPN needed to be expressed by tumor cells in monolayer culture condition and thus, its expression had to be determined initially in potential candidate cell lines.
Therefore, whole-cell protein lysates of 2D-cultured human and murine cSCC cell lines derived from various cSCC tumors or metastasis were used for Western blotting (Figure 8 A and B). Detected intensities of PDPN protein expressions varied between different human cSCC cell lines. Moreover, this analysis demonstrated a shift of electrophoretic mobility of PDPN suggesting potential cancer-specific posttranslational modifications such as glycosylation. The human SCL-II and MET-4 cell lines were selected based on their tumor origin, PDPN expression intensity and diverse electrophoretic shift. SCL-II cells were isolated from a facial undifferentiated primary tumor and MET-4 cells were established from an undifferentiated metastatic cSCC (Tilgen et al. 1983, Popp et al. 2000, Proby et al. 2000). Thus, these two selected human cell lines represent tumors at different stages of cSCC progression. Comparing these two lines, MET-4 cells expressed lower PDPN levels as SCL-II cells, but the electrophoretic mobility of PDPN was shifted in SCL-II cells probably due to differential glycosylation patterns. Besides human cSCC cells, the murine cSCC cell line BDVII was chosen allowing syngeneic injections into mice. This cell line was generated by chemical induction of cSCC in C57BL/6 mice (Fusenig et al. 1978). BDVII cells strongly expressed PDPN (~ 42 kDa) and its electrophoretic mobility was shifted differently compared to SCL-II and MET-4 cells (~55 kDa and ~49 kDa, Figure 8 A and B). Notably, the expression intensity between human and murine PDPN cannot be compared as different antibody clones (human D2-40 and murine 8.1.1) were used for the detection.

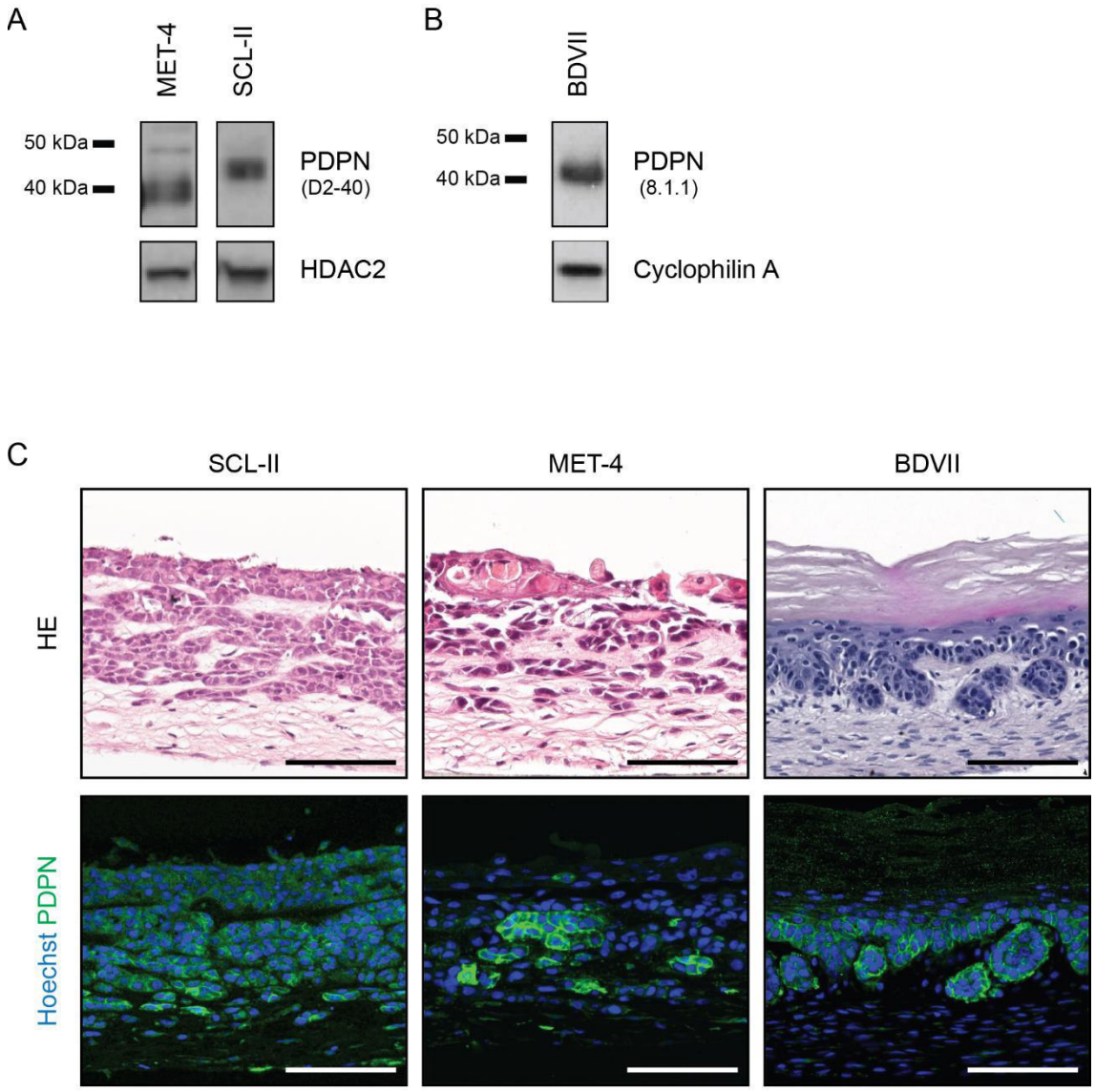

Figure 8 PDPN protein expression in human and murine cSCC cell lines.
Western blot analysis of 2D-cultured A) human cell lines and B) murine BDVII cells showed varying protein levels. Protein expression of HDAC2 and Cyclophilin A were used as loading control. C) Representative images of histological and IF analysis of PDPN expression of selected human and murine cell lines in the 3D organotypic SCM. All tumor cells formed multiple epithelial layers and invaded into the dermal compartment. Different PDPN expression pattern was observed. Nuclei were stained with Hoechst. Scale bar 100 µm, image quality was optimized by adjustment of brightness, contrast and gamma.

The expression levels of PDPN were additionally analyzed in 3D context using the organotypic skin cancer model (SCM). SCL-II, MET-4 and BDVII cells were seeded on top of human dermal fibroblasts (hDFs) and cultured for two weeks. Histological analysis showed that tumor cells grew on top of the dermal compartment reflecting the characteristics of original tumor samples (Figure 8 C; Tilgen et al. (1983), Popp et al. (2000), Proby et al. (2000)). SCL-II and MET-4 cells formed a multilayered epithelium

without differentiation, whereas BDVII cells formed cornified layers. IF staining demonstrated that PDPN expression was not only restricted to invasively growing cells. All SCL-II cells expressed PDPN homogenously on a moderate level, whereas only a proportion of MET-4 cells showed PDPN staining in different intensities. In the murine BDVII culture, PDPN was strongly expressed in all active tumor cells, but it was gradually lost when cells entered terminal differentiation.

Hence, the two human SCL-II and MET-4 as well as the murine BDVII cSCC cell lines were selected. Their origin, the differences in PDPN expression intensities as well as potential different glycosylation patterns made these cell lines particular attractive to investigate the causative link between PDPN expression and cSCC progression.

3.2.2 Establishment of Podoplanin Deletion in Human and Murine Cutaneous Squamous Cell Carcinoma Cell Lines

3.2.2.1 Generation of Podoplanin Knockout and Control Cells

To examine the impact of PDPN loss in tumor cells on the invasive potential in functional *in vitro* and *in vivo* experiments, the CRISPR/Cas9 system was chosen to constitutively ablate *PDPN* in selected human and murine cSCC cell lines. *PDPN*-deficient and control cells were generated in a multistep procedure (Figure 9). Accordingly, SCL-II, MET-4 and BDVII cells were transduced with the lentiviral vector lentiCRISPRv2 encoding the endonuclease Cas9 and a guide RNA (gRNA) specifically targeting either human *PDPN* or murine *Pdpn*. To delete *PDPN* in human cell lines two gRNAs were transduced targeting two different exons of *PDPN* generating two sublines (*PDPN* knockout 1 (KO1) and KO2, Table 4, Figure 9 A). To generate murine *Pdpn*-deficient cells one gRNA was used (Figure 9 B). Moreover, appropriate Cas9-expressing control cells (ctrl) were generated in parallel to exclude potential effects of Cas9 in further experiments. Therefore, human and murine cSCC cells were lentivirally transduced with Cas9 as described, but here a gRNA was utilized which targeted a Renilla-luciferase gene originated from sea pansy. Subsequently, all transduced sublines were treated with puromycin for one week to select cells which stably integrated the construct.

To distinguish murine BDVII tumor cells upon injection from host cells, BDVII wild-type (WT), control and *Pdpn* KO cells were additionally labeled with the V5-Firefly-Luciferase-mCherry (V5) via lentiviral transduction followed by bulk FACSort (Figure 9 B).

To evaluate successful *PDPN* deletion as well as marker expression, PDPN protein and marker expression were verified on protein level on a single cell level.

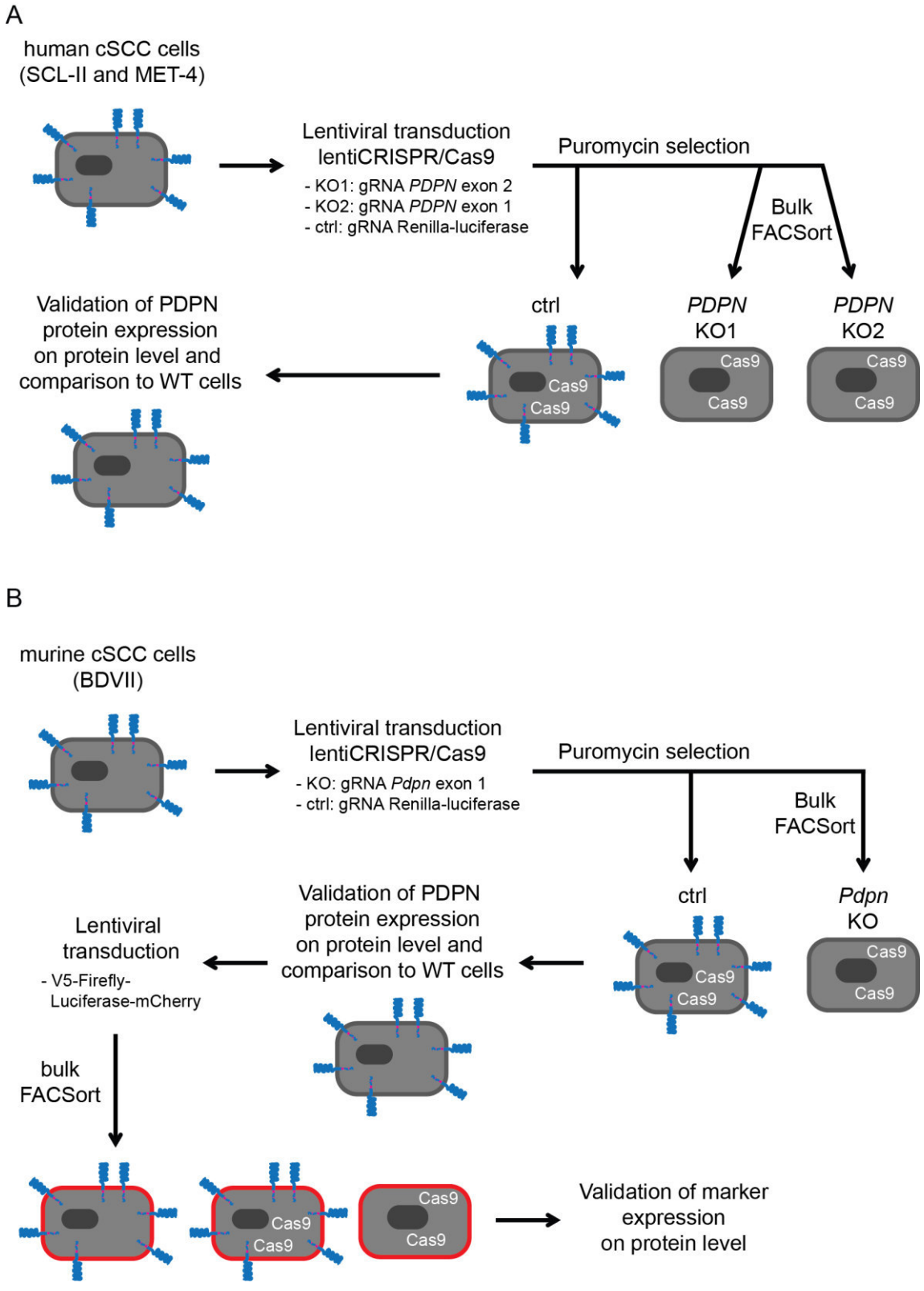

Figure 9 *In vitro* generation of *PDPN* KO and control cells.
CRSPR/Cas9-mediated *PDPN* KO and generation of Cas9-expressing controls (ctrl) in A) human and B) murine cSCC cells using lentiviral infection. Additional labeling of murine BDVII cells. Validation of PDPN and marker expression was performed on protein level.

3.2.2.2 Validation of Podoplanin and Marker Expression in Generated Human and Murine Cutaneous Squamous Cell Carcinoma Cell Lines

After generation of polyclonal *PDPN* KO and control sublines, the presence or absence of PDPN protein expression, respectively, as well as labeling of the BDVII-V5 cells were validated by immunofluorescence (IF) staining and FACS analysis.

To verify PDPN protein levels an IF staining of cultured cells was performed. Strong PDPN expression was found in BDVII WT- and control-V5 cells (Figure 10 A). No PDPN was observed in the KO-V5 culture. SCL-II WT and control cells expressed PDPN at a moderate level, whereas KO1 and KO2 showed no PDPN signal (Figure 11 A). MET-4 control cells showed varying PDPN levels. Single cells expressing low levels of PDPN were detected in MET-4 KO cultures (Figure 11 A arrowheads).

In order to test whether generated *PDPN* KO cultures retained their PDPN-negative status over time, FACS analyses at different time points were performed. Nearly 100 % of BDVII WT- and control-V5 cells showed high PDPN expression (Figure 10 B and C). *Pdpn* KO-V5 cells maintained around 3 % PDPN-expressing cells over several passages. Furthermore, analysis of mCherry expression revealed that more than 90 % of all murine sublines were positive for the introduced marker. SCL-II WT and control cells expressed PDPN on a moderate level (Figure 10 B and D). Notably, SCL-II KO1 and KO2 cultures contained less than 3 % of PDPN-positive cells from low to high culture passage (Figure 11 B and D). PDPN-positivity in MET-4 WT and control cells ranged from 55 to 90 % (Figure 11 C and D). In generated MET-4 KO1 and KO2 cultures, the proportion of PDPN-positive cells increased over time from 1 % to around 11-14 %. Although an additional FACSort of MET-4 KO cultures could have lowered the remaining PDPN-positive population, this procedure was left out to retain a short cultivation period. In consequence, low passage cultures were used for subsequent functional analyses. The residual small amount of PDPN-expressing cells in all generated KO sublines was taken into account.

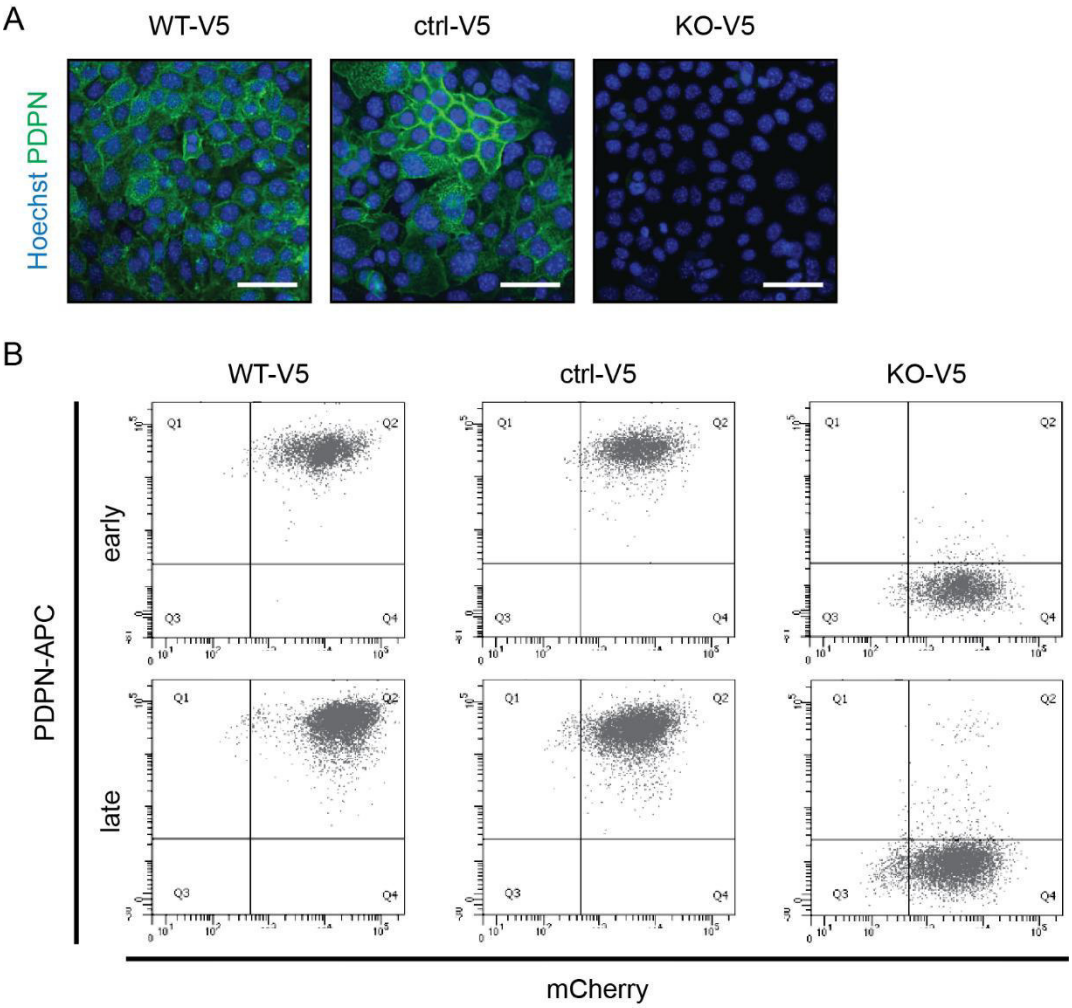

C

Cell line	Q1 [%]		Q2 [%]		Q3 [%]		Q4 [%]	
	early	late	early	late	early	late	early	late
WT-V5	0.5	0.5	99.5	99.5	0.0	0.0	0.0	0.0
ctrl-V5	0.9	1.4	99.1	98.6	0.0	0.0	0.0	0.0
KO-V5	0.0	0.3	2.5	3.0	2.5	5.9	95.0	90.8

Figure 10 Validation of PDPN and marker expression in murine cSCC cells.
A) PDPN expression was observed by IF staining. WT- and control (ctrl)-V5 cells showed strong PDPN expression. No PDPN signal was detected in KO-V5 cells. B) FACS analysis confirmed PDPN-positive population in WT- and ctrl-V5 cultures. The small amount of PDPN-positive cells in KO-V5 subline was retained from early to late passages. WT-, ctrl- and KO-V5 cells expressed moderate to high mCherry levels. C) Overview of percentage portion in quadrant 1 to 4 (Q1-4) in early and late culture passages. Nuclei were stained with Hoechst. Scale bar 50 µm, image quality was optimized by adjustment of brightness, contrast and gamma.

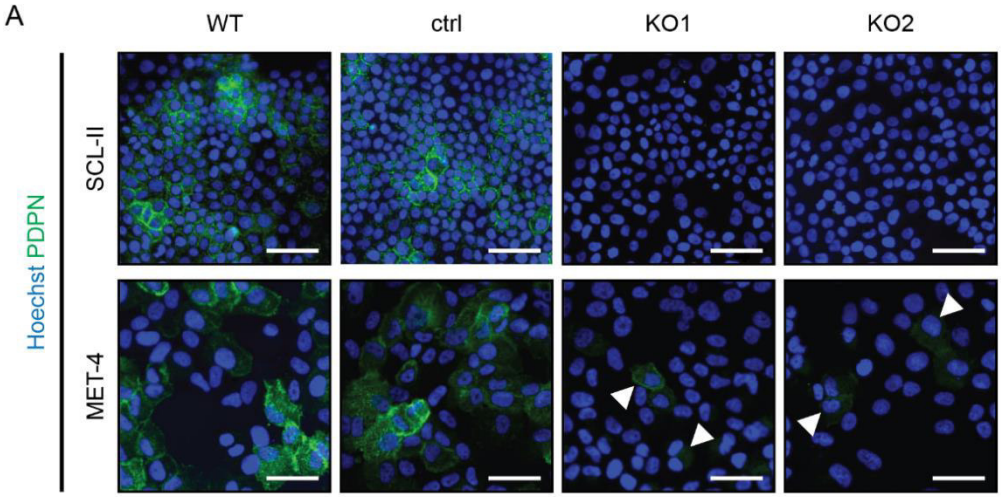

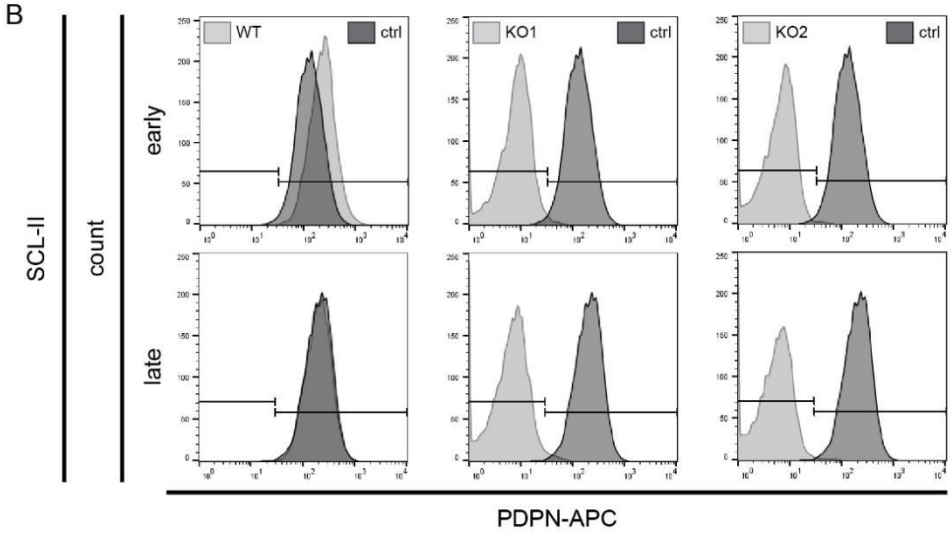

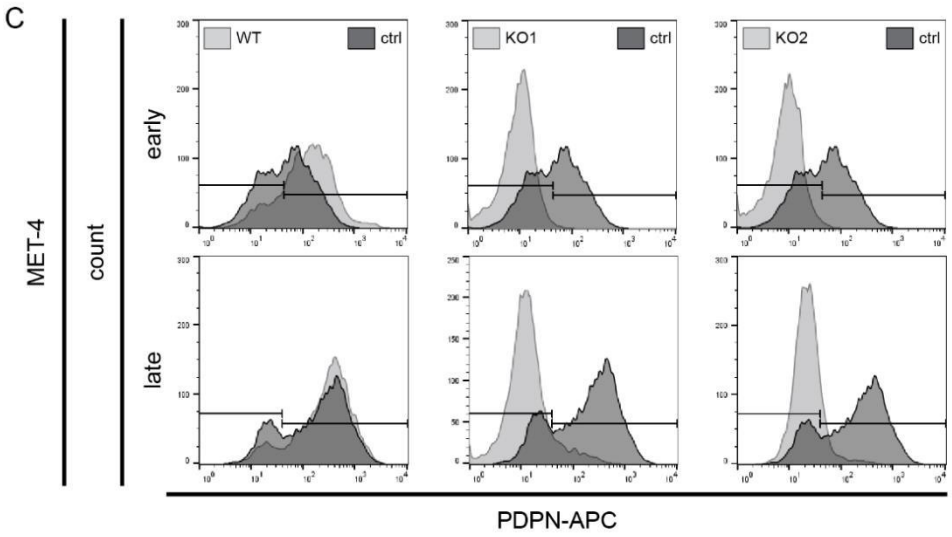

D

SCL-II	PDPN-neg [%]		PDPN-pos [%]	
	early	late	early	late
WT	0.2	0.5	99.8	99.5
ctrl	99.2	99.5	0.8	0.5
KO1	98.7	97.8	1.3	2.2
KO2	99.2	98.9	0.8	1.1

MET-4	PDPN-neg [%]		PDPN-pos [%]	
	early	late	early	late
WT	21.1	12.1	78.9	87.9
ctrl	45.9	22.5	54.1	77.5
KO1	99.0	88.8	1.0	11.2
KO2	98.9	86.2	1.1	13.8

Figure 11 PDPN protein evaluation in human cSCC cell lines.
A) IF assessment of PDPN in SCL-II and MET-4 cells. FACS analysis of B) SCL-II and C) MET-4 cells. SCL-II WT and control (ctrl) cells showed moderate PDPN expression, no IF staining was detected in KO1 and KO2 sublines. PDPN-positive cells in KO cultures remained below 3 %. MET-4 WT and ctrl cells expressed varying PDPN levels and only single cells in KO1 and KO2 showed low PDPN expression (arrowheads) in early passage with was increasing over time. D) Overview of percentage portion in early and late culture passages. Nuclei were stained with Hoechst. Scale bar 50 µm, image quality was optimized by adjustment of brightness, contrast and gamma.

Moreover, I further examined whether the cellular morphology in monolayer-cultured cells was changed upon *PDPN* deletion as it was already demonstrated that the loss of this protein can result in a change from the epithelial morphology to a more mesenchymal-like phenotype (reviewed in Lamouille 2014). Bright-field microscopy depicted that all established cells showed similar morphology (Figure 12). Neither the lack of *PDPN* nor the constitutive Cas9 expression in control cells resulted in different cellular morphology.

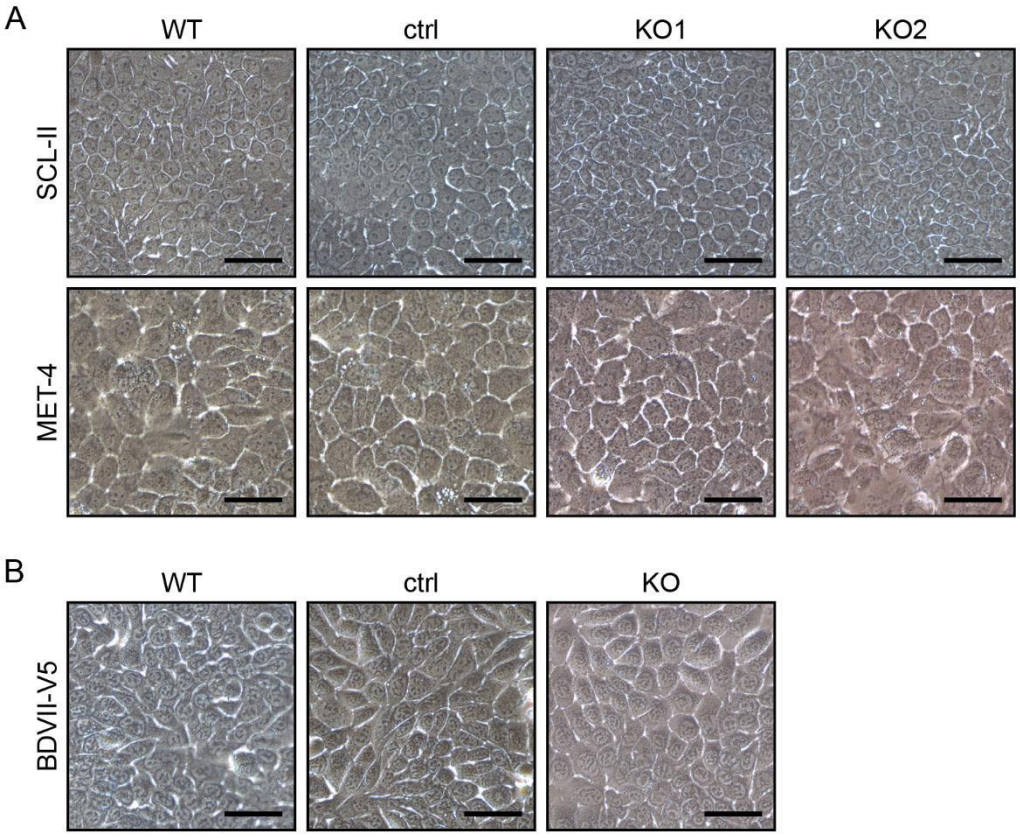

Figure 12 Morphological analysis of generated *PDPN* KO and control sublines.
A) Human and B) murine cSCC cells showed similar cobblestone-like morphology despite constitutive Cas9 expression and deletion of *PDPN*. Scale bar 50 µm, image quality was optimized by adjustment of brightness, contrast and gamma.

Taken together, applying the CRISPR/Cas9 technology human as well as murine *PDPN* KO and Cas9 control sublines were successfully established. Generated *PDPN*-proficient and -deficient SCL-II, MET-4 and BDVII cells are suitable for different functional *in vitro* experiments to examine differences in proliferation, migration and invasion. Moreover, the effect of PDPN on these tumor characteristics will be tested in an orthotopic mouse model applying murine BDVII cells.

3.2.3 Functional Investigation of Podoplanin Loss in Cutaneous Squamous Cell Carcinoma Cell Lines *in Vitro*

The impact of PDPN on cSCC proliferation was not defined yet. Performing different *in vitro* experiments, no difference in proliferation was described upon *Pdpn* loss in primary murine keratinocytes, whereas the downregulation of *PDPN* in human oral SCC (OSCC) cells was associated with reduced proliferation (Baars et al. 2015, Tsuneki et al. 2013). Additionally, migration and invasion were proposed as crucial tumor characteristics related to PDPN expression (Martin-Villar et al. 2006, Wicki et al. 2006). Hence, these three aspects were examined by employing generated human and murine cSCC cell lines.

3.2.3.1 Loss of Podoplanin neither Influences Cell Proliferation nor Viability in 2D Culture System[1]

Cell proliferation was determined by manual cell counting using the Neubauer Chamber combining with trypan blue staining to exclude dead cells. Cell viability was examined by employing the XTT assay in which cellular metabolic activity is detected by absorbance measurement. Proliferation and viability of human and murine cSCC cell lines were observed on three consecutive days. Manual counting as well as measurement of absorbance revealed that the cell number and metabolic activity in all cell lines was increasing over time (Figure 13 A and B; Schneider, 2019). In SCL-II and BDVII-V5 cells *PDPN* KO resulted in similar cell numbers and absorbance signal compared to control cells. Similar results were obtained for MET-4 cells (data not shown). Moreover, similar cell numbers were already observed after 24 h indicating indirectly that there was no effect on adhesion upon *PDPN* abrogation, since not attached cells would have been washed off the cell culture plate during the preparation for cell counting.

[1] These experiments were performed by Jakob Schneider as part of his Bachelor thesis supervised by myself.

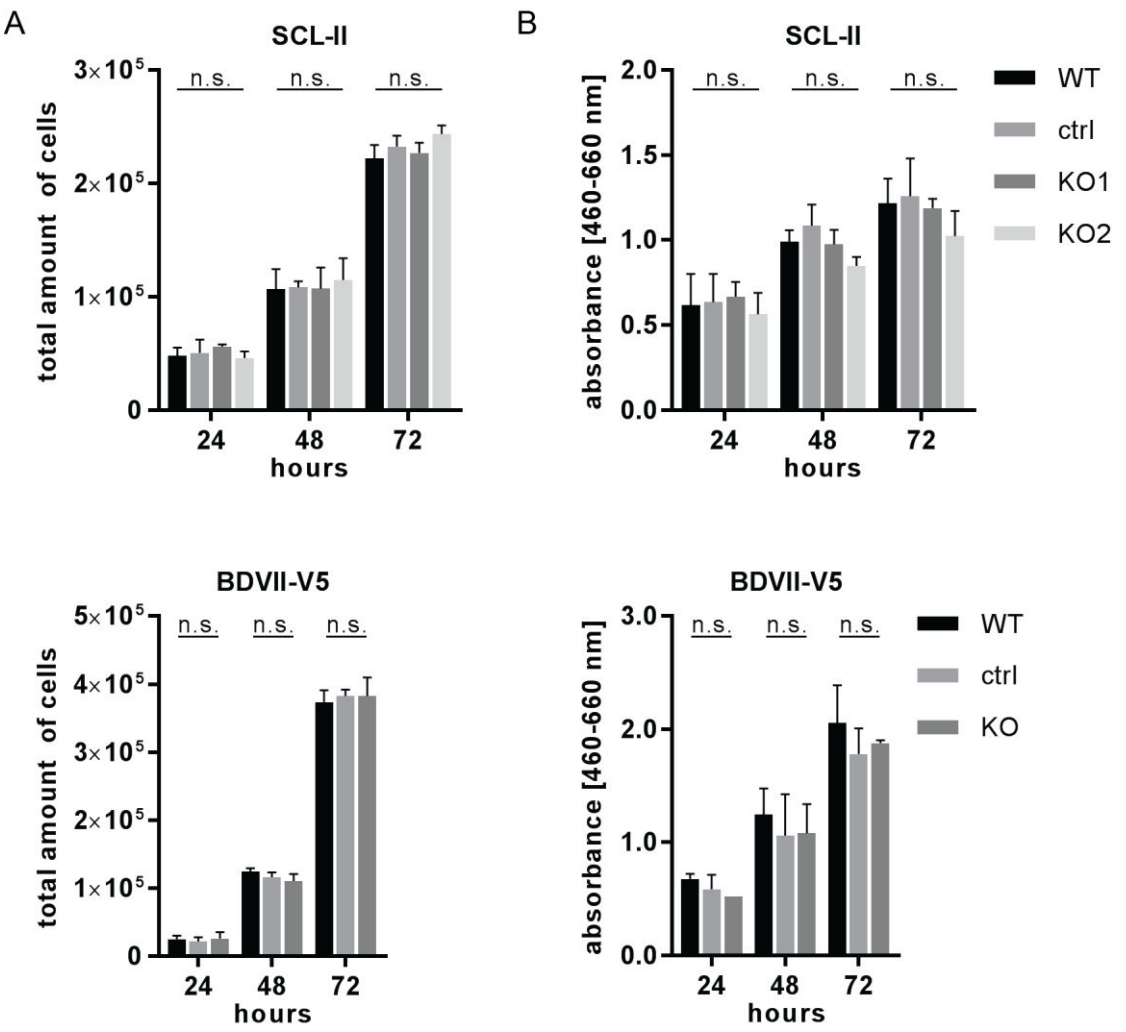

Figure 13 *PDPN* deletion neither affected proliferation nor viability in human and murine cSCC cells.
A) Proliferation was examined by manual counting using the Neubauer chamber and trypan blue to identify dead cells. B) XTT assay was performed to determine cell viability. Both tests were done 24, 48 and 72 h after cell seeding. Cell amount and viability were increasing over time in human and murine cSCC cells. No difference was obtained comparing KO with control (ctrl). Values are plotted as mean and SD of n=3 independent experiments with technical triplicates. Unpaired two-tailed Welch's t test was performed with a 95 % confidence level. N.s. not significant.

3.2.3.2 Impact of Podoplanin on Cellular Transmigration

In order to examine the possible rate limiting function of PDPN on the migratory potential of cSCC cells, the Boyden Chamber Matrigel (BCM) assay was performed using generated human and murine *PDPN* KO and Cas9 control cells. Tumor cells were seeded on top of matrigel-coated filters and cell line-specific incubation time allowed

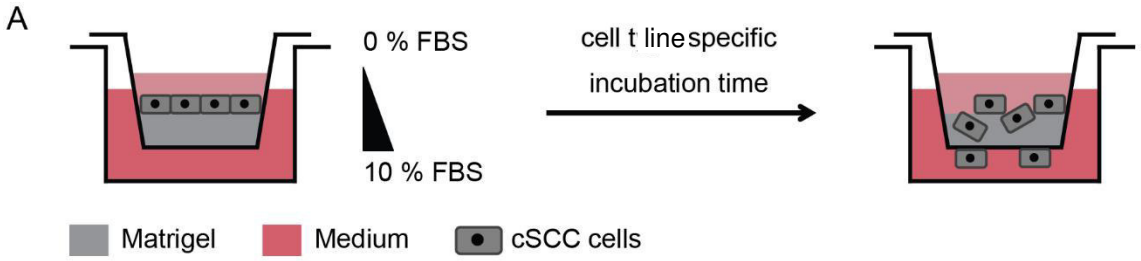
A
0 % FBS
10 % FBS
cell t linespecific
incubation time
Matrigel
Medium
cSCC cells

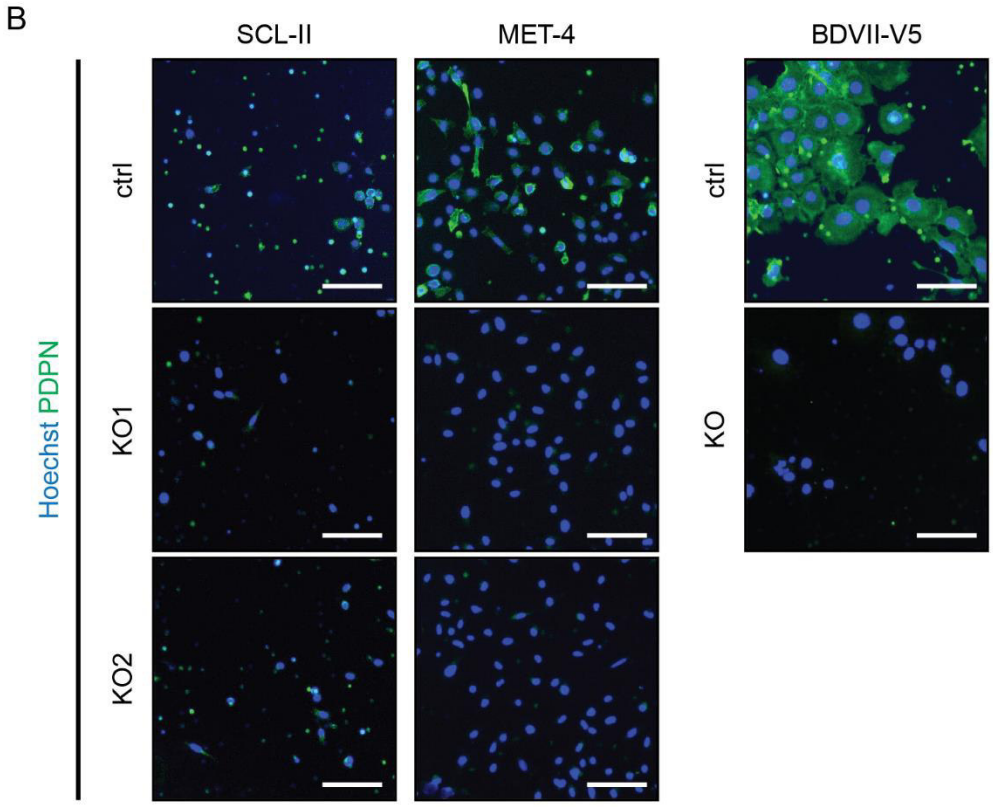
B
SCL-II
MET-4
BDVII-V5
ctrl
KO1
KO2
KO
Hoechst PDPN

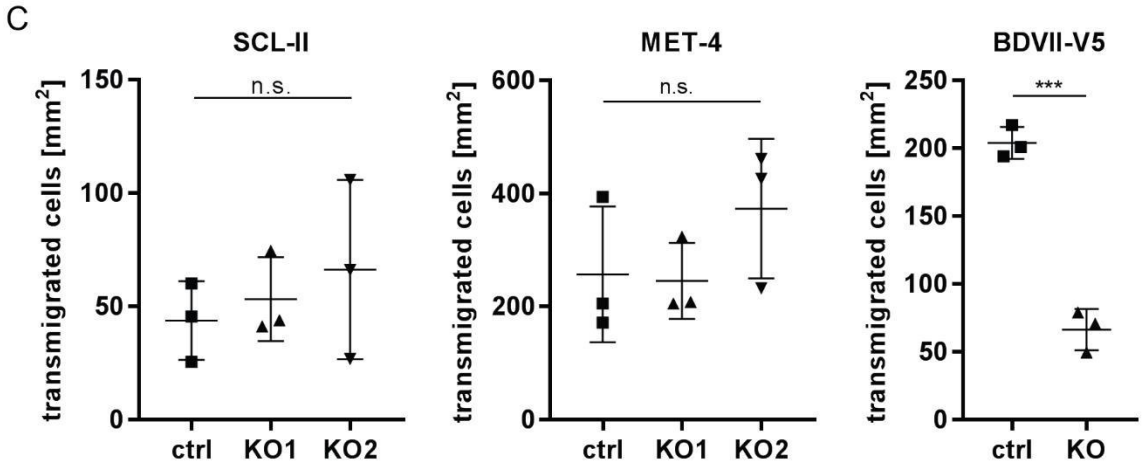
C
SCL-II
MET-4
BDVII-V5
transmigrated cells [mm²]
n.s.
n.s.
***
ctrl
KO1
KO2
KO

Figure 14 Examination of the transmigratory capacity upon the loss of *PDPN* in cSCC cell lines.
A) In the BCM assay matrigel was used as an artificial BM through which tumor cells needed to transmigrate according to a serum gradient (FBS). Transmigrated cells were stained for PDPN and Hoechst. Hoechst staining was utilized for automatic counting of transmigrated cells. B) Transmigrated control (ctrl) cells expressed PDPN. No PDPN signal was detected in transmigrated KO cells. C) *PDPN* loss in human SCL-II and MET-4 cells did not affect transmigration. Contrary, the deletion of *Pdpn* in murine BDVII cells resulted in a significant reduction. Values are plotted as mean and SD of n=3 independent experiments with technical triplicates. 5 fields per technical replicate were analyzed. Unpaired two-tailed Welch's t test was performed with a 95 % confidence level. N.s. not significant, *** $p < 0.001$. Scale bar 100 µm, image quality was optimized by adjustment of brightness, contrast and gamma.

cells to transmigrate through the Matrigel layer according to a serum gradient (Figure 14 A). Transmigrated cells were stained for PDPN protein expression to verify its absence in KO sublines. Nuclei of transmigrated cells were stained with Hoechst and counted automatically utilizing a macro in ImageJ.

In agreement of initial characterization (Figure 10 and 11), no PDPN expression was detected in either transmigrated KO sublines, whereas control cells express PDPN (Figure 14 B). The transmigration of SCL-II cells was inefficient as only 50 cells per square millimeter migrated through the matrigel. In contrast, MET-4 cells showed a stronger transmigratory ability with more than 200 cells per square millimeter. The deletion of *PDPN* in human cSCC cell lines showed similar transmigratory capacity as control cells (Figure 14 C).

In comparison, the murine BDVII control-V5 cells showed similar transmigration potential as MET-4 cells. In murine cells, the loss of *Pdpn* resulted in a significant reduction of transmigration (200 to 50 cells/mm^2; Figure 14 C).

Since the deletion of *PDPN* showed different transmigratory effects in human compared to murine cSCC cells, the invasive capacity of all selected cancer cells was tested in the more complex fibroblast-derived matrix (fdm)-based SCM. Furthermore, this organotypic culture system reflects better physiological aspects.

3.2.3.3 Tumor Cell Invasion upon Podoplanin Deletion Using the Organotypic Co-Culture System

To study PDPN-dependent tumor cell invasiveness more profoundly and to complement already obtained results, the 3D organotypic SCM was used (Figure 4; Berning et al. (2015)). Control and *PDPN* KO cells derived from SCL-II, MET-4 and BDVII cell lines were seeded on top of the dermal equivalent generated by multiple seeding steps of hDFs. Cultures were cultivated up to four weeks and morphology was examined at different time points using histological and IF staining.

In the organotypic model system, both human cell lines formed a multilayered epithelial compartment with no sign of differentiation reflecting the histology of original tumor samples (Figures 15 and 16; Tilgen et al. (1983), Popp et al. (2000), Proby et al. (2000), Berning et al. (2015)). IF assessment of SCL-II control cells showed only moderate PDPN expression in all tumor cells (Figure 15). Only focal PDPN expression was detected in MET-4 control cells (Figure 16). These results confirmed 2D culture properties of PDPN expression. Moreover, PDPN was expressed by either control cell lines independent of invasive behavior. No PDPN signal was detected in KO cells. Some single PDPN-positive tumor cells were observed in MET-4 KO1, even though early passaged cells were applied. Visual analysis of 3D culture sections showed that SCL-II and MET-4 tumor cells grew invasively into the dermal equivalent independent of PDPN expression confirming BCM data (Figure 14). This invasive growth was increasing over time. In SCL-II cultures small cell groups were detected indicating collective tumor cell invasion. MET-4 cells invaded as single cells.

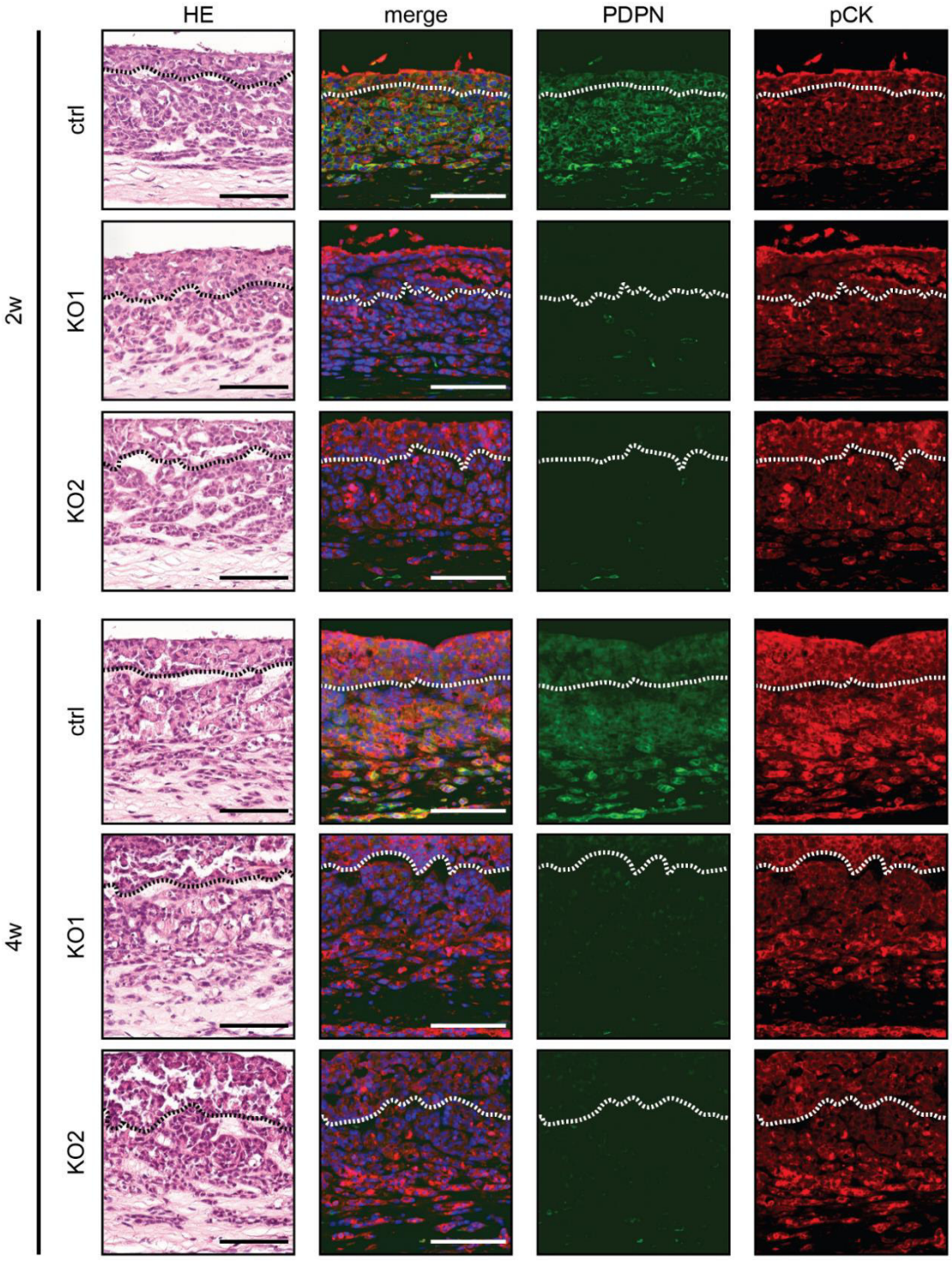

Figure 15 No effect of *PDPN* loss in human SCL-II cells cultured in the SCM.
Histological and IF stainings showed multilayered epithelium with no sign of differentiation. Invasive SCL-II tumor cell growth into the dermal equivalent increasing over time was observed which was independent of PDPN expression. Control (ctrl) cells expressed moderate PDPN and no PDPN expression was detected in KO1 or KO2. Pan Cytokeratin (pCK) was used as epithelial cell marker. Nuclei were stained with Hoechst for nuclear counterstain. Dashed line represents BM. N=1 with 1-3 technical replicates. Representative images are displayed. Scale bar 100 µm, image quality was optimized by adjustment of brightness, contrast and gamma. HE hematoxylin and eosin, w weeks.

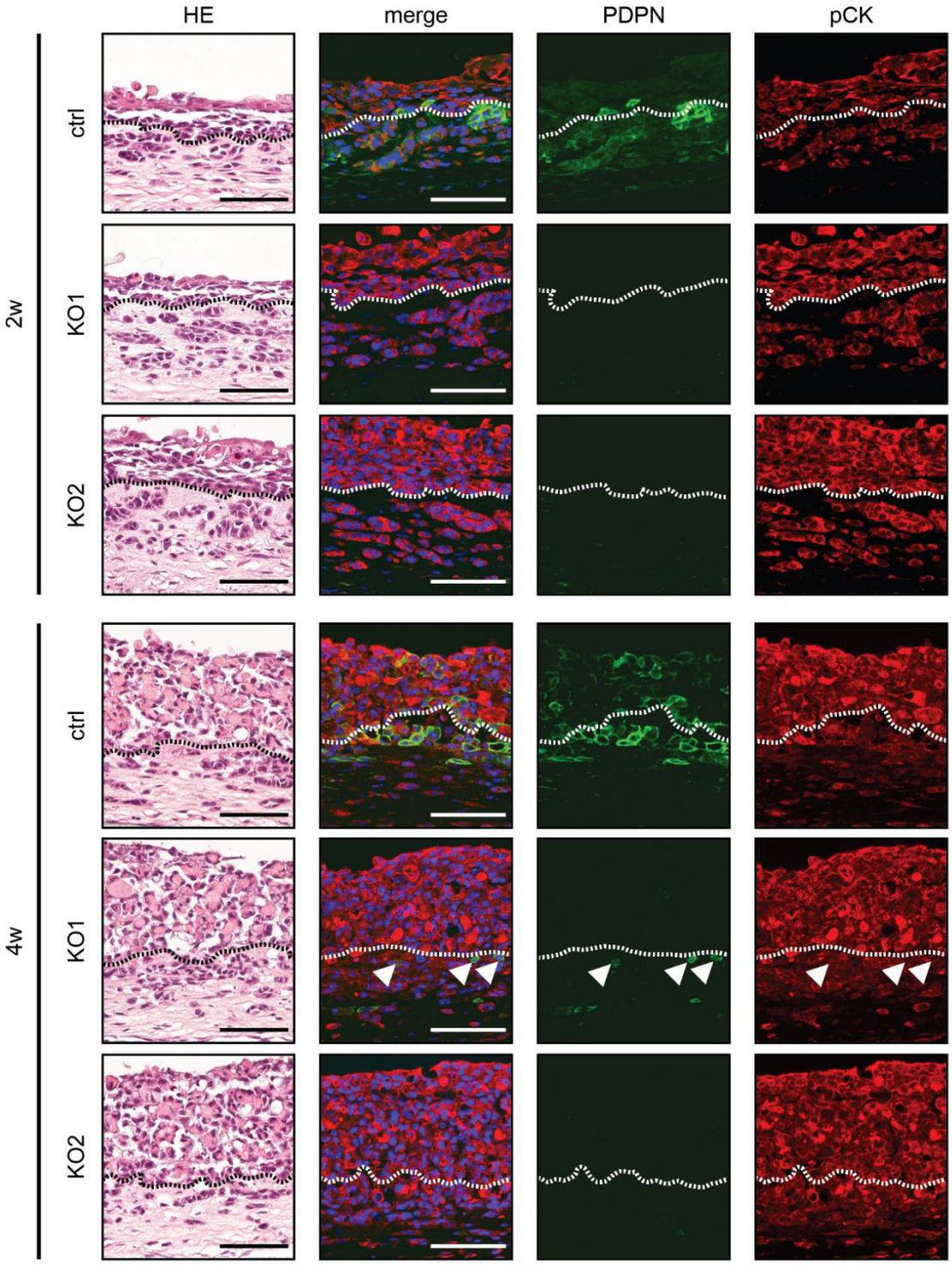

Figure 16 *PDPN* deletion did not interfere human MET-4 cell invasion in 3D context.
MET-4 control (ctrl), KO1 and KO2 tumor cells formed a multilayered epithelium without cornification and invaded into the dermal compartment assessed by HE and IF. Invasion was increasing over time in a PDPN-independent manner. Ctrl cells expressed varying PDPN levels and no PDPN expression was observed in KO2. Single KO1 cells showed a PDPN-positive reaction (arrowheads) Epithelial cells were stained with pan Cytokeratin (pCK). Hoechst was used for nuclear counterstain. Dashed line represents BM. N=1 with 1-3 technical replicates. Representative images are displayed. Scale bar 100 µm, image quality was optimized by adjustment of brightness, contrast and gamma. HE hematoxylin and eosin, w weeks.

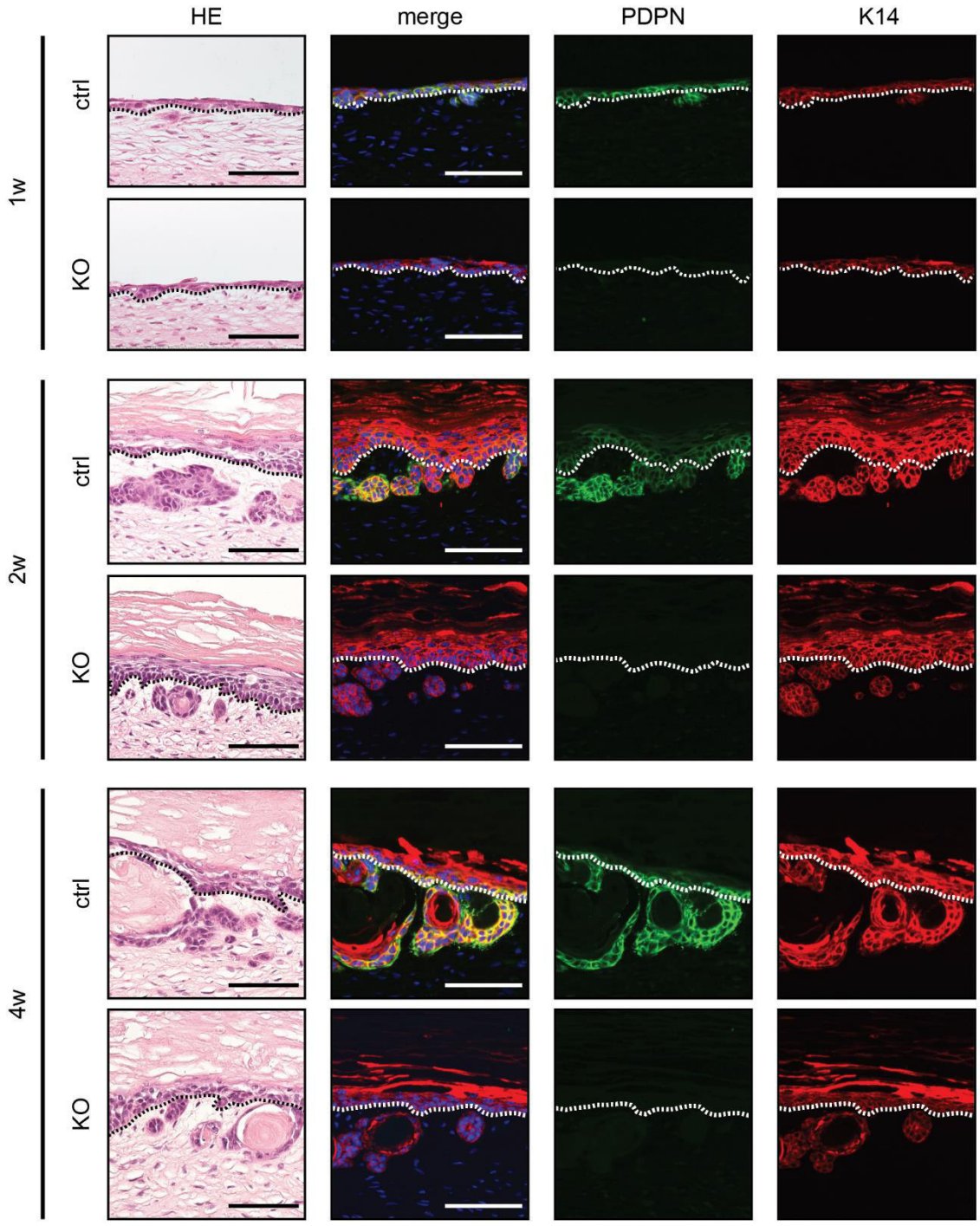

Figure 17 *Pdpn* loss in murine BDVII-V5 cells diminished tumor cell invasion in the 3D model.

Histological and IF assessment revealed formation of multilayered epithelium with terminal differentiation independent of PDPN expression. Tumor cells grew invasively into dermal compartment increasing over time and formed horn pearls. KO cells invaded less. Proliferative active control (ctrl) cells expressed high PDPN, whereas no PDPN was observed in differentiated cells. KO cells did not express PDPN. K14 was used as epithelial cell marker. Hoechst was used for nuclear counterstain. Dashed line represents BM. N=3 with technical triplicates. Representative images are displayed. Scale bar 100 µm, image quality was optimized by adjustment of brightness, contrast and gamma. HE hematoxylin and eosin, w weeks.

Cultured murine BDVII-V5 cells revealed that these cells formed a fully differentiated multilayered epithelium over time independent of PDPN expression (Figure 17). These characteristics resembled the histology of original tumors (Fusenig et al. 1978). Tumor cells invaded collectively as tumor buds were observed in the dermal compartment. Larger areas of invaded cells showed cornified regions. Strong PDPN expression was observed in non-differentiated V5-labeled control tumor cells, whereas *Pdpn* KO-V5 cells showed no PDPN-positive staining. Notably, the visual examination of tissue sections revealed that *Pdpn* loss in BDVII-V5 cells resulted in reduced invasion confirming the findings of the BCM experiment (Figure 14). The time point of two weeks indicated already this difference between KO and control cultures, which became more obvious after four weeks of culture.

In conclusion, the lack of *PDPN* did neither influence proliferation nor viability of cSCC tumor cells. However, the transmigratory and invasive capabilities of human and murine cSCC cells studied in the BCM assay and the SCM differed upon *PDPN* abrogation. The loss of *Pdpn* in the BDVII-V5 cells resulted in decreased transmigration and invasion in *in vitro* assays. Thus, to further characterize PDPN-dependent migratory behavior in functional experiments, the differences between *Pdpn* KO and control cells originated from the murine BDVII cell line became the focus of the following investigation.

3.2.3.4 Quantitative Analysis of Podoplanin-Dependent Invasion of BDVII Cells in the 3D Model

I showed that the invasive behavior of cSCC cancer cells depended on PDPN expression. Consequently, the extent of tumor cell invasion was quantified and several immunostainings were performed to characterize tumor properties in the organotypic system.

3.2.3.4.1 Decreased Invasion in Tumor Cells Lacking Podoplanin

To verify the visual impression of reduced invasion of *Pdpn* KO compared to control BDVII-V5 cells in the SCM (Figure 17), a quantitative analysis based on HE staining was performed. Therefore, bright-field images were used to execute semi-automated quantification using ImageJ. In this macro, the basement membrane (BM) was drawn manually. Tumor cells located below this set line and within the dermal equivalent were defined as invaded cancer cells. Tissue above the BM was excluded from the analysis.

Based on eosin staining of histological analysis (Figure 17), invaded tumor cells depicted a higher contrast compared to extracellular matrix (ECM) and hDFs. This property was used to quantify tumor cell invasion as area of tumor cells and distance which were covered by them.

Statistical analysis revealed that the deletion of *Pdpn* in BDVII-V5 cells resulted in significant decreased invasive area compared to control-V5 cells at any assessed time point (Figure 18 A). Moreover, the distance of invaded V5-marked KO cells was diminished in average and KO cells invaded less deep into the dermal compartment compared to control-V5 cells (Figure 18 B and C).

Taken together, the findings of the simplified transmigration assay (Figure 14) as well as of the more sophisticated 3D organotypic SCM (Figure 17) highlighted a driving role of PDPN in cSCC invasion.

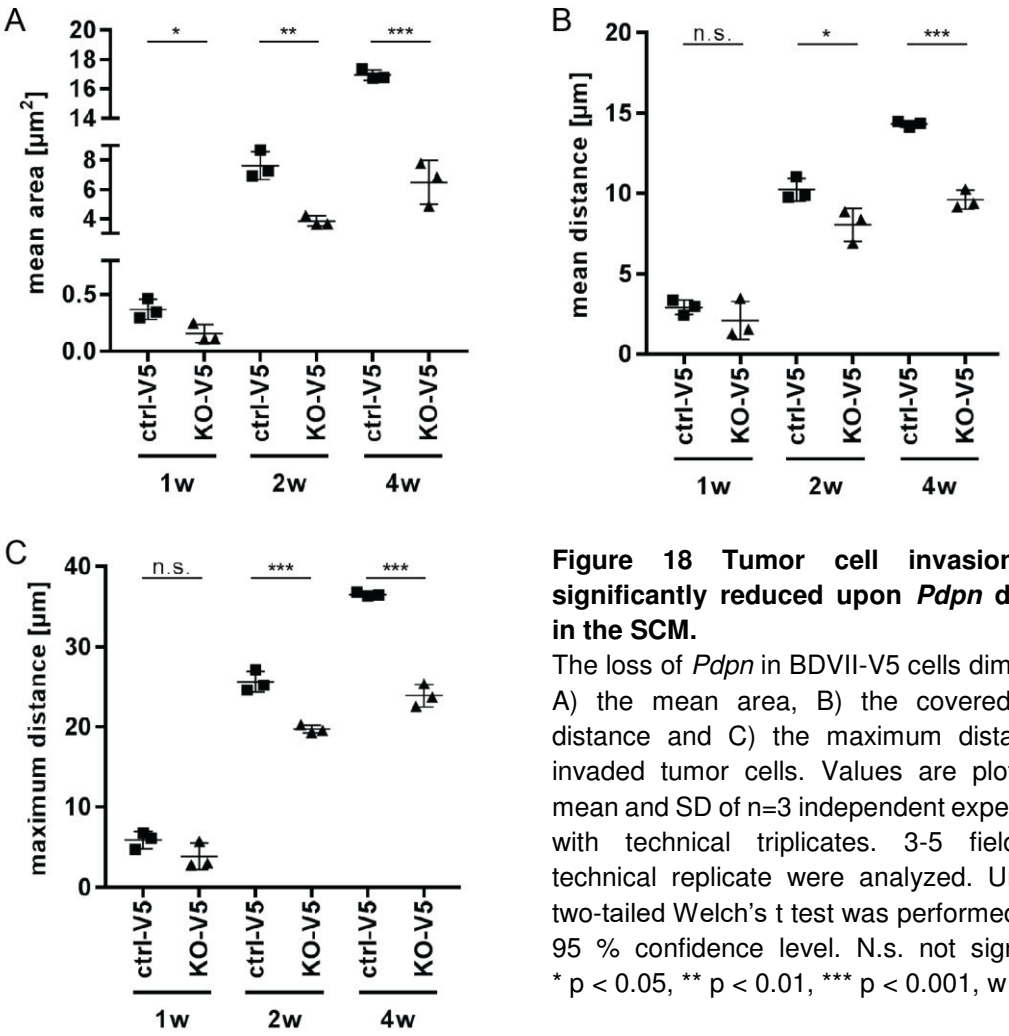

Figure 18 Tumor cell invasion was significantly reduced upon *Pdpn* deletion in the SCM.

The loss of *Pdpn* in BDVII-V5 cells diminished A) the mean area, B) the covered mean distance and C) the maximum distance of invaded tumor cells. Values are plotted as mean and SD of n=3 independent experiments with technical triplicates. 3-5 fields per technical replicate were analyzed. Unpaired two-tailed Welch's t test was performed with a 95 % confidence level. N.s. not significant, * $p < 0.05$, ** $p < 0.01$, *** $p < 0.001$, w week

3.2.3.4.2 Loss of Podoplanin Does Not Affect Tumor Cell Proliferation[2]

Besides collective tumor cell invasion, increased proliferation is changing multicellular positioning (Friedl et al. 2012). Tumor cells which are located at the periphery are pushed into the stroma due to expansive growth (Friedl et al. 2012). In order to determine whether increased proliferation of PDPN-expressing cells accounted for the increased invasive phenotype, Ki67 as proliferative marker was assessed.

Based on visual analysis no difference in the amount of Ki67-positive tumor cells was observed between *Pdpn*-proficient and -deficient BDVII-V5 cells at any time point (Figure 19, Schneider 2019).

These data confirmed proliferation and viability results of performed 2D culture experiments (Figure 13).

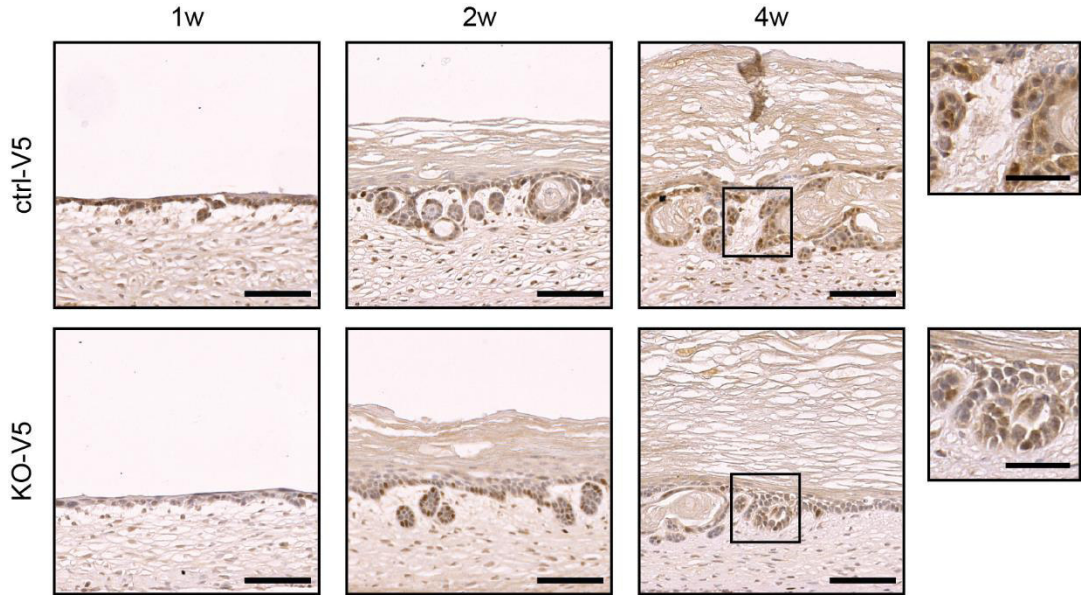

Figure 19 Lack of *Pdpn* did not affect BDVII-V5 tumor cell proliferation in the 3D organotypic culture.
Ki67 IHC was performed to evaluate proportion of proliferating BDVII-V5 tumor cells cultured in the SCM. Amount of Ki67-positive tumor cells was visually estimated. No difference between *Pdpn* KO- and control (ctrl)-V5 cultures were observed at any time point. N=3 with technical triplicates. Representative bright-field images are depicted. Scale bar 100 µm; zoom 50 µm, image quality was optimized by adjustment of brightness, contrast and gamma. W week.

[2] This experiment was performed by Jakob Schneider as part of his Bachelor thesis supervised by myself.

3.2.3.4.3 Tumor Cell Invasion Was Epithelial-Mesenchymal Transition-Independent in 3D Context

In collective tumor cell invasion epithelial-mesenchymal transition (EMT) was reported to be either absent or partial (reviewed in Friedl et al. (2012)). In EMT-independent invasion, tumor cells maintain their epithelial marker expression (e.g. keratins or E-cadherin), whereas tumor cells undergoing partial EMT gain mesenchymal marker expression such as N-cadherin or vimentin additionally to epithelial features. Descriptive analysis of cSCC patients' material showed that PDPN-positive cancer cells invaded collectively without undergoing EMT (Hesse et al. 2016). However, whether differentiated cSCC can also represent a partial phenotype has not been shown yet. Hence, I explored E-cadherin as well as vimentin expression levels in invading BDVII-V5 tumor cells cultured in the SCM.
IF staining demonstrated that all undifferentiated tumor cells expressed E-cadherin independent of PDPN expression or invasive behavior at any analyzed time point (Figure 20). Vimentin was detected in hDFs in the dermal compartment, but not in any tumor cell.
These results underscored that PDPN-driven cSCC invasion in the utilized 3D organotypic SCM emerged in the absence of EMT.

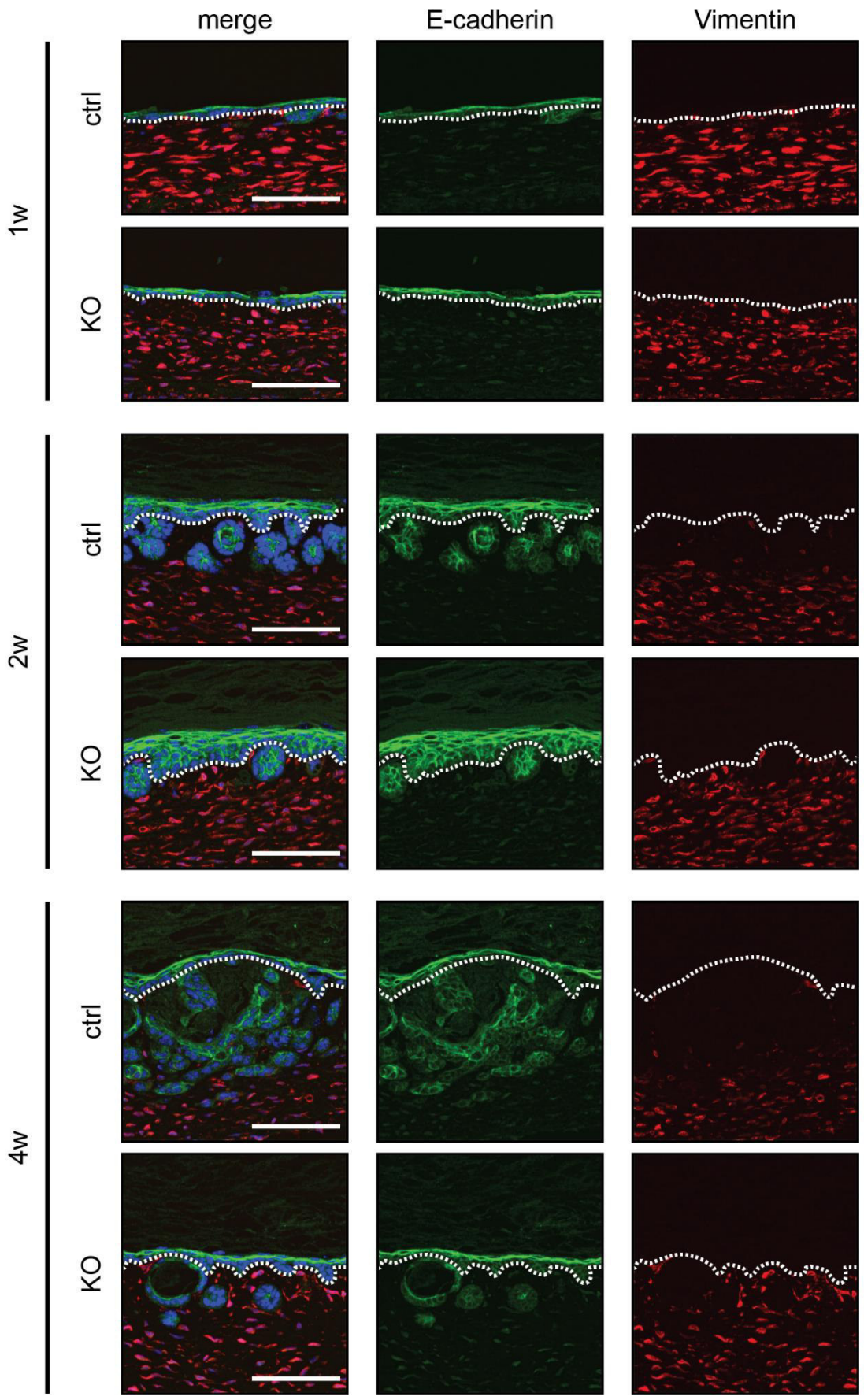
merge
E-cadherin
Vimentin
1w
2w
4w
ctrl
KO
ctrl
KO
ctrl
KO

Figure 20 EMT-independent invasion upon *Pdpn* deletion in murine cSCC cells in 3D context.
IF staining revealed that E-cadherin, but no vimentin, was expressed by PDPN-positive and -negative tumor cells. High levels of vimentin were observed in hDF. Hoechst was used for nuclear counterstain. Dashed line represents BM. N=3 with technical triplicates. Representative images are displayed. Scale bar 100 µm, image quality was optimized by adjustment of brightness, contrast and gamma. W weeks.

3.2.3.5 Podoplanin Loss Does Not Impair Downstream Signaling

Tumor cell invasion in PDPN-overexpressing cells was shown to be mediated by ERM proteins (Scholl et al. 1999, Martin-Villar et al. 2006, Wicki et al. 2006). The activation of these proteins result in cytoskeleton rearrangements and hence, in increased migration and invasion (Martin-Villar et al. 2006, Wicki et al. 2006). Consequently, the recruitment of ezrin, which is mainly expressed in epithelial cells, was examined since I showed that the loss of *Pdpn* in murine cSCC cells diminished tumor cell invasion (reviewed in Fehon et al. (2010)). To assess the subcellular localization of ezrin, the filament K5 was additionally visualized.

Confocal microscopy of 2D-cultured *Pdpn*-proficient and -deficient BDVII-V5 cells revealed that K5 filaments were expressed throughout the cell defining, amongst others, cell shape (Figure 21 A). Ezrin expression was enhanced close to the plasma membrane. However, no differential recruitment of ezrin to the plasma membrane was observed in *Pdpn* KO- and control-V5 cells.

Nevertheless, I wondered whether the cytoskeleton was differential modulated ezrin-independently in PDPN-positive tumor cells leading to enhanced invasion. The myosin light chain 2 (MLC2) is responsible for actin contraction among other effectors (Wyckoff et al. 2006). For activation, MLC2 gets phosphorylated (P-MLC2) by MLC kinase and dephosphorylated by myosin phosphatase (MP) leading to inactivation (Totsukawa et al. 2004). MP is inactivated by ROCK and thus, P-MLC2 remains active resulting in enhanced cell migration (Fukata et al. 2001). To test whether the cytoskeleton was rearranged in cSCC tumor cells in a PDPN-dependent manner, P-MLC2 expression was examined in BDVII-V5 tumor cells cultured in monolayer culture. E-cadherin expressed was detected to visualize the plasma membrane.

P-MLC2 was detected as dotted signal in tumor cells (Figure 21 B). Visual assessment indicated similar P-MLC2 expression in *Pdpn* KO compared to control cells.

These findings demonstrated that the PDPN downstream activation of ezrin and consequent cytoskeleton rearrangements were not differentially regulated in 2D-cultured *Pdpn* KO cells.

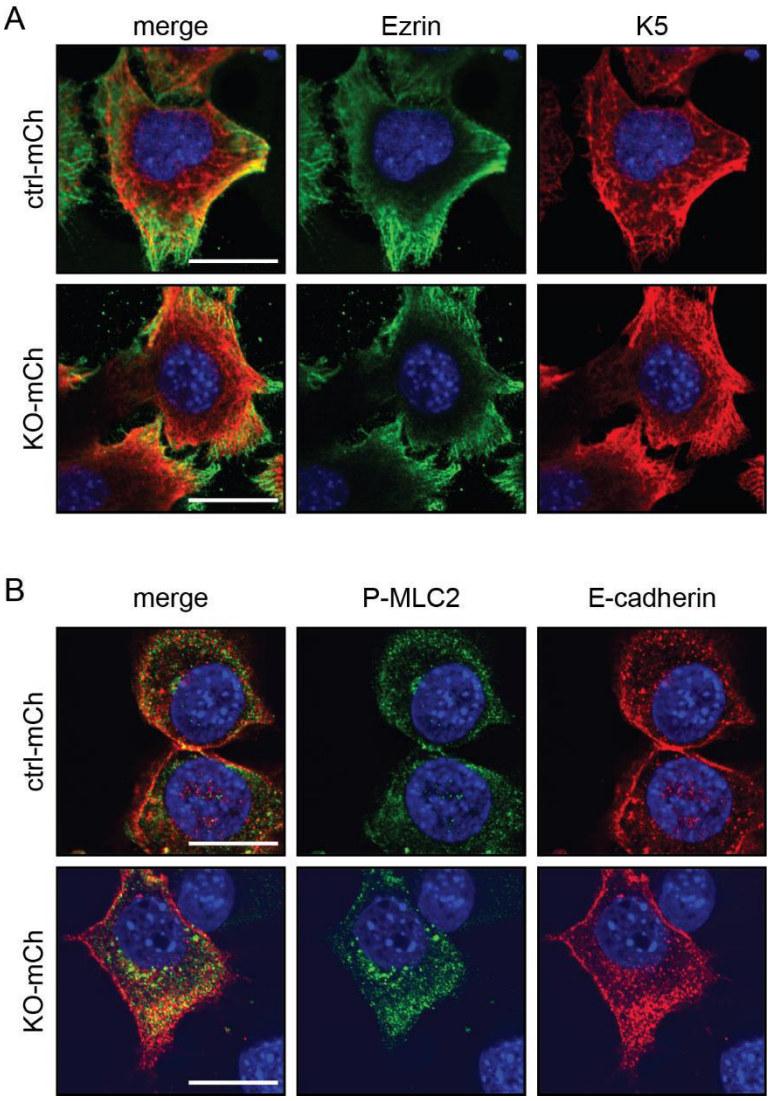

Figure 21 Neither ezrin recruitment nor cytoskeleton modulation were affected by *Pdpn* deletion.
A) IF assessment of ezrin in monolayer cultured control (ctrl)- and KO-V5 cells revealed no differential recruitment of ezrin to the plasma membrane. K5 was used as marker for the cytoskeleton. B) Similar P-MLC2 was detected in control-V5 and KO-V5 cancer cells. E-cadherin stained the plasma membrane. N=1 with 10 images per condition. Nuclei were stained with Hoechst. Representative images are displayed. Scale bar 20 µm, image quality was optimized by adjustment of brightness, contrast and gamma.

3.2.4 Generation of Cas9-Deficient mCherry-Labeled Control and Podoplanin-Compromised BDVII Cells

The abrogation of *Pdpn* in the murine BDVII-V5 cells displayed a significant reduction in transmigration and invasion *in vitro*. The BDVII-V5 cells express constantly the Cas9 protein as they were generated using lentiviral transduction (Figure 9 B). Hence, re-introducing PDPN WT or mutant constructs (e.g. CLEC-2- or ERM-binding mutants) to study the underlying molecular mechanisms would result in the deletion of the re-introduced *Pdpn* by the constant expression of the Cas9-gRNA-complex. Thus, the *Pdpn* construct for re-expressing PDPN needs to be modified in order to prevent Cas9-mediated cutting. The gRNA and the protospacer adjacent motif (PAM) are mediating Cas9 binding (Pyzocha et al. 2014, Sternberg et al. 2014). Since the used gRNA is targeting the coding region in exon 1 of *Pdpn*, any amino acid exchange in this region of the *Pdpn* sequence needs to be omitted. The PAM sequence is located directly upstream of the gRNA binding site. Unfortunately, this sequence is a Tryptophan which has a unique codon. Thus, no silent mutation can be introduced in the *Pdpn* sequence and whether the special indole ring of Tryptophan is involved in gene expression was not reported. However, in order to maintain PDPN functionality and to perform mechanistical studies in the future by re-introducing a WT or mutant form of PDPN, new *Pdpn* KO and control cells lacking continuous Cas9 expression were required. This strategic approach was not pursued initially as the transfection of the BDVII cell line was rather inefficient. In order to use these newly generated cells, the same validation approach as well as transmigration experiment were performed.

3.2.4.1 Generation and Validation of mCherry-Labeled Podoplanin Knockout and Control BDVII Cells

To generate mCherry-labeled *Pdpn* KO and Cas9 control cells, in the first of multiple steps (Figure 22), BDVII WT cells were lentivirally transduced with a construct encoding the mCherry marker. Subsequent bulk FACSort guaranteed the generation of a pure mCherry-expressing cell population (WT-mCh). In order to generate transient Cas9-expressing *Pdpn* KO and control cells, the same constructs as employed for the generation of V5-labeled BDVII cells were transfected into BDVII WT-mCh cells followed by a bulk FACSort (section 3.2.2.1).

Finally, generated BDVII WT-, control- and *Pdpn* KO-mCh cells were validated on protein level to verify PDPN and mCherry marker expression.

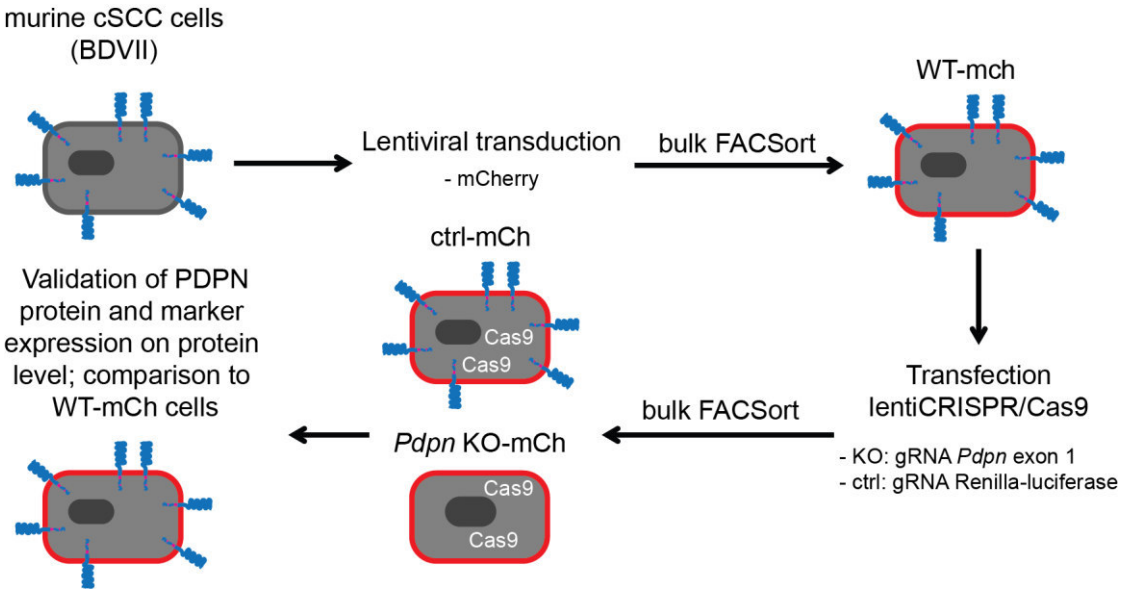

Figure 22 Establishment of transiently transfected mCherry-labeled WT, control and *Pdpn* KO BDVII cells.
The mCherry construct was lentivirally transduced into BDVII WT cells with subsequent bulk FACSort. WT-mCh cells were transfected with lentiCRISPR/Cas9 constructs generating Cas9 control (ctrl)- and *Pdpn* KO-mCh cells. PDPN and marker expression were validated on protein level.

IF analysis confirmed that WT- and control-mCh cells expressed PDPN while no PDPN staining was observed in *Pdpn* KO-mCh culture (Figure 23 A). FACS analysis confirmed PDPN expression in WT- and control-mCh cells from low to high cell passages (Figure 23 B and C). Less than 2 % of PDPN-positive cells were detected in the established KO-mCh culture. That proportion was retained over time until cells reached high passage number. FACS analysis of the cells showed additionally that all three sublines expressed the introduced mCherry marker. Western blot analysis demonstrated similar PDPN levels for WT- and control-mCh cells (Figure 23 D). No PDPN was detected in the KO-mCh subline. Importantly, no Cas9 protein expression was detected in control- and KO-mCh cells compared to initial lentivirally transduced Cas9- and KO-V5 cells, which expressed Cas9. Furthermore, cell morphology was analyzed visually. Bright-field microscopy of cultured cells displayed similar cobble-stone-like structure between WT-, control- and *Pdpn* KO-mCh monolayer cultures (Figure 23 E).

A

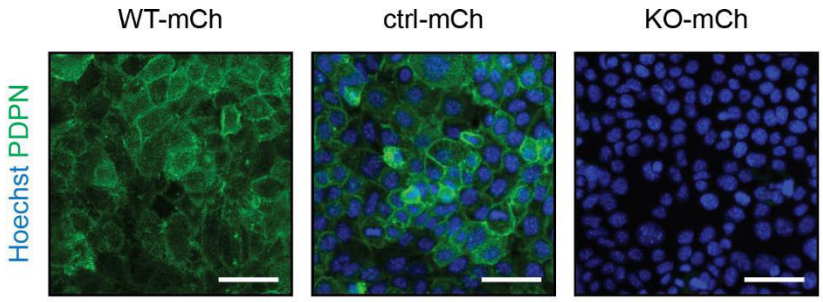

B

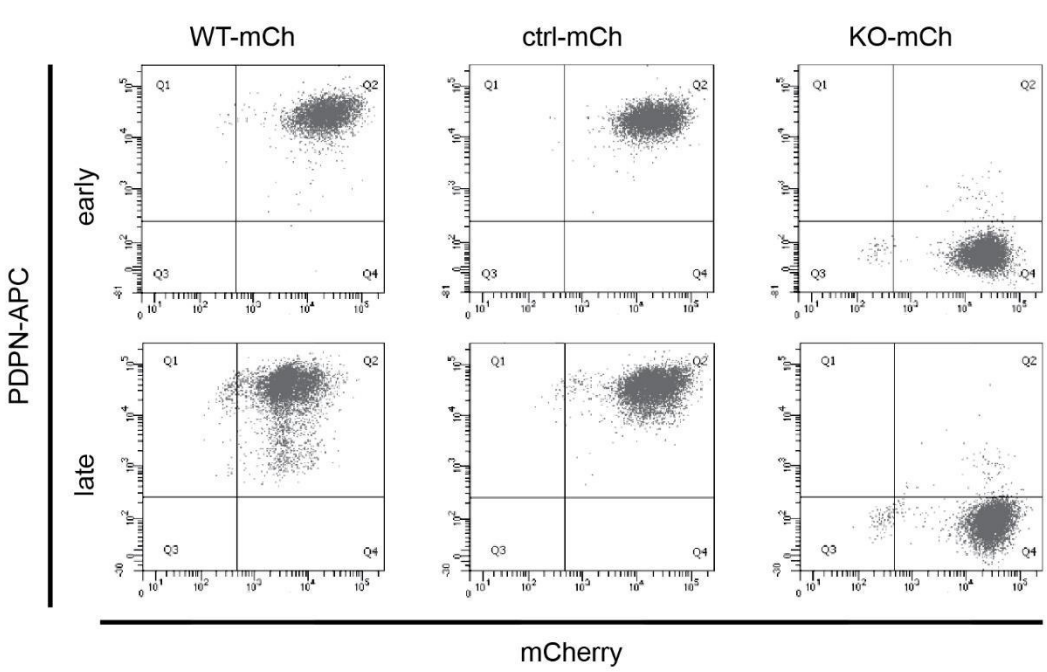

C

Cell line	Q1 [%]		Q2 [%]		Q3 [%]		Q4 [%]	
	early	late	early	late	early	late	early	late
WT-mCh	0.3	2.1	99.7	97.9	0.0	0.0	0.0	0.0
ctrl-mCh	0.0	0.5	100.0	99.5	0.0	0.0	0.0	0.0
KO-mCh	0.0	0.0	0.8	1.1	0.8	1.3	98.4	97.6

D

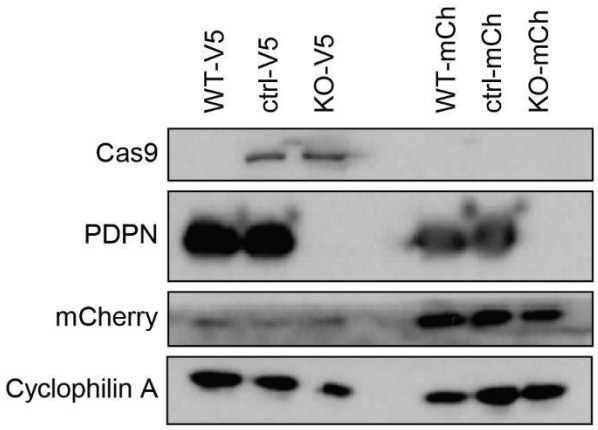

E

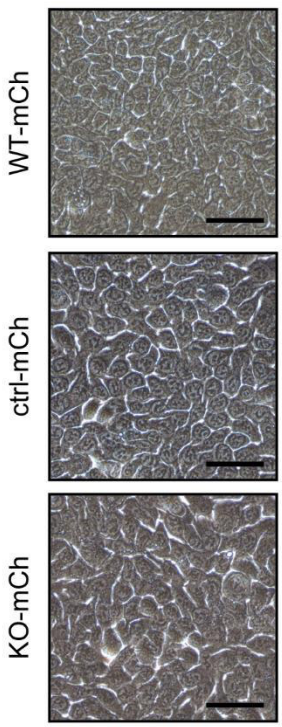

Figure 23 Evaluation of PDPN and mCherry expression in BDVII cells.
A) BDVII WT- and control (ctrl)-mCh cells expressed strongly PDPN observed by IF. KO-mCh cells did not show any PDPN signal. B) FACS analysis confirmed PDPN-positive population in WT- and ctrl-mCh cultures as well as PDPN-negative population in KO-mCh culture. The small amount of PDPN-positive cells in KO-mCh culture was retained from early to late passages. Moderate to high mCherry levels were expressed by WT-, ctrl- and KO-mCh cells. C) Overview of percentage portion in quadrant 1 to 4 (Q1-4) in early and late culture passages. D) Western blot analysis confirmed presence or absence of PDPN in WT, ctrl and KO cells either labeled with V5 or mCh, respectively. No Cas9 protein was detected in transiently transfected ctrl- and KO-mCh sublines compared to transduced V5-cells. E) Bright-field microscopy revealed similar morphology of mCh-labeled BDVII sublines. Nuclei were stained with Hoechst. Scale bar 50 µm, image quality was optimized by adjustment of brightness, contrast and gamma.

In addition, cell proliferation and viability were examined in BDVII-mCh cells (chapter 3.2.3.1). Manual cell determination showed that the abrogation of *Pdpn* did not affect proliferation as similar cell numbers were detected for WT-, control- and KO-mCh cells (Figure 24 A). Moreover, results of the cell viability test indicated no difference between BDVII-mCh sublines (Figure 24 B).

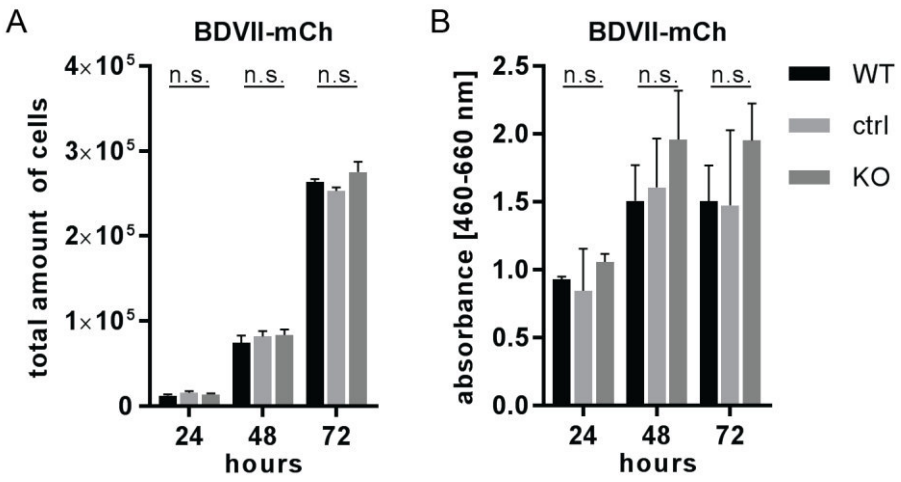

Figure 24 Loss of *Pdpn* had no effect on BDVII-mCh tumor cell proliferation and viability.
A) Proliferation was examined by manual counting using the Neubauer chamber and trypan blue to identify dead cells. B) XTT assay was performed to determine cell viability. Both tests were done 24, 48 and 72 h after cell seeding. Cell amount and viability increased over time in BDVII-mCh cSCC cells. No difference was obtained comparing KO with control (ctrl) cells. Values are plotted as mean and SD of n=3 independent experiments with technical triplicates. Unpaired two-tailed Welch's t test was performed with a 95 % confidence level. N.s. not significant.

Taken together, I was able to establish *Pdpn* KO and control BDVII-mCh cell populations via transient transfection, which lack Cas9 expression.

3.2.4.2 Podoplanin Deletion Decreases Transmigration in BDVII-mCherry Cells

The newly generated and validated control- and *Pdpn* KO-mCh BDVII cells were tested for their transmigratory capacity in order to confirm that these sublines show the same phenotype as previously generated BVII-V5 cells. Therefore, the BCM assay was performed as described (Figure 14 A).

IF staining of transmigrated cells confirmed strong PDPN expression in control-mCh cells, whereas no PDPN-positive KO-mCh cell was detected (Figure 25 A). *Pdpn* deletion resulted in reduced transmigration compared to control-mCh cells (Figure 25 B).

Thus, *Pdpn*-proficient and -deficient BDVII-mCh cells, which were generated by transient Cas9 expression showed similar results as their BDVII-V5 counterparts.

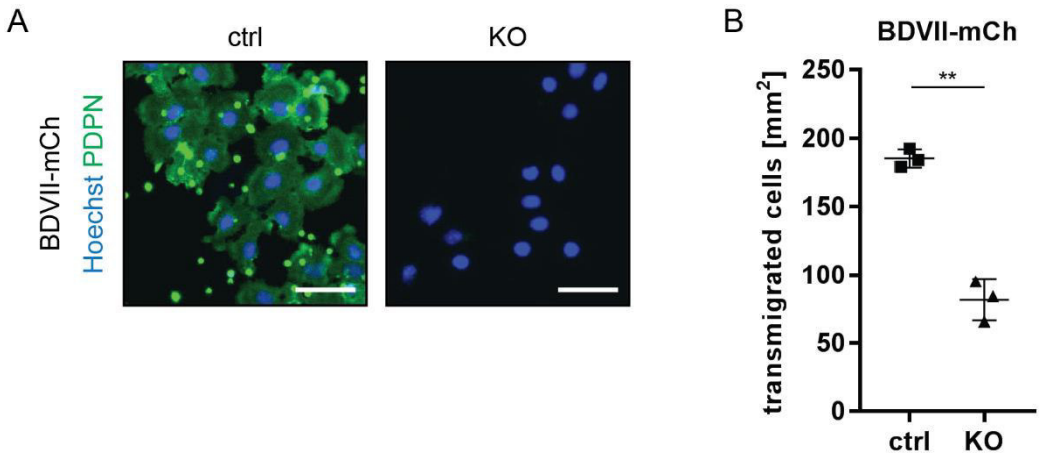

Figure 25 Investigation of the transmigratory potential in *Pdpn* KO- and control-mCh BDVII cells.

A) Transmigrated control (ctrl)-mCh cells expressed PDPN. No PDPN signal was detected in transmigrated KO-mCh cells. B) Transmigration was significantly reduced upon the loss of *Pdpn*. Values are plotted as mean and SD of n=3 independent experiments with technical triplicates. 5 fields per technical replicate were analyzed. Unpaired two-tailed Welch's t test was performed with a 95 % confidence level. ** $p < 0.01$. Scale bar 100 µm, image quality was optimized by adjustment of brightness, contrast and gamma.

In summary, the applied LOF approach led to the establishment of two different sets of labeled *Pdpn* KO and control murine BDVII cSCC cells. After successful validation of PDPN as well as marker expression level, these sublines were used in functional *in vitro* experiments. The loss of *Pdpn* in these murine tumor cells, which represent a differentiated cSCC morphology, did neither influence proliferation nor cell viability in either monolayer or 3D context. Notably, in both established cell sets *Pdpn* KO resulted in diminished cell transmigration. These results were supported by using the most advanced 3D organotypic

model system showing that the loss of *Pdpn* impaired tumor cell invasion into the dermal equivalent significantly. The examination of EMT showed neither a loss of the epithelial marker E-cadherin nor a gain of the mesenchymal marker vimentin in tumor cells. These results indicated a causal relation between PDPN expression and tumor cell invasion in an EMT-independent manner.

3.3 Impact of Podoplanin Deletion during Skin Cancer Progression *in Vivo*

The lack of *Pdpn* in cSCC cells impaired tumor cell migration and invasion *in vitro*. Together with the performed descriptive analysis of PDPN protein expression in well-differentiated cSCC patients' material and additional clinical studies, these results strongly supported the previous assumption on a crucial role of PDPN in cSCC carcinogenesis and invasive behavior (Vinicius de et al. 2011, Wojciechowska-Zdrojowy et al. 2016). Thus, the impact of *Pdpn* deletion was investigated in an orthotopic mouse model to examine the link between PDPN expression and cSCC tumor cell invasion and cancer progression *in vivo* and to complement *in vitro* experiments.

I decided to use an intradermal (i.d.) injection approach as developing tumors can be investigated in an organ-specific microenvironment reflecting characteristics of both, original murine tumors and human physiology. Moreover, injected tumors form and progress rather fast and hence, tissue can be analyzed within weeks to months. Immunosuppressed patients are at higher risk to develop cSCC (Waldman and Schmults 2019). Thus, I chose a model system which is mimicking skin carcinogenesis in these patients by defining the function of PDPN in the progression of cSCC in T cell-deficient nude mice (Rj:NMRI-Foxn1$^{nu/nu}$).

Generated *Pdpn* KO and control BDVII-mCh cSCC cells were injected i.d. into nude mice. Two different experimental strategies were pursued: time- and size-matched tumor analysis. For the time-matched approach, KO and control tumors were harvested on the same day post-injection, when tumor volumes reached around two-thirds of the allowed maximum in one group (max. 1.5 cm in diameter). This time point was applied to test whether PDPN interferes with cSCC cancer development in general like tumor outgrowth and final tumor volume. Further, PDPN-positive and -negative tumors were harvested when they reached a volume of approximately 60 mm^3 in order to study the influence of PDPN at an earlier tumor stage as well as to analyze potential differences in tumor characteristics at the same tumor size. In both procedures, tumor growth was monitored

regularly (Equation 1). Final tumor volumes were detected more precisely by measuring directly all three dimensions before harvesting the tissue (Equation 2). Harvested tumors were characterized by indicative histological analysis defining the nature of the tumor. Notably, mice were euthanized when termination criteria were reached such as ulcers. These animals were excluded from the analysis as well as tumors which showed additional skin reactions.

3.3.1. Loss of Podoplanin Results in Smaller Tumor Volumes and Delayed Tumor Outgrowth

During the first injection round, tumor diameter of i.d. injected control-mCh cells reached around 9 mm 14 days after injection. Thus, this time point was chosen for the time-matched analysis to have sufficient flexibility to include tumors, which might reach the maximal tumor volume faster in subsequent injection rounds.

Tumor development upon injection of BDVII-mCh cells was monitored over time and in general, all injected BDVII-mCh sublines formed i.d. tumors (Figure 26 A). Comparing final volumes of tumors derived from WT- and control-mCh cells, no difference was observed (Figure 26 B). The loss of *Pdpn* resulted in smaller tumor volumes obtained in the time-matched analysis (Figure 26 B). Moreover, the size-matched experiment indicated that KO-mCh cells reached the required volume of around 60 mm^3 on average 1.4 days later than control-mCh cells (Figure 26 C and D).

Independent of PDPN expression, well-differentiated tumors were formed and all tumor cells expressed the introduced mCherry marker (Figure 27 A and B). Moreover, small groups of tumor cells were observed within the stroma suggesting collective tumor cell invasion (Figure 27 B). In order to confirm PDPN protein levels in developed tumors, PDPN expression was examined by IF. Co-staining for the epithelial cell marker pan cytokeratin (pCK) demonstrated that PDPN was only detected in control-mCh tumors (Figure 27 C). No PDPN expression was observed in KO-mCh tumor cells. Independent of PDPN-expressing cancer cells, a weak PDPN-positive reaction was also detected in tumor microenvironment (TME), which were most likely CAFs.

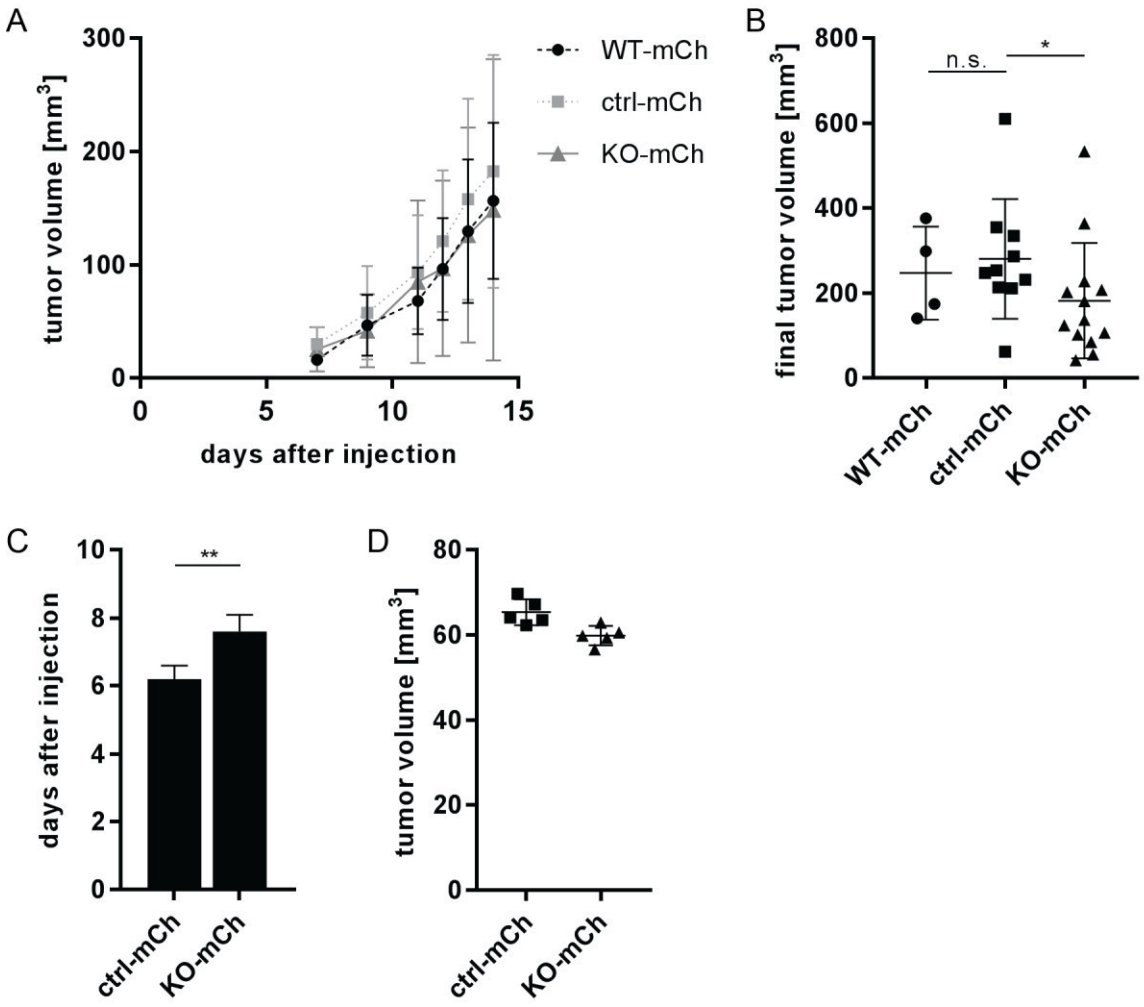

Figure 26 Reduced tumor volume and delayed outgrowth of *Pdpn* KO-mCh tumors.
A) Tumor volumes were monitored over time in time-matched experiment. WT-mCh n=4, control (ctrl)-mCh n=10, KO-mCh n=13. B) Loss of *Pdpn* resulted in decreased tumor volume in time-matched analysis. C) Tumor outgrowth was decelerated in *Pdpn* KO-mCh tumors. N=5. D) Ctrl- and KO-mCh tumors were isolated when tumors reached ~60 mm^3. Unpaired one-tailed Mann-Whitney test was performed with a 95 % confidence level for time-matched analysis and unpaired two-tailed Welch t test for size-matched experiment. N.s. not significant, * $p < 0.05$, ** $p < 0.01$.

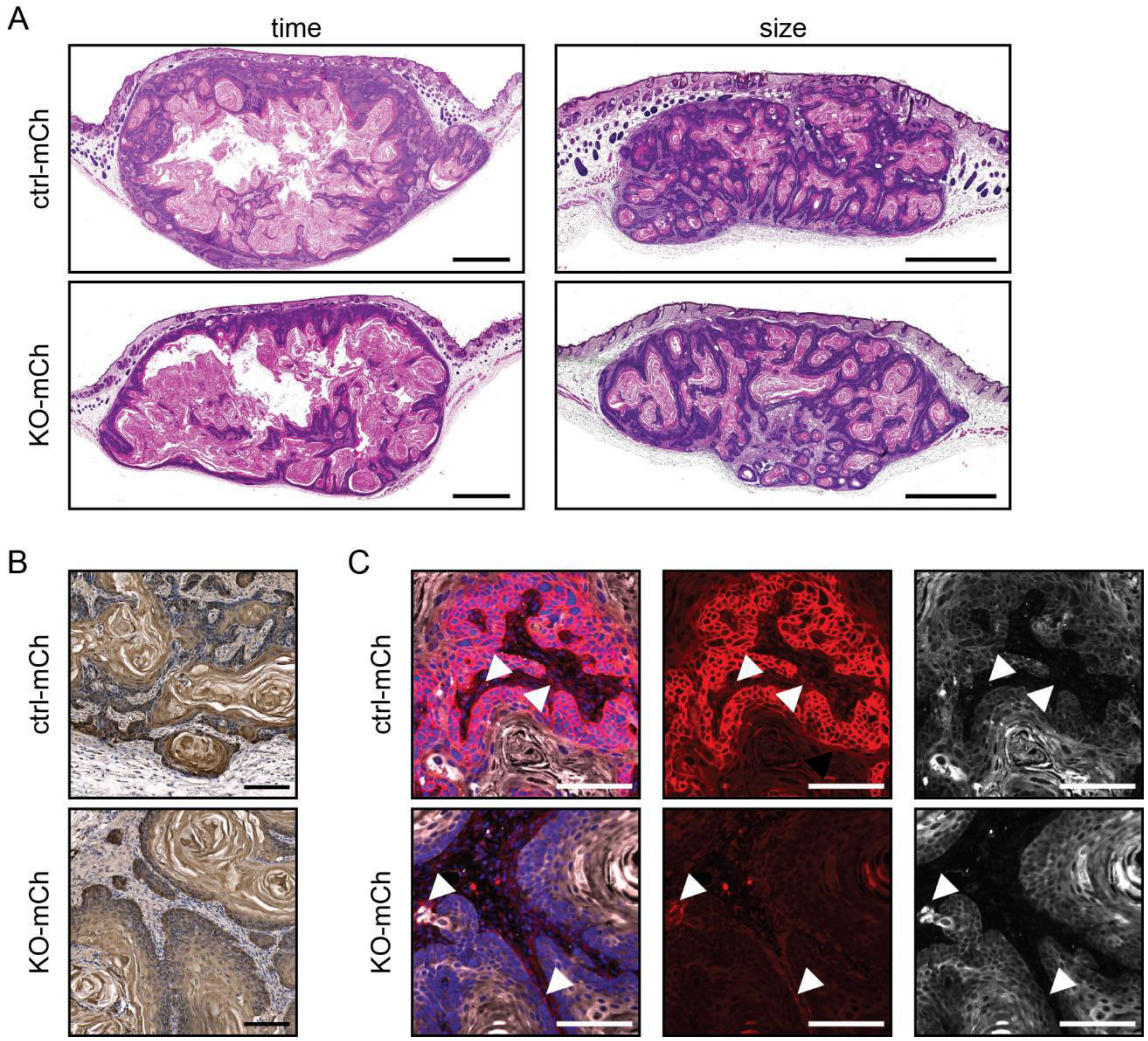

Figure 27 Orthotopically applied BDVII-mCh cells formed well-differentiated cSCCs.
A) Well-differentiated tumors were established independent of PDPN expression upon i.d. injection. B) Tumor cells expressed mCherry marker. Small groups of tumor cells were detected in the stroma. C) Tumors derived from control (ctrl)-mCh cells expressed highly PDPN at the invasive front. No PDPN expression was obtained in *Pdpn* KO-mCh tumors. Additionally, a weak PDPN-positive reaction was observed in CAFs independent of PDPN expression of tumor cells (arrowheads). Hematoxylin or Hoechst were used to stain nuclei. Representative images are depicted. Scale bar A) 1000 µm, B) and C) 100 µm, image quality was optimized by adjustment of brightness, contrast and gamma.

3.3.2 Diminished Proliferation in Podoplanin-Deficient Tumor Cells

PDPN-expressing control-mCh cells gave rise to larger tumors at a shorter time compared to *Pdpn* KO-mCh cells. In order to determine whether PDPN expression affected tumor cell proliferation or apoptosis *in vivo*, different histological stainings were performed.
Comparing control- and KO-mCh tumors no difference was observed in apoptosis as examined visually by cleaved caspase 3 expression (Figure 28 A). Hardly any tumor cell showed a positive staining indicating that the vast majority of tumor cells were in a viable state. Hence, Ki67 was analyzed, which is expressed in all phases of cycling cells. Visual examination showed similar expression of Ki67 in nearly all cells of PDPN-positive and -negative tumors supporting that almost no tumor cells was apoptotic (Figure 28 B). However, using this method no statement can be done about how efficient tumor cells are undergoing cell division. To further investigate differential proliferation rate *in vivo*, BrdU was injected intraperitoneally (i.p.) four hours before animals were euthanized. Thereby, BrdU was incorporated into DNA during S-phase of cycling cells. Staining of BrdU indicated visually a potential difference and therefore, manual counting of regions of interests was performed (Figure 28 C). Quantification revealed that less cells incorporated BrdU in *Pdpn*-negative tumors suggesting that PDPN-expressing control tumor cells entered S-phase more efficient than *Pdpn* KO cells (Figure 28 D).
Taken together, i.d. injection of murine BDVII-mCh cells lacking *Pdpn* resulted in slower cycling tumor cells and hence, in smaller tumors and delayed tumor outgrowth, respectively.

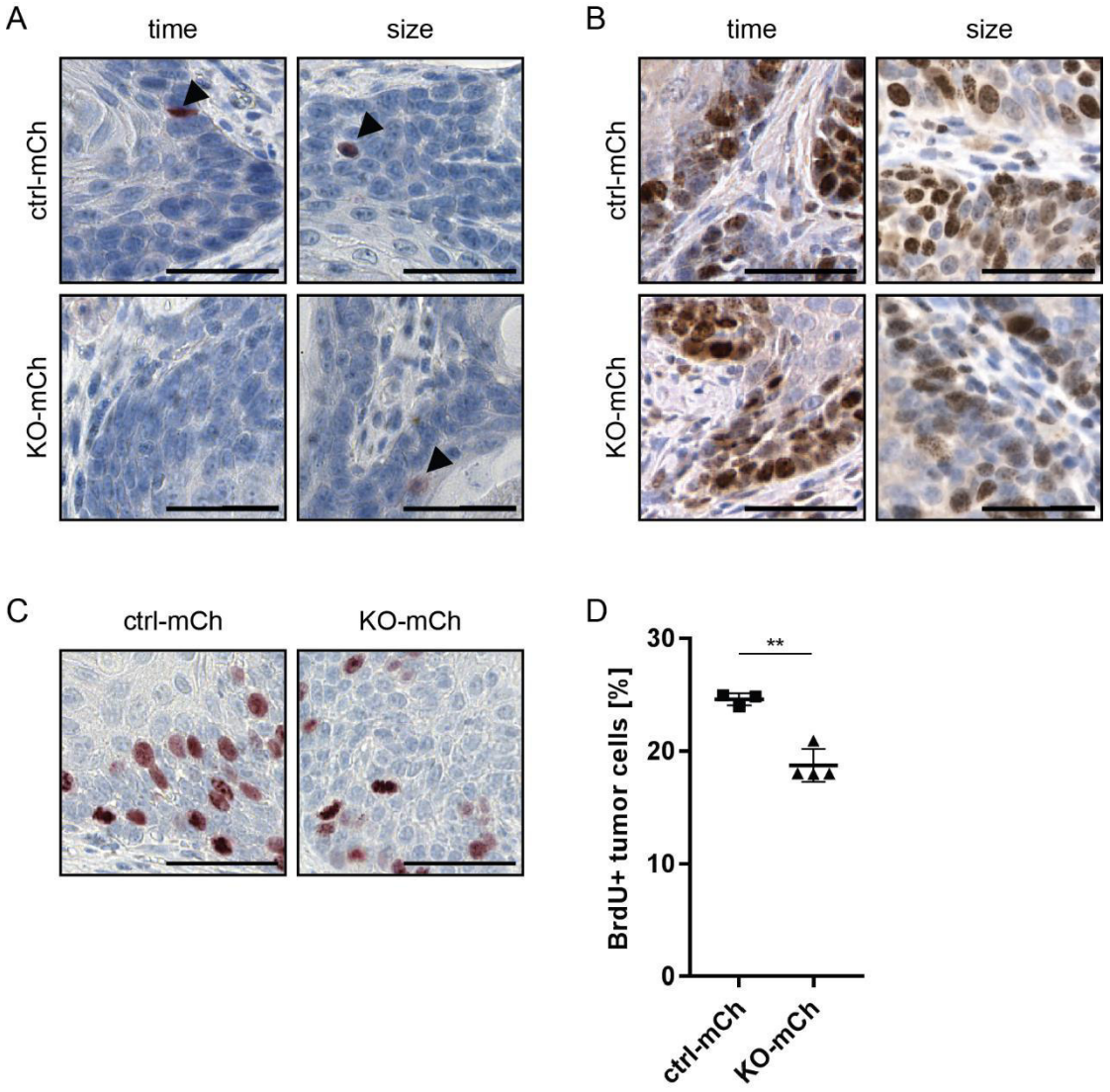

Figure 28 *Pdpn*-negative tumor cells entered S-phase less efficient *in vivo*.
A) Only single apoptotic tumor cells were detected by cleaved caspase 3 staining. No difference was observed between tumors derived from control (ctrl)- or KO-mCh cells. B) Ki67 staining revealed that majority of tumor cells was within the cell cycle. Ctrl-mCh n=7 and KO-mCh n=9. C) *Pdpn* KO tumors incorporated less BrdU. D) Decreased BrdU-positive tumor cells were detected in KO tumors. Ctrl-mCh n=3 and *Pdpn* KO-mCh n=4. Nuclei were counterstained with hematoxylin. Representative bright-field images are depicted. Scale bar 50 µm. Unpaired two-tailed Welch's t test was performed with a 95 % confidence level. ** $p < 0.01$. Image quality was optimized by adjustment of brightness, contrast and gamma.

3.3.3. Reduced Invasion upon Podoplanin Deletion in an Epithelial-Mesenchymal Transition-Independent Manner

The expansive growth of PDPN-expressing tumor cells resulted in a larger tumor volume. Besides enhanced proliferation, malignant progression of solid cancer such as cSCC is also promoted by tumor cells, which are invading locally into the TME without undergoing EMT (reviewed in Friedl et al. (2012)). Employing the 3D organotypic SCM, I demonstrated that PDPN-positive BDVII-V5 cells invaded more and deeper into the dermal equivalent (Figure 18). These data implied a fundamental role of PDPN in tumor cell invasion *in vitro*. Hence, the invasive capacity of *Pdpn* KO- and control-mCh tumor cells was studied in tumor samples.

Laminin is one major component of the BM and gets lost upon tumor cell invasion (Watt 2014, Poltavets et al. 2018). Therefore, I performed co-staining of laminin and K14, as epithelial cell marker, in order to determine stroma infiltrating tumor cells. Undifferentiated tumor cells, either derived from control- or KO-mCh cells, showed K14 expression and laminin was detected at the outer edge of the tumor bulk (Figure 29 A). Small groups of tumor cells, which were not connected to the bulk and partially lost laminin, were observed indicating collective tumor cell invasion.

For quantitative analysis, images of the tumor margin were analyzed semi-automatically utilizing an ImageJ macro. Invading tumor cells were determined as described in the following: groups of tumor cells at the tumor edge, which were not connected to the tumor bulk, were selected by K14 signal. Laminin coverage at the outer edge of these infiltrative buds was detected. K14 areas with laminin coverage below 15 % were defined as invading tumor cells. The area of these invading cells was determined according to K14 staining. This quantitative analysis demonstrated a trend close to significance that *Pdpn* abrogation reduced the amount of tumor cells invading the stroma (Figure 29 B).

Examination of the SCM revealed that tumor cells were invading collectively in the absence of EMT (Figure 20) and orthotopic injected control- and KO-mCh BDVII cells showed small groups of mCherry-positive tumor cells within the stroma indicating collective tumor cell invasion (Figure 27 B). Thus, E-cadherin as epithelial and vimentin as mesenchymal markers were analyzed assessing EMT. *Pdpn*-proficient and -deficient tumor cells expressed E-cadherin whereas vimentin was detected in fibroblasts (Figure 29 C). Only single tumor cells expressed vimentin additionally to E-cadherin indicating that these cells underwent partial EMT.

To sum up, the orthotopic injection mouse model highlighted the significance of PDPN in cSCC tumor cell invasion, since less infiltrative tumor cells upon *Pdpn* loss were observed.

Moreover, i.d. tumors derived from either *Pdpn*-positive or -negative cells established in an EMT-independent manner.

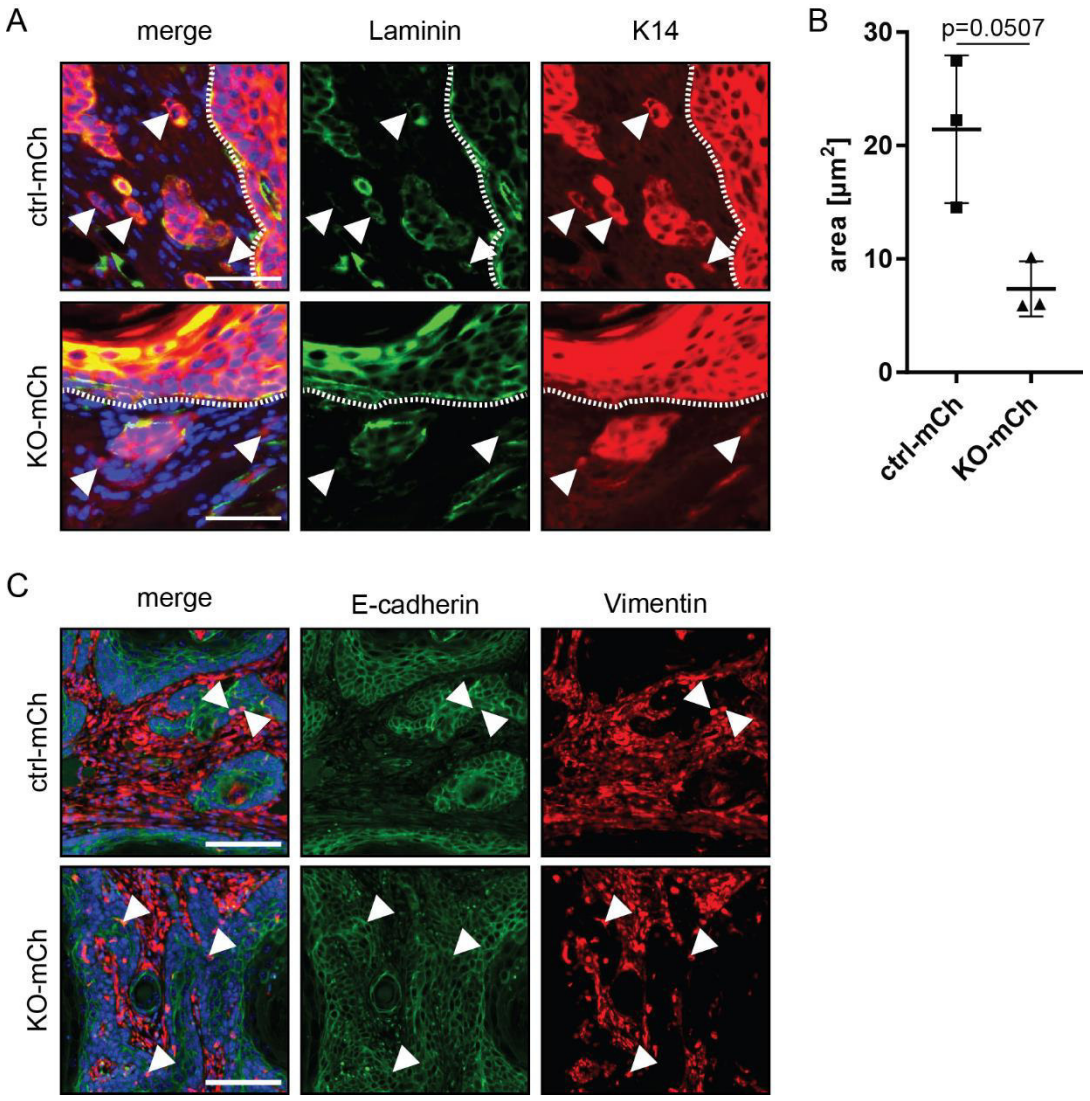

Figure 29 Lowered tumor cell invasion in an EMT-independent manner upon *Pdpn* deletion.

A) Undifferentiated control (ctrl)- and KO-mCh tumor cells expressed K14. Small groups of tumor cells invaded into the stroma and lost laminin expression partially. Dashed line represents BM of tumor bulk. B) Quantitative analysis of laminin-K14-co-staining revealed that KO-mCh tumor cells tended to infiltrate less into the stroma. Values are plotted as cumulative sum and SD of n=3 tumors derived from either ctrl- or KO-mCh cells. For each tumor, 3 non-consecutive sections with 5 fields per section were analyzed. Unpaired two-tailed Welch's t test was performed with a 95 % confidence level. C) IF staining revealed that independent of PDPN expression tumor cells expressed E-cadherin, but no vimentin. Only single tumor cells showed partial EMT by expressing both, vimentin and E-cadherin (arrowhead). High levels of vimentin were observed in fibroblasts. Nuclei were stained with Hoechst. Representative images are displayed. Scale bar A) 50 µm and C) 100 µm, image quality was optimized by adjustment of brightness, contrast and gamma.

In conclusion, *Pdpn* KO and control murine BDVII cSCC cells formed well-differentiated tumors upon orthotopic injection into nude mice. Histological analysis revealed that stromal cells also showed a PDPN-positive reaction independent of the PDPN status of injected tumor cells. Consequently, the chosen i.d. injection model recapitulated characteristics of human patient material (Figure 7). Importantly, tumor cells lacking *Pdpn* entered S-phase less efficiently resulting in diminished tumor volume and decelerated tumor outgrowth. Furthermore, small groups of either PDPN-positive or -negative tumor cells infiltrated into the stroma in an EMT-independent manner. Notably, reduced infiltrative capacity was observed upon *Pdpn* KO. Thus, this employed *in vivo* approach underscored the importance of PDPN in cSCC carcinogenesis since the deletion of this glycoprotein impaired both, tumor growth and tumor cell invasion.

4 DISCUSSION

4 DISCUSSION

Multiple studies have revealed that the expression of podoplanin (PDPN) is associated with tumor progression in solid cancer derived from human patients or mouse models (Schacht et al. 2005, Durchdewald et al. 2008, Cueni et al. 2010, Honma et al. 2012, Kunita et al. 2018). 90 % of cutaneous squamous cell carcinoma (cSCC) strongly express PDPN in tumor cells particularly at the leading edge of the tumor as well as in cancer-associated fibroblasts (CAFs; Wicki and Christofori (2007), Honma et al. (2012), Wojciechowska-Zdrojowy et al. (2016)). This enhanced PDPN expression correlates with poor patient survival and results in increased metastasis as demonstrated by descriptive clinical investigations (Toll et al. 2012, Vinicius de et al. 2011, Wojciechowska-Zdrojowy et al. 2016). Mechanistically, strong PDPN expression was shown to increase migration and invasion in gain-of-function (GOF) *in vitro* experiments (Scholl et al. 1999, Martin-Villar et al. 2006, Wicki et al. 2006). However, the exact mechanism seems to be contextual since different modes of action were reported in tumorigenic and non-tumorigenic epithelial cells. Thus, only little is known about the role of PDPN in skin cancer development. The fact that the incidence of cSCC is increasing as well as late stages of this cancer entity are difficult to treat highlights that there is a substantial need for novel treatment options.

In this study, I show for the first time that PDPN drives proliferation and collective invasion of well-differentiated cSCC cancer cells. Subsequent to the detection of PDPN in cancer cells at the invasive front in differentiated cSCC, the causality of PDPN expression on cSCC progression was addressed in functional assays by using the CRISPR/Cas9 technology. The employed orthotopic injection model showed that the tumor volume as well as tumor outgrowth were significantly reduced or delayed, respectively, in tumors derived from *Pdpn*-deficient cells that were due to diminished cancer cell proliferation. Moreover, functional *in vitro* and *in vivo* experiments demonstrated that the invasive capacity was impaired and moreover, independent of epithelial-mesenchymal transition (EMT) upon the loss of *Pdpn* in murine cSCC cells. These findings underscore the importance of PDPN in the progression of differentiated cSCC by promoting cancer cell proliferation and invasion.

4.1 Differentiated Cutaneous Squamous Cell Carcinoma Express Podoplanin

The expression of PDPN has been described in various human tumors such as cervix, breast, head and neck as well as cSCC (Martin-Villar et al. 2005, Schacht et al. 2005, Vinicius de et al. 2011, Honma et al. 2012, Toll et al. 2012, Lan et al. 2014, Hesse et al. 2016, Kunita et al. 2018). Independent of the tumor entity, PDPN expression was localized in tumor cells at the invasive front suggesting that this glycoprotein acts as a driver of invasiveness and cancer progression. Two descriptive studies reported that PDPN expression correlated negatively with differentiation, in particular, well-differentiated tumors showed only low levels of PDPN if at all, whereas poorly-differentiated expressed high levels of this glycoprotein (Schacht et al. 2005, Vinicius de et al. 2011). In this thesis, I analyzed one moderately- and five well-differentiated human cSCCs. Examined tumors expressed PDPN in tumor cells at the tumor-stroma border, which is in contrast to published data (Schacht et al. 2005, Vinicius de et al. 2011). Previously, PDPN was reported to be upregulated in basal keratinocytes around the wound margins (Baars et al. 2015). By using an *in vivo* loss-of-function (LOF) approach, in which *Pdpn* is deleted specifically in Keratin 14 (K14)-expressing keratinocytes, the authors showed that the deficiency of *Pdpn* was dispensable for re-epithelialization during wound healing and, notably, for cornification (Baars et al. 2015). Thus, there is no causal link between PDPN expression and keratinocyte or epidermal tumor differentiation, respectively. Moreover, I observed PDPN expression in the stroma pointing to PDPN-positive CAFs, which was also reported by Wojciechowska and co-workers (Wojciechowska-Zdrojowy et al. 2016).
Consequently, based on these findings, I hypothesized that PDPN plays a major role also in differentiated cSCC. In order to define its function, a LOF approach was utilized which is discussed in the following chapters.

4.2 Podoplanin Does neither Affect Morphology nor Proliferation *in Vitro*

Since PDPN is expressed in cSCC at any stage of differentiation according to my results and published reports, I selected the two human cSCC cell lines SCL-II and MET-4 as well as murine BDVII cells to investigate the role of PDPN in cSCC carcinogenesis (Schacht et al. 2005, Vinicius de et al. 2011). SCL-II and MET-4 cells represent undifferentiated tumors from different stages, as they were isolated from a facial primary lesion and a lymph node

metastasis, respectively (Tilgen et al. 1983, Popp et al. 2000, Proby et al. 2000). The murine BDVII cell line was established from a well-differentiated murine tumor that developed upon 7,12-Dimethylbenz-[a]-anthracene (DMBA) treatment in the course of a chemical carcinogenesis protocol (Fusenig et al. 1978). *PDPN* knockout (KO) and control sublines were established for these three cSCC cell lines using the CRISPR/Cas9 technology and detection of PDPN protein levels verified successful generation.

Functional analysis in monolayer culture revealed that the lack of *PDPN* did neither influence morphology nor proliferation in either SCL-II, MET-4 or BDVII tumor cells. Previously, only studies with other cell types than cutaneous epithelial cancer cells were performed. *In vitro* cultivation of primary murine *Pdpn* KO keratinocytes, which were generated by an *in vivo* LOF approach, did not alter proliferation in comparison to *Pdpn*-proficient control keratinocytes (Baars et al. 2015). Proliferation was neither influenced in non-tumorigenic keratinocytes nor in breast cancer cells upon ectopic overexpression of PDPN, which is in agreement with my studies (Scholl et al. 1999, Wicki et al. 2006). However, PDPN-dependent proliferation seems to be context-dependent, since orthotopic tumor cell injections, which were performed in this study, showed diminished tumor cell proliferation, which will be discussed in chapter 4.6.1.

4.3 Transmigration and Invasion Are Diminished in Murine Tumor Cells Lacking Podoplanin

The deficiency of *PDPN* in human and murine cSCC cells did not impair tumor cell features in monolayer culture. Hence, in order to investigate the functional consequences of PDPN on migration and invasion, I used two different more advanced *in vitro* procedures. First, established human and murine control and *PDPN* KO cells were applied in the Boyden Chamber matrigel (BCM) assay. This method is commonly performed to assess the transmigratory capacity of cells *in vitro* since it is quick, quantitative and reproducible (Bloomfield et al. 2001, Kleinman and Jacob 2001). In this experimental approach, cells are seeded on top of matrigel-coated filters. Cells transmigrate through the matrigel along a serum-gradient during a cell line-specific incubation time and the number of transmigrated cells can be quantified. Despite giving insights into the transmigratory potential of intrinsic tumor cell factors, the BCM assay, however, lacks the complexity of a tissue context, which is present *in vivo*. Hence, to further complement the understanding of tumor cell invasion *in vitro*, the 3D organotypic skin cancer model (SCM) was used as the second method (Berning et al. 2015). In comparison to traditional systems, the SCM

is more elaborated. Briefly, epithelial cancer cells grow air-exposed on top of a fibroblast feeder layer consisting of primary dermal fibroblasts that produce matrix themselves. Thus, this organotypic system allows analyzing the cell behavior in a more appropriate environment, since this model mimics the epidermal-dermal context.

Functional analysis of human and murine cSCC cells revealed that the transmigratory and invasive potential differed in both the BCM assay as well as in the SCM upon *PDPN* deletion. SCL-II and MET-4 cells lacking *PDPN* showed similar transmigratory and invasive behavior compared to control cells. Strikingly, the loss of *Pdpn* in murine BDVII cells resulted in decreased transmigration in the BCM as well as in reduced invasive area and covered invaded distance in the SCM. The different transmigratory and invasive behavior of human and murine cell lines might be due to various reasons. The level of PDPN expression is only moderate in SCL-II and MET-4 cells, whereas all murine BDVII cells strongly express PDPN. Hence, the delta of PDPN expression between KO and control cells originated from SCL-II and MET-4 cell lines might not be high enough to be able to detect an effect. Other aspects, which could explain the unaltered migration of human cells upon *PDPN* loss, might be due to their tumor origin and morphology. SCL-II and MET-4 cell lines were established from human undifferentiated primary tumor lesion or lymph node metastasis, respectively, whereas BDVII cells were isolated from a murine well-differentiated primary tumor, which emerged upon a chemical tumorigenesis protocol (Fusenig et al. 1978, Tilgen et al. 1983, Popp et al. 2000, Proby et al. 2000). Hence, various genes are differentially mutated in these cell lines. For instance, BDVII cells harbor a mutant form of the *Ha-Ras* proto-oncogene and SCL-II a mutant form of the tumor suppressor *TRP53*, whereas both genes are not mutated in MET-4 cells (Fusenig et al. 1978, Tilgen et al. 1983, Popp et al. 2000, Proby et al. 2000). In order to investigate the importance of PDPN in cSCC progression in this study, these cell lines were selected particularly because of these differences to extend the spectrum to a variety of cSCCs representing different tumor characteristics. However, additional molecular alterations favoring migration and invasion were probably gained in the course of cancer development in individual original human tumors. Thus, it cannot be excluded that known gene mutations as well as additional alterations might trigger compensatory responses upon *PDPN* loss. Baars and colleagues demonstrated that the depletion of *Pdpn* in basal keratinocytes did neither impair skin development nor wound healing assuming that other yet undefined molecular mechanisms were balancing the loss of *Pdpn* (Baars et al. 2015). Potential candidates could be other proteins with similar location and function such as CD44. CD44 like PDPN links the plasma membrane to the cytoskeleton via the interaction with the ezrin, radaxin and moesin (ERM) protein family resulting in increased invasion (Hirao et al. 1996, Yonemura et al. 1998, Isacke and Yarwood 2002). Since more human

cSCC cell lines are available that are used in skin cancer research (chapter 1.2.1), the impact of PDPN should be analyzed in these cell lines additionally. These further investigations would complement the understanding of PDPN function in the human cell system and potential species-specific alterations that were observed in this study could be excluded.

Thus, I used *Pdpn* KO and control BDVII cells for further studies of PDPN's role in differentiated cSCC. My findings of the murine BDVII cell behavior in dependence of PDPN are in line with published data. Ectopic expression of human PDPN in non-tumorigenic Madin-Darby canine kidney (MDCK) cells or the MCF7 breast cancer cell line resulted in enhanced migration assessed by the BCM assay (Martin-Villar et al. 2006, Wicki et al. 2006). Invasively growing BDVII cells in the SCM showed cornified pearls within the dermal compartment. On the one hand, this characteristic reflects the morphology of original DMBA-induced tumors (Fusenig et al. 1978). On the other hand, this feature mimics 90 % of human cSCC that display a well-differentiated morphology (Stenman et al. 2018). Thus, the BDVII cell line used in the SCM presents a valid model system that recapitulates PDPN-dependent invasion in cSCC.

Subsequently, a more detailed analysis of 3D-cultured BDVII cells was performed to determine the invasive character. The proliferative behavior of organotypically cultured cells was examined since expansive cancer cell growth results in passive migration, which could be one reason for enhanced invasiveness in PDPN-positive BDVII cells. Ki67 staining demonstrated that proliferative activity was similar in *Pdpn* KO and control cells. These findings supported 2D *in vitro* analysis discussed in chapter 4.2. No reports examining PDPN-dependent proliferation in 3D are available and reported *in vivo* data will be discussed in the corresponding chapter (4.6.1).

Moreover, I observed small groups of invading cells in *Pdpn* KO and control cultures suggesting collective tumor cell invasion. So far, collective invasion of differentiated cutaneous epithelial tumors was associated with partial EMT or absence of EMT (Friedl et al. 2012, Lan et al. 2014, Hesse et al. 2016). Detection of the epithelial marker E-cadherin and the mesenchymal marker vimentin revealed that *Pdpn* KO and control BDVII cells invaded in the absence of EMT, which corresponds to clinical patient data (Lan et al. 2014, Hesse et al. 2016). The impact of PDPN on EMT was so far either analyzed in 2D culture systems or *in vivo*, which will discussed in chapter 4.6.2. Previous 2D *in vitro* investigations utilized *PDPN* GOF approaches in different cell lines. Scholl and colleagues examined murine non-tumorigenic keratinocytes and showed that the expression of E-cadherin as well as K14 were lost and vimentin was enhanced upon murine *Pdpn* overexpression (Scholl et al. 2000). Similar morphological changes were observed in MDCK cells overexpressing human *PDPN*, where E-cadherin expression was reduced, while N-

cadherin was increased, indicating these cells underwent the so-called cadherin switch (Martin-Villar et al. 2006, Fernandez-Munoz et al. 2011). Moreover, the epithelial keratin filament 8 was also decreased and vimentin expression was enhanced upon PDPN overexpression indicating that ectopic PDPN overexpression triggered EMT (Martin-Villar et al. 2006, Fernandez-Munoz et al. 2011). In contrast to these studies, ectopic PDPN overexpression did not affect E-cadherin levels in MCF7 breast cancer cells and also not EMT (Wicki et al. 2006). In conclusion, the abrogation of epithelial markers and the gain of mesenchymal protein expression upon PDPN overexpression were shown to be context-dependent in monolayer culture.

4.4 Intracellular Podoplanin Signaling via Ezrin Is Not Influenced in Monolayer Culture

The invasive capacity of PDPN-expressing cells was reported to be mediated through the interaction with the ERM protein family (Scholl et al. 1999, Martin-Villar et al. 2006, Wicki et al. 2006). ERM proteins are activated via phosphorylation mediated by kinases including Rho GTPases (RhoA, Rac1 and Cdc42) at the plasma membrane followed by binding to PDPN resulting in actin cytoskeleton remodeling and thus, migration and invasion (Scholl et al. 1999, Bretscher et al. 2002, Martin-Villar et al. 2006). Confocal microscopy of 2D-cultured BDVII cSCC cells revealed that PDPN-positive tumor cells recruited ezrin to the plasma membrane. Subsequently, phosphorylated myosin light chain 2 (P-MLC2) was expressed indicating induced cytoskeleton rearrangements. However, the deletion of *Pdpn* did not abrogate ezrin translocation and a similar activity of P-MLC2 was observed. Previously, ectopic overexpression of PDPN in MDCK cells resulted in PDPN-ERM-mediated RhoA activation and enhanced invasiveness in the presence of EMT *in vitro* (Martin-Villar et al. 2006). However, a similar *in vitro* experimental approach ectopically overexpressing PDPN in MCF7 cells demonstrated ezrin recruitment and EMT-independent invasion without the activation of Rho GTPases (Wicki et al. 2006). Interestingly, PDPN-expressing B16.F10 melanoma cells recruited ERM, which was abolished upon *Pdpn* knockdown (KD; Pedro and Shields (2018)). Moreover, the authors identified an alternative mechanism without activation of Rac1 or Cdc42 but including PAK1-RhoA. Altogether, this suggests a cell context-dependent regulation of ERM proteins and Rho GTPases. Therefore, further examination, especially in a 3D context, is required in order to decipher the underlying mechanism of PDPN-induced invasion in cSCC *in vitro*. Descriptive analysis by using immunostainings of SCM or tumor sections

might be a possibility. However, proper determination of subcellular ezrin localization could be difficult due to the close cellular interaction and potential overlap of individual cells within tissues. Martín-Villar and co-workers ectopically expressed PDPN in which the cytoplasmic tail was deleted or the ERM-binding site was mutated and showed that the modification of the intracellular (IC) PDPN domain diminished ezrin recruitment (Martin-Villar et al. 2006). Hence, the utilization of a *Pdpn* mutant lacking the ERM binding site represents the most appropriate approach.

4.5 Orthotopic Injection Mouse Model Recapitulates Well-Differentiated Human Cutaneous Squamous Cell Carcinoma

Although more complex *in vitro* model systems like the SCM allow the examination of migratory and invasive behavior of cancer cells, they still lack the complexity of whole tissues and organisms. Consequently, an *in vivo* mouse model is required to decipher all factors of carcinogenesis like tumor growth or interaction of tumor cells with stromal cells in dependency of PDPN. Since organ transplant recipients and other immunosuppressed patients are at higher risk to develop cSCC, I decided to study the role of PDPN in cSCC progression in an orthotopic model using athymic nude mice that lack T cells (Stenman et al. 2018, Waldman and Schmults 2019). Nevertheless, it is noteworthy to mention that the incidence in immunocompetent patients is increasing due to cumulative sun exposure, for instance. Thus, the function of PDPN in this patient cohort should be considered in different model systems additionally such as (i) orthotopic injections into immunocompetent mice or (ii) genetic engineered mouse models (GEMMs). In the later model system, mice, which lack *Pdpn* specifically in keratinocytes by using, for instance, a K14-Cre recombinase, can be utilized. Since PDPN is not tumorigenic autonomously, this GEMM needs to be combined with the multistage DMBA/12-O-tetradecanoylphorbol-13-acetate (TPA) carcinogenesis protocol (explained in detail in section 1.3.2). Durchdewald and co-workers treated the back skin of wild-type (WT) mice with the tumor promoter TPA and established papilloma (PAP), which can be defined as a potential pre-malignant lesion of cSCC, showed a PDPN upregulation in tumor cells at the invasive front (Durchdewald et al. 2008). Consequently, this *in vivo* approach would represent an appropriate model to characterize the impact of PDPN. However, in order to investigate cSCC carcinogenesis, the additional tumor initiator DMBA needs to be applied before TPA treatment so that initially formed PAP transform to cSCCs over time. In the research group of Prof. Dr. Peter Angel, *Pdpn* floxed as well as K14-Cre mice were established in the mouse strain C57BL/6 (Baars et

al. 2015). Unfortunately, this mouse strain is highly resistant to the chemical-based protocol resulting in low tumor incidences and multiplicities compared to a susceptible strain like 129/SvEv (Reiners and Singh 1997, Yamakage et al. 2000, Gebhardt et al. 2008). Consequently, C57BL/6 *Pdpn* floxed and K14-Cre mice would have needed to be backcrossed into the DMBA/TPA-sensitive mouse strain 129/SvEv. Successful backcrossing requires at least ten generations resulting in a minimum of approximately one and a half years before starting the actual experiment, which would have been beyond the scope of this study.

Thus, in this dissertation, I focused on the impact of PDPN in cSCC tumorigenesis in immunosuppressed patients. Therefore, labeled *Pdpn* KO and control murine BDVII cells were injected i.d. into nude mice that lack T cells. Established tumors displayed a well-differentiated morphology upon i.d. injection of both *Pdpn*-proficient and -deficient BDVII cells. Moreover, tumor cells derived from control cells strongly expressed PDPN at the tumor-stroma border. Stromal cells, most likely CAFs, showed a PDPN-positive reaction as well, in tumors derived from control and *Pdpn* KO cells. Thus, this model is suitable to study the impact of PDPN in cSCC progression, since formed tumors recapitulate the human situation (Vinicius de et al. 2011, Toll et al. 2012, Lan et al. 2014, Hesse et al. 2016, Wojciechowska-Zdrojowy et al. 2016).

4.6 Deletion of Podoplanin Results in Smaller Tumors and Delayed Tumor Outgrowth

Time- and size-matched analysis of i.d. injected control and *Pdpn* KO cancer cells revealed that the abrogation of *Pdpn* resulted in smaller tumors and delayed outgrowth. These findings support the proposed function of PDPN in cSCC, as clinical data reported a correlation of PDPN-expressing tumor cells and poor patient survival (Vinicius de et al. 2011). An *in vivo* study using short hairpin (sh) RNA-mediated *PDPN* KD in the human vulva SCC cell line A431 demonstrated that tumor volume was reduced upon i.d. injection into T cell-deficient BALB/c nude mice (Kunita et al. 2018). Wicki and colleagues employed a transgenic pancreas mouse model resulting in PDPN overexpression in insulin-producing β-cells and showed that the overexpression increased pancreatic tumor incidence as well as malignancy (Wicki et al. 2006). In contrast to these studies, primary tumor growth of breast carcinoma xenografts was reduced upon orthotopic injection into the mammary fatpad of MCF7 cells that ectopically overexpressed PDPN (Cueni et al. 2010). Interestingly, in PDPN-expressing breast cancer xenografts, the number of lymph

vessels and lymph node metastasis was increased. These data indicate that, depending on the context, PDPN expression cannot only affect primary tumor growth but also drives tumor malignancy by increasing the amount of metastasis. Thus, my findings together with published reports underline the crucial role of PDPN in epithelial tumors.

4.6.1 Podoplanin Abrogation Impaired Proliferation *in Vivo*

To elucidate the diminished tumor volume and delayed outgrowth in PDPN-negative tumors, proliferation and apoptosis in tumor cells were examined *in vivo*. Almost all PDPN-positive and -negative tumor cells were proliferating and not apoptotic, as assessed by presence of Ki67 and absence of cleaved caspase-3 expression, respectively. Thus, these results supported *in vitro* data. However, Ki67 is expressed in all phases of the cell cycle. In order to get a more detailed insight, BrdU incorporation upon intraperitoneal injection was additionally determined, since BrdU labels only cells that enter S-phase after injection until mice are sacrificed (~ 4 hours). Statistical analysis revealed that BrdU incorporated less in *Pdpn* KO compared to control tumors, indicating less efficient entry into S-phase upon *Pdpn* loss and thus, slower cycling cells and reduced proliferation. Consequently, smaller tumor volume and delayed tumor outgrowth can be explained by decreased tumor cell proliferation upon *Pdpn* deletion. In previous studies, the *in vivo* GOF of *PDPN* in pancreatic insulin-producing β-cells did neither affect proliferation nor apoptosis, as examined by BrdU and TUNEL assay, respectively (Wicki et al. 2006). Contrary in the lung increased proliferation in type I alveolar cells lacking *Pdpn* was detected using proliferating cell nuclear antigen that is expressed in the nuclei of cells during S-phase (Ramirez et al. 2003). These converse findings as well as my results observed in monolayer and 3D culture systems (chapter 4.2 and 4.3) suggest that the impact of PDPN on proliferation depends on the cellular context. Thus, cell-autonomous pathways that induce proliferation could be excluded since no difference was observed in 2D-cultured cells. In the organotypic co-culture system, soluble factors secreted by fibroblasts might have an impact on tumor cell proliferation; however, BrdU labeling should be performed to get a more detailed insight on whether the efficiency of S-phase entry is impaired upon *Pdpn* loss in 3D context. Altogether, the findings of the *in vivo* model highlighted that PDPN-dependent factors, which are most probably secreted by stromal cells or induced in tumor cells upon the contact with cells of the tumor microenvironment (TME), have an impact on cancer cell proliferation.

4.6.2 Loss of Podoplanin Reduces Invasiveness in an Epithelial-Mesenchymal Transition-Independent Manner

Since I observed an invasive phenotype upon the deletion of *Pdpn in vitro*, I wondered whether tumor cells lacking *Pdpn* showed reduced invasion *in vivo* as well. Invading tumor cells can be defined according to the breakdown of the basement membrane (BM; Spaderna et al. (2006), Watt (2014)). Laminin is one component of BM, which is expressed by fibroblasts and keratinocytes or tumor cells, respectively (Simpson et al. 2011, Watt 2014). Therefore, I detected laminin in combination with K14, which marked basal tumor cells. Quantitative analysis showed a tendency of less invaded tumor cells in *Pdpn* KO tumors, which was, however, not statistically significant. This effect might become significant by increasing sample size since only a small number with three tumors each was analyzed with high variation between samples. Kunita and co-workers injected vulva SCC cells i.d. into nude mice, which resulted in decreased tumor cell invasion upon shRNA-mediated *PDPN* KD (Kunita et al. 2018). They determined invasion according to the circularity of the tumor on hematoxylin and eosin-stained sections. Based on my own experience, i.d. injected tumors can display different shapes from circular via elliptical to even more elongated. Therefore, I suggest using the examination of laminin in combination with K14 as performed in my studies (Spaderna et al. 2006). Moreover, I observed that the majority of invading sheets as well as the tumor bulk of control and *Pdpn* KO tumors did not undergo EMT as tumor cells still expressed E-cadherin and expression of vimentin was not gained. Noteworthy, some single cells at the leading edge co-expressed E-cadherin and vimentin indicating partial EMT. Performing exogenous PDPN overexpression studies, it was shown previously that PDPN resulted in enhanced invasion in an EMT-independent manner in a pancreas *in vivo* model (Wicki et al. 2006). Clinically, PDPN expression was associated with EMT-dependent and -independent invasiveness. E-cadherin expression was attenuated in poorly differentiated cSCC, whereas membranous expression was reported in well-differentiated tumors, which was linked to collective cancer invasion (Lan et al. 2014, Hesse et al. 2016). Furthermore, another study demonstrated partial downregulation of E-cadherin at the invasive front, whereas the EMT-associated transcription factor twist as well as vimentin were upregulated (Toll et al. 2013). The descriptive analysis of human SCC of different entities showed that PDPN and E-cadherin were co-expressed and detected an enlarged invading tumor front indicating collective invasion according to Friedl and colleagues (Wicki et al. 2006, Friedl et al. 2012). Thus, in agreement with literature, in my studies PDPN-positive and -negative cSCC cells invaded collectively without driving an EMT-like behavior, whereas invasiveness was impaired in *Pdpn* KO tumors.

4.7 Potential Mechanism of Podoplanin-Dependent Cancer Cell Proliferation and Invasion

The descriptive analysis as well as the application of LOF experiments performed in this study conclude that PDPN has a decisive role in cSCC carcinogenesis by driving tumor cell proliferation and invasion. Despite that these findings shed some light on the limited knowledge of the molecular basis of cSCC, additional investigations are needed to explore the underlying mechanism of PDPN-dependent cSCC progression to develop novel potential treatment options.

Since proliferation and invasion are distinct hallmarks of cancer, this raises the question of whether there is one or multiple underlying signaling pathways. The transcriptional regulation of PDPN was reported to be controlled by various context-specific signaling pathways and transcription factors in non-tumorigenic cells as well as in *in vivo* models (Li et al. 2015, Renart et al. 2015, Kunita et al. 2018, Quintanilla et al. 2019). So far, several signaling pathways have been proposed in combination with PDPN, however, these investigations focused on SCC or other cellular model systems different from cSCC.

Kunita and co-workers utilized a human papilloma virus-driven mouse model in which the viral oncogenes E6 and E7 are expressed under the control of K14-promoter in immunocompetent FVB/n mice resulting in the development of cervix SCC upon additional treatment with estradiol (Kunita et al. 2018). Gene expression profiling of established cervix SCCs as well as additional *in vitro* and *in vivo* experiments using various SCC cell lines revealed that PDPN upregulation was accompanied by enhanced type-I interferon (IFN) as well as cytokine-mediated signaling pathways in tumor cells. The authors suggested tumor-infiltrating immune cells secrete multiple factors such as IFN-γ, transforming growth factor beta (TGF-β) and interleukin (IL)-6 resulting in the activation of various signaling pathways in tumor cells like STAT1 or SMAD-proteins besides PDPN. Moreover, the shRNA-mediated KD of *PDPN* or *STAT1* diminished tumor volume and invasion in BALB/c nude mice. However, analyzed SCC cells responded differently upon cytokine and/or IFN treatment implying that the impact of PDPN in cancer progression seems to be strongly contextual. Although these authors suggest that SMAD-dependent TGF-β signaling is involved in tumor vulva SCC progression, in cSCC a contradictory role of SMAD-dependent TGF-β signaling was described. Frequent mutations in the TGF-β receptors or diminished expression of SMAD proteins have been reported suggesting a tumor suppressive function of TGF-β in this skin cancer entity (Hoot et al. 2008, Pickering et al. 2014). Moreover, Rose and co-workers revealed that cSCC progression is associated with the abrogation of canonical TGF-β signaling pathway (Rose et al. 2018).

Notably, TGF-β can also trigger other non-SMAD pathways and downstream targets such as PI3K or MAPK resulting in enhanced proliferation and invasion (reviewed in Akhurst (2017)). This non-canonical TGF-β signaling has been already associated with PDPN-dependent malignant SCC progression. Li and colleagues demonstrated in oral SCC (OSCC) that PDPN was upregulated in tumor cells at the invasive front together with the Cdc42 GTPase and complementing GOF and LOF *in vitro* approaches indicated induced invasion in a PDPN-Cdc42-dependent manner (Li et al. 2015). Recently, the same authors described the underlying mechanism that is based on paracrine PDPN-TGF-β signaling (Li et al. 2018). Briefly, PDPN-positive OSCC tumor cells secret TGF-β which activates fibroblasts. Consequently, CAFs secrete TGF-β as well that trans-induces epidermal growth factor receptor (EGFR) signaling. Subsequently, EGFR activates phosphoinositide 3-kinase (PI3K)/AKT and mitogen-activated protein kinase (MAPK) pathways resulting in proliferation and invasion of OSCC cells. This non-canonical TGF-β signal transduction might also explain the effect observed in BCM, in which PDPN-positive tumor cells alone transmigrated more efficiently through matrigel than their PDPN-negative counterparts that indicates a cell-autonomous or paracrine signaling between tumor cells via TGF-β *in vitro*. Noteworthy, non-canonical TGF-β signaling was not reported yet in cSCC progression and besides trans-inducing EGFR, TGF-β activates Rho GTPases as well that induces cytoskeletal rearrangement and thus, enhanced migration and invasion (Edlund et al. 2002). Several reports have shown that PDPN-induced Rho GTPase activity is mediated through ERM proteins (Martin-Villar et al. 2006, Wicki et al. 2006, Pedro and Shields 2018). However, whether TGF-β modulates the cytoskeleton in an ERM-dependent or -independent manner was not shown yet.

Besides IFNs, cytokines or growth factors, proliferation can also be induced by ezrin. Previous *in vitro* studies utilizing epithelial kidney cells demonstrated that ezrin interacted with the regulatory subunit of the PI3K resulting in PI3K activation and thus, in activation of the PI3K/AKT pathway and proliferation (Gautreau et al. 1999). Chuan and colleagues demonstrated that c-Myc enhanced ezrin expression resulting in increased motility of human prostate cancer cells *in vitro* (Chuan et al. 2010). Moreover, they reported a positive regulation of c-Myc by ezrin that was mediated by the activation of AKT and downregulation the glycogen synthase kinase 3 beta (GSK-3β). Notably, proliferation and invasion were diminished in dominant negative ezrin variants mutants *in vitro*. In another *in vitro* study, reduced proliferation was observed upon small interfering RNA (siRNA)-mediated ezrin KD in lung cancer cells (Li et al. 2012).

In conclusion, various potential signaling pathways and most interestingly the TGF-β, IL-6 and IFN-γ cascade as well as the PDPN downstream signaling via ERM proteins (also discussed in chapter 4.4) should be considered while defining the impact of PDPN on

cSCC progression. There are still many unanswered question, hence, further investigations are required in order to unravel the underlying molecular mechanism of PDPN-induced cSCC tumor cell proliferation and invasion. Apart from the potential role of the IL-6 and TGF-β signaling as well as ERM proteins, one should keep in mind that other pathways or additional interaction partners might contribute to the mechanism as well.

4.8 Conclusion and Future Perspective

In this dissertation I showed that PDPN acts as a driver of tumorigenesis in differentiated cSCC. *In vitro* and *in vivo* LOF experiments demonstrated that PDPN induces tumor cell proliferation and invasion. Additional future studies are required to define involved signaling pathways.

To tackle this, I suggest generating PDPN mutants in order to evaluate whether the interaction of PDPN with its known extracellular partner CLEC-2, the IC binding of the ERM proteins or possibly other, yet unknown proteins are essential for tumor cell invasion and proliferation. For this purpose, I have initiated experiments, in which specific point mutations are introduced into the murine *Pdpn* gene sequence that inhibit the known specific interactions: (i) mutation of the CLEC-2 binding site resulting in the transition of Thr34 to Ala34; (ii) change of charged to uncharged amino acids in the IC amino acid sequence being responsible for ERM-binding (KK…R→NN…Q). In previous studies, the same *Pdpn* mutants were generated and showed a diminished PDPN function. Bianchi and colleagues revealed that the mutant PDPN-CLEC-2 binding site resulted in reduced CLEC-2 activation *in vitro* and prolonged bleeding time due to decreased platelet activation *in vivo* (Bianchi et al. 2014). Moreover, Martín-Villar and co-workers mutated the ERM binding site and ectopically overexpressed this mutant in MDCK cells, which resulted in reduced migratory ability compared to PDPN WT-expressing cells (Martin-Villar et al. 2006). The generated mutants will be used in different functional *in vitro* and *in vivo* experiments, as performed in this study and will give insights into interaction partners and signaling pathways that contribute to PDPN-induced proliferation and invasion in cSCC.

Various signaling pathways have already been described that are involved or accompany PDPN-driven SCC carcinogenesis. Therefore, I propose to perform a gene expression analysis of tumor samples. Depending on the outcome of the *Pdpn* mutant study, genetic profiles of tumors derived from control, *Pdpn* KO and mutant cSCC cells should be examined. This analysis will reveal whether similar or other signaling pathways as described are differentially regulated in differentiated cSCC.

Altogether, these findings will further contribute to the understanding whether PDPN, its interaction partners or IC downstream effectors might represent a promising target for the development of a novel cSCC therapy. PDPN is expressed in different health tissue and it has been demonstrated that its molecular mass varies between tissues. This implies that the post-translational addition of sugar residues might be organ-specific. The development of a cancer-specific PDPN antibody that only binds to PDPN, which is expressed by tumor cells but not by healthy tissue, indicated that the glycosylation can be modified in a tumor-specific manner (Kato and Kaneko 2014). Thus, such antibodies might represent a possibility to develop chimeric antigen receptor (CAR) T cells, which can specifically target tumor cells that express PDPN with an abnormal glycosylation. However, a potential drawback might be the differential modification of the sugar residues between individual patients, which has not been investigated yet. Notably, *in vitro* protein expression analysis of different cSCC cell lines established from various patient tumor samples implies that the glycosylation might vary between individuals as well as primary and metastatic lesions (data not shown). Thus, an antibody that targets cancer-specific glycosylation of PDPN would not represent the most appropriate therapeutic strategy, since not all tumors might display similar glycosylation pattern, which would provoke the development of personalized antibody therapy.

Therefore, the proposed mechanistical study using *Pdpn* mutants is crucial to define the mode of action in PDPN-dependent cSCC progression. If the CLEC-2 mutant phenocopies the behavior of *Pdpn* KO cells, future studies should focus on the interaction of PDPN and CLEC-2 in cSCC as well as on the discovery of potential additional PDPN interaction partners. Several antibodies were developed that neutralize the PDPN-CLEC-2 interaction and subsequent PDPN-mediated platelet aggregation as well as pulmonary metastasis *in vitro* and *in vivo* approaches (reviewed in Takemoto et al. (2017)). Furthermore, tumor cells that are covered by platelets are protected from shear stress and elimination by immune cells. However, the validation of developed antibodies strongly depends on appropriate model systems that are limited and moreover, the blockage of this interaction can cause enhanced bleeding in patients with thrombocytopenia due to chemotherapeutic toxicity. Thus, further investigations are still required. If the cytoplasmic tail mimics the effect of *Pdpn* KO cells, the IC signaling via ERM and Rho GTPases might represent potential targets. It is important to keep in mind that also other transmembrane proteins like CD44, which is commonly upregulated in epithelial cancers, can trigger migration via the induction of ERM proteins as well (Hirao et al. 1996, Yonemura et al. 1998, Isacke and Yarwood 2002). Since the ERM binding site in CD44 and PDPN differ, the blockage of their downstream targets like ERM proteins or Rho GTPases would be recommendable to prevent compensatory mechanisms. The small-molecule Quinocarmycin was reported to

target radixin and thereby inhibiting its interaction with actin and CD44 (Kahsai et al. 2006). However, a previously performed clinical phase I trial in refractory solid malignancies demonstrated that this drug is poorly tolerable besides its inability to reach an inhibitory effect *in vivo* tumor growth (Bunnell 2001). Consequently, it was not investigated further in phase II studies. Inhibitors blocking Rho GTPases and their effectors are already under investigation, however, the biggest challenge is their druggability and inhibitors are still at early stages of development (reviewed in Lin and Zheng (2015)).

In conclusion, the described interventions targeting PDPN or its known extracellular or IC partners would rather impair further progression than eradicating the existing tumor. The blockage of PDPN-CLEC-2 axis would increase the exposure to tumor-infiltrating immune cells, since tumor cell coverage by platelets would be impaired as well as the activation of DCs would be diminished, which normally suppress the pro-tumorigenic immune response via T cells (Acton et al. 2014). Inhibiting the IC downstream signaling would result in reduced tumor cell invasion as cytoskeletal remodeling mediated via ERM or Rho GTPases would be impaired. Although these proposed strategies would not eliminate the tumor, they would represent a first success, since locally advanced late-stage tumors have a poor prognostic outcome (Vinicius de et al. 2011). In order to eradicate cSCC cells, signaling pathways need to be identified, which accompany PDPN-expressing tumor cells at the invasive front or which are dependent on PDPN expression.

5 REFERENCES

5 REFERENCES

ABEL EL, ANGEL JM, KIGUCHI K AND DIGIOVANNI J. 2009. Multi-stage chemical carcinogenesis in mouse skin: fundamentals and applications. Nat Protoc 4: 1350-1362.

ACKERMAN AB AND MONES JM. 2006. Solar (actinic) keratosis is squamous cell carcinoma. Br J Dermatol 155: 9-22.

ACTON SE ET AL. 2014. Dendritic cells control fibroblastic reticular network tension and lymph node expansion. Nature 514: 498-502.

AKHURST RJ. 2017. Targeting TGF-beta Signaling for Therapeutic Gain. Cold Spring Harb Perspect Biol 9.

ALAM M AND RATNER D. 2001. Cutaneous squamous-cell carcinoma. N Engl J Med 344: 975-983.

ALONSO L AND FUCHS E. 2003. Stem cells of the skin epithelium. Proc Natl Acad Sci U S A 100 Suppl 1: 11830-11835.

ANGEL P, SZABOWSKI A AND SCHORPP-KISTNER M. 2001. Function and regulation of AP-1 subunits in skin physiology and pathology. Oncogene 20: 2413-2423.

ASTARITA JL, ACTON SE AND TURLEY SJ. 2012. Podoplanin: emerging functions in development, the immune system, and cancer. Front Immunol 3: 283.

AUGSBURGER D ET AL. 2017. Current diagnostics and treatment of fibrosarcoma - perspectives for future therapeutic targets and strategies. Oncotarget 8: 104638-104653.

BAARS S, BAUER C, SZABOWSKI S, HARTENSTEIN B AND ANGEL P. 2015. Epithelial deletion of podoplanin is dispensable for re-epithelialization of skin wounds. Exp Dermatol 24: 785-787.

BASTIAN BC. 2014. The molecular pathology of melanoma: an integrated taxonomy of melanocytic neoplasia. Annu Rev Pathol 9: 239-271.

BENJAMIN CL AND ANANTHASWAMY HN. 2007. p53 and the pathogenesis of skin cancer. Toxicol Appl Pharmacol 224: 241-248.

BERENBLUM I AND SHUBIK P. 1947. A new, quantitative, approach to the study of the stages of chemical cartinogenesis in the mouse's skin. Br J Cancer 1: 383-391.

BERNING M, PRATZEL-WUNDER S, BICKENBACH JR AND BOUKAMP P. 2015. Three-Dimensional In Vitro Skin and Skin Cancer Models Based on Human Fibroblast-Derived Matrix. Tissue Eng Part C Methods 21: 958-970.

BIANCHI R, FISCHER E, YUEN D, ERNST E, OCHSENBEIN AM, CHEN L, OTTO VI AND DETMAR M. 2014. Mutation of threonine 34 in mouse podoplanin-Fc reduces CLEC-2 binding and toxicity in vivo while retaining antilymphangiogenic activity. J Biol Chem 289: 21016-21027.

BLOOMFIELD KL, BALDWIN BL, HARKIN DG AND TONISSEN KF. 2001. Modification of the Boyden chamber to improve uniformity of cell invasion of matrigel-coated membranes. Biotechniques 31: 1242, 1244, 1246.

BONNOTTE B, GOUGH M, PHAN V, AHMED A, CHONG H, MARTIN F AND VILE RG. 2003. Intradermal injection, as opposed to subcutaneous injection, enhances immunogenicity and suppresses tumorigenicity of tumor cells. Cancer Res 63: 2145-2149.

BOUKAMP P. 2005a. Non-melanoma skin cancer: what drives tumor development and progression? Carcinogenesis 26: 1657-1667.

BOUKAMP P. 2005b. UV-induced skin cancer: similarities--variations. Journal der Deutschen Dermatologischen Gesellschaft = Journal of the German Society of Dermatology : JDDG 3: 493-503.

BOUKAMP P, BREITKREUTZ D, STARK HJ AND FUSENIG NE. 1990. Mesenchyme-mediated and endogenous regulation of growth and differentiation of human skin keratinocytes derived from different body sites. Differentiation 44: 150-161.

BOUKAMP P, PETRUSSEVSKA RT, BREITKREUTZ D, HORNUNG J, MARKHAM A AND FUSENIG NE. 1988. Normal keratinization in a spontaneously immortalized aneuploid human keratinocyte cell line. J Cell Biol 106: 761-771.

BOUTWELL RK. 1964. Some Biological Aspects of Skin Carcinogenisis. Prog Exp Tumor Res 4: 207-250.

BREITENEDER-GELEFF S ET AL. 1999. Angiosarcomas express mixed endothelial phenotypes of blood and lymphatic capillaries: podoplanin as a specific marker for lymphatic endothelium. Am J Pathol 154: 385-394.

BRETSCHER A, EDWARDS K AND FEHON RG. 2002. ERM proteins and merlin: integrators at the cell cortex. Nat Rev Mol Cell Biol 3: 586-599.

BURTON KA, ASHACK KA AND KHACHEMOUNE A. 2016. Cutaneous Squamous Cell Carcinoma: A Review of High-Risk and Metastatic Disease. Am J Clin Dermatol 17: 491-508.

CANDI E, SCHMIDT R AND MELINO G. 2005. The cornified envelope: a model of cell death in the skin. Nat Rev Mol Cell Biol 6: 328-340.

CHUAN YC, IGLESIAS-GATO D, FERNANDEZ-PEREZ L, CEDAZO-MINGUEZ A, PANG ST, NORSTEDT G, POUSETTE A AND FLORES-MORALES A. 2010. Ezrin mediates c-Myc actions in prostate cancer cell invasion. Oncogene 29: 1531-1542.

CUENI LN, HEGYI I, SHIN JW, ALBINGER-HEGYI A, GRUBER S, KUNSTFELD R, MOCH H AND DETMAR M. 2010. Tumor lymphangiogenesis and metastasis to lymph nodes induced by cancer cell expression of podoplanin. Am J Pathol 177: 1004-1016.

DAVIES LC, ROSAS M, JENKINS SJ, LIAO CT, SCURR MJ, BROMBACHER F, FRASER DJ, ALLEN JE, JONES SA AND TAYLOR PR. 2013. Distinct bone marrow-derived and tissue-resident macrophage lineages proliferate at key stages during inflammation. Nat Commun 4: 1886.

DOUGLAS YL, MAHTAB EA, JONGBLOED MR, UHRIN P, ZAUJEC J, BINDER BR, SCHALIJ MJ, POELMANN RE, DERUITER MC AND GITTENBERGER-DE GROOT AC. 2009. Pulmonary vein, dorsal atrial wall and atrial septum abnormalities in podoplanin knockout mice with disturbed posterior heart field contribution. Pediatr Res 65: 27-32.

DURCHDEWALD M, GUINEA-VINIEGRA J, HAAG D, RIEHL A, LICHTER P, HAHN M, WAGNER EF, ANGEL P AND HESS J. 2008. Podoplanin is a novel fos target gene in skin carcinogenesis. Cancer Res 68: 6877-6883.

EDLUND S, LANDSTRÖM M, HELDIN C-H AND ASPENSTRÖM P. 2002. Transforming growth factor-beta-induced mobilization of actin cytoskeleton requires signaling by small GTPases Cdc42 and RhoA. Molecular biology of the cell 13: 902-914.

EFERL R AND CASANOVA E 2015. Mouse Models of Cancer. Methods in Molecular Biology, 1 ed: Humana Press.

EFERL R AND WAGNER EF. 2003. AP-1: a double-edged sword in tumorigenesis. Nat Rev Cancer 3: 859-868.

FARR AG, BERRY ML, KIM A, NELSON AJ, WELCH MP AND ARUFFO A. 1992. Characterization and cloning of a novel glycoprotein expressed by stromal cells in T-dependent areas of peripheral lymphoid tissues. J Exp Med 176: 1477-1482.

FEHON RG, MCCLATCHEY AI AND BRETSCHER A. 2010. Organizing the cell cortex: the role of ERM proteins. Nat Rev Mol Cell Biol 11: 276-287.

FERNANDEZ-MUNOZ B, YURRITA MM, MARTIN-VILLAR E, CARRASCO-RAMIREZ P, MEGIAS D, RENART J AND QUINTANILLA M. 2011. The transmembrane domain of podoplanin is required for its association with lipid rafts and the induction of epithelial-mesenchymal transition. Int J Biochem Cell Biol 43: 886-896.

FERNANDEZ FIGUERAS MT. 2017. From actinic keratosis to squamous cell carcinoma: pathophysiology revisited. J Eur Acad Dermatol Venereol 31 Suppl 2: 5-7.

FINCH JS, ALBINO HE AND BOWDEN GT. 1996. Quantitation of early clonal expansion of two mutant 61st codon c-Ha-ras alleles in DMBA/TPA treated mouse skin by nested PCR/RFLP. Carcinogenesis 17: 2551-2557.

FRIEDL P, SAHAI E, WEISS S AND YAMADA KM. 2012. New dimensions in cell migration. Nat Rev Mol Cell Biol 13: 743-747.

FU J ET AL. 2008. Endothelial cell O-glycan deficiency causes blood/lymphatic misconnections and consequent fatty liver disease in mice. J Clin Invest 118: 3725-3737.

FUCHS E. 2008. Skin stem cells: rising to the surface. J Cell Biol 180: 273-284.

FUCHS E AND GREEN H. 1980. Changes in keratin gene expression during terminal differentiation of the keratinocyte. Cell 19: 1033-1042.

FUCHS E AND RAGHAVAN S. 2002. Getting under the skin of epidermal morphogenesis. Nature reviews Genetics 3: 199-209.

FUKATA Y, AMANO M AND KAIBUCHI K. 2001. Rho-Rho-kinase pathway in smooth muscle contraction and cytoskeletal reorganization of non-muscle cells. Trends Pharmacol Sci 22: 32-39.

FUSENIG NE, AMER SM, BOUKAMP P AND WORST PK. 1978. Characteristics of chemically transformed mouse epidermal cells in vitro and in vivo. Bull Cancer 65: 271-279.

GANDARILLAS A, SCHOLL FG, BENITO N, GAMALLO C AND QUINTANILLA M. 1997. Induction of PA2.26, a cell-surface antigen expressed by active fibroblasts, in mouse epidermal keratinocytes during carcinogenesis. Mol Carcinog 20: 10-18.

GARY R AND BRETSCHER A. 1995. Ezrin self-association involves binding of an N-terminal domain to a normally masked C-terminal domain that includes the F-actin binding site. Mol Biol Cell 6: 1061-1075.

GAUTREAU A, POULLET P, LOUVARD D AND ARPIN M. 1999. Ezrin, a plasma membrane-microfilament linker, signals cell survival through the phosphatidylinositol 3-kinase/Akt pathway. Proc Natl Acad Sci U S A 96: 7300-7305.

GEBHARDT C ET AL. 2008. RAGE signaling sustains inflammation and promotes tumor development. J Exp Med 205: 275-285.

GERDES MJ ET AL. 2006. Activator protein-1 activity regulates epithelial tumor cell identity. Cancer Res 66: 7578-7588.

GITTENBERGER-DE GROOT AC, MAHTAB EA, HAHURIJ ND, WISSE LJ, DERUITER MC, WIJFFELS MC AND POELMANN RE. 2007. Nkx2.5-negative myocardium of the posterior heart field and its correlation with podoplanin expression in cells from the developing cardiac pacemaking and conduction system. Anat Rec (Hoboken) 290: 115-122.

HARVEY M, MCARTHUR MJ, MONTGOMERY CA, JR., BUTEL JS, BRADLEY A AND DONEHOWER LA. 1993. Spontaneous and carcinogen-induced tumorigenesis in p53-deficient mice. Nat Genet 5: 225-229.

HESSE K, SATZGER I, SCHACHT V, KOTHER B, HILLEN U, KLODE J, SCHAPER K AND GUTZMER R. 2016. Characterisation of Prognosis and Invasion of Cutaneous Squamous Cell Carcinoma by Podoplanin and E-Cadherin Expression. Dermatology 232: 558-565.

HIRAO M, SATO N, KONDO T, YONEMURA S, MONDEN M, SASAKI T, TAKAI Y, TSUKITA S AND TSUKITA S. 1996. Regulation mechanism of ERM (ezrin/radixin/moesin) protein/plasma membrane association: possible involvement of phosphatidylinositol turnover and Rho-dependent signaling pathway. J Cell Biol 135: 37-51.

HONMA M, MINAMI-HORI M, TAKAHASHI H AND IIZUKA H. 2012. Podoplanin expression in wound and hyperproliferative psoriatic epidermis: regulation by TGF-beta and STAT-3 activating cytokines, IFN-gamma, IL-6, and IL-22. J Dermatol Sci 65: 134-140.

HOOT KE, LIGHTHALL J, HAN G, LU S-L, LI A, JU W, KULESZ-MARTIN M, BOTTINGER E AND WANG X-J. 2008. Keratinocyte-specific Smad2 ablation results in increased epithelial-mesenchymal transition during skin cancer formation and progression. The Journal of clinical investigation 118: 2722-2732.

HUANG PY AND BALMAIN A. 2014. Modeling cutaneous squamous carcinoma development in the mouse. Cold Spring Harb Perspect Med 4: a013623.

ISACKE CM AND YARWOOD H. 2002. The hyaluronan receptor, CD44. Int J Biochem Cell Biol 34: 718-721.

JENNINGS L AND SCHMULTS CD. 2010. Management of high-risk cutaneous squamous cell carcinoma. J Clin Aesthet Dermatol 3: 39-48.

JU T AND CUMMINGS RD. 2002. A unique molecular chaperone Cosmc required for activity of the mammalian core 1 beta 3-galactosyltransferase. Proc Natl Acad Sci U S A 99: 16613-16618.

KAHSAI AW, ZHU S, WARDROP DJ, LANE WS AND FENTEANY G. 2006. Quinocarmycin Analog DX-52-1 Inhibits Cell Migration and Targets Radixin, Disrupting Interactions of Radixin with Actin and CD44. Chemistry & Biology 13: 973-983.

KANEKO MK ET AL. 2007. Functional glycosylation of human podoplanin: glycan structure of platelet aggregation-inducing factor. FEBS Lett 581: 331-336.

KANELLOS G AND FRAME MC. 2016. Cellular functions of the ADF/cofilin family at a glance. J Cell Sci 129: 3211-3218.

KATO Y, FUJITA N, KUNITA A, SATO S, KANEKO M, OSAWA M AND TSURUO T. 2003. Molecular identification of Aggrus/T1alpha as a platelet aggregation-inducing factor expressed in colorectal tumors. J Biol Chem 278: 51599-51605.

KATO Y AND KANEKO MK. 2014. A cancer-specific monoclonal antibody recognizes the aberrantly glycosylated podoplanin. Sci Rep 4: 5924.

KEMP CJ. 2005. Multistep skin cancer in mice as a model to study the evolution of cancer cells. Semin Cancer Biol 15: 460-473.

KERJASCHKI D ET AL. 2004. Lymphatic neoangiogenesis in human kidney transplants is associated with immunologically active lymphocytic infiltrates. J Am Soc Nephrol 15: 603-612.

KERSTEN K, DE VISSER KE, VAN MILTENBURG MH AND JONKERS J. 2017. Genetically engineered mouse models in oncology research and cancer medicine. EMBO Mol Med 9: 137-153.

KLEINMAN HK AND JACOB K. 2001. Invasion assays. Curr Protoc Cell Biol Chapter 12: Unit 12 12.

KRISHNAN H, OCHOA-ALVAREZ JA, SHEN Y, NEVEL E, LAKSHMINARAYANAN M, WILLIAMS MC, RAMIREZ MI, MILLER WT AND GOLDBERG GS. 2013. Serines in the intracellular tail of podoplanin (PDPN) regulate cell motility. J Biol Chem 288: 12215-12221.

KRISHNAN H, RETZBACH EP, RAMIREZ MI, LIU T, LI H, MILLER WT AND GOLDBERG GS. 2015. PKA and CDK5 can phosphorylate specific serines on the intracellular domain of podoplanin (PDPN) to inhibit cell motility. Exp Cell Res 335: 115-122.

KUMPF S ET AL. 2012. Hairless promotes PPARgamma expression and is required for white adipogenesis. EMBO Rep 13: 1012-1020.

KUNITA A, BAERISWYL V, MEDA C, CABUY E, TAKESHITA K, GIRAUDO E, WICKI A, FUKAYAMA M AND CHRISTOFORI G. 2018. Inflammatory cytokines induce podoplanin expression at the tumor invasive front. Am J Pathol.

LAN YJ, CHEN H, CHEN JQ, LEI QH, ZHENG M AND SHAO ZR. 2014. Immunolocalization of vimentin, keratin 17, Ki-67, involucrin, beta-catenin and E-cadherin in cutaneous squamous cell carcinoma. Pathol Oncol Res 20: 263-266.

LEDERLE W, HARTENSTEIN B, MEIDES A, KUNZELMANN H, WERB Z, ANGEL P AND MUELLER MM. 2010. MMP13 as a stromal mediator in controlling persistent angiogenesis in skin carcinoma. Carcinogenesis 31: 1175-1184.

LEITER U, KEIM U, EIGENTLER T, KATALINIC A, HOLLECZEK B, MARTUS P AND GARBE C. 2017. Incidence, Mortality, and Trends of Nonmelanoma Skin Cancer in Germany. J Invest Dermatol 137: 1860-1867.

LI Q, GAO H, XU H, WANG X, PAN Y, HAO F, QIU X, STOECKER M, WANG E AND WANG E. 2012. Expression of ezrin correlates with malignant phenotype of lung cancer, and in vitro knockdown of ezrin reverses the aggressive biological behavior of lung cancer cells. Tumour Biol 33: 1493-1504.

LI Y-Y, ZHOU C-X AND GAO Y. 2018. Interaction between oral squamous cell carcinoma cells and fibroblasts through TGF-β1 mediated by podoplanin. Experimental Cell Research 369: 43-53.

LI YY, ZHOU CX AND GAO Y. 2015. Podoplanin promotes the invasion of oral squamous cell carcinoma in coordination with MT1-MMP and Rho GTPases. Am J Cancer Res 5: 514-529.

LIN Y AND ZHENG Y. 2015. Approaches of targeting Rho GTPases in cancer drug discovery. Expert Opin Drug Discov 10: 991-1010.

LOMAS A, LEONARDI-BEE J AND BATH-HEXTALL F. 2012. A systematic review of worldwide incidence of nonmelanoma skin cancer. Br J Dermatol 166: 1069-1080.

LOWE KL ET AL. 2015. Podoplanin and CLEC-2 drive cerebrovascular patterning and integrity during development. Blood 125: 3769-3777.

MACNEIL S. 2007. Progress and opportunities for tissue-engineered skin. Nature 445: 874-880.

MARTIN-VILLAR E, BORDA-D'AGUA B, CARRASCO-RAMIREZ P, RENART J, PARSONS M, QUINTANILLA M AND JONES GE. 2015. Podoplanin mediates ECM degradation by squamous carcinoma cells through control of invadopodia stability. Oncogene 34: 4531-4544.

MARTIN-VILLAR E, FERNANDEZ-MUNOZ B, PARSONS M, YURRITA MM, MEGIAS D, PEREZ-GOMEZ E, JONES GE AND QUINTANILLA M. 2010. Podoplanin associates with CD44 to promote directional cell migration. Mol Biol Cell 21: 4387-4399.

MARTIN-VILLAR E, MEGIAS D, CASTEL S, YURRITA MM, VILARO S AND QUINTANILLA M. 2006. Podoplanin binds ERM proteins to activate RhoA and promote epithelial-mesenchymal transition. J Cell Sci 119: 4541-4553.

MARTIN-VILLAR E, SCHOLL FG, GAMALLO C, YURRITA MM, MUNOZ-GUERRA M, CRUCES J AND QUINTANILLA M. 2005. Characterization of human PA2.26 antigen (T1alpha-2, podoplanin), a small membrane mucin induced in oral squamous cell carcinomas. Int J Cancer 113: 899-910.

MEIDES A, GUTSCHALK CM, DEVEL L, BEAU F, CZARNY B, HENSLER S, NEUGEBAUER J, DIVE V, ANGEL P AND MUELLER MM. 2014. Effects of selective MMP-13 inhibition in squamous cell carcinoma depend on estrogen. Int J Cancer 135: 2749-2759.

MICALLEF L, BELAUBRE F, PINON A, JAYAT-VIGNOLES C, DELAGE C, CHARVERON M AND SIMON A. 2009. Effects of extracellular calcium on the growth-differentiation switch in immortalized keratinocyte HaCaT cells compared with normal human keratinocytes. Exp Dermatol 18: 143-151.

MIGDEN MR ET AL. 2018. PD-1 Blockade with Cemiplimab in Advanced Cutaneous Squamous-Cell Carcinoma. N Engl J Med 379: 341-351.

MUFFLER S, STARK HJ, AMOROS M, FALKOWSKA-HANSEN B, BOEHNKE K, BUHRING HJ, MARME A, BICKENBACH JR AND BOUKAMP P. 2008. A stable niche supports long-term maintenance of human epidermal stem cells in organotypic cultures. Stem Cells 26: 2506-2515.

NAGARAJAN P, ASGARI MM, GREEN AC, GUHAN SM, ARRON ST, PROBY CM, ROLLISON DE, HARWOOD CA AND TOLAND AE. 2018. Keratinocyte Carcinomas: Current concepts and future research priorities. Clin Cancer Res.

NAKAZAWA Y, SATO S, NAITO M, KATO Y, MISHIMA K, ARAI H, TSURUO T AND FUJITA N. 2008. Tetraspanin family member CD9 inhibits Aggrus/podoplanin-induced platelet aggregation and suppresses pulmonary metastasis. Blood 112: 1730-1739.

NAVARRO-NUNEZ L, LANGAN SA, NASH GB AND WATSON SP. 2013. The physiological and pathophysiological roles of platelet CLEC-2. Thromb Haemost 109: 991-998.

NOSE K, SAITO H AND KUROKI T. 1990. Isolation of a gene sequence induced later by tumor-promoting 12-O-tetradecanoylphorbol-13-acetate in mouse osteoblastic cells (MC3T3-E1) and expressed constitutively in ras-transformed cells. Cell Growth Differ 1: 511-518.

PAN Y ET AL. 2014. Podoplanin requires sialylated O-glycans for stable expression on lymphatic endothelial cells and for interaction with platelets. Blood 124: 3656-3665.

PEDRO L AND SHIELDS JD. 2018. Podoplanin interaction with caveolin-1 promotes tumour cell migration and invasion. bioRxiv: 488304.

PICKERING CR ET AL. 2014. Mutational landscape of aggressive cutaneous squamous cell carcinoma. Clinical cancer research : an official journal of the American Association for Cancer Research 20: 6582-6592.

POLTAVETS V, KOCHETKOVA M, PITSON SM AND SAMUEL MS. 2018. The Role of the Extracellular Matrix and Its Molecular and Cellular Regulators in Cancer Cell Plasticity. Front Oncol 8: 431.

POPP S, WALTERING S, HERBST C, MOLL I AND BOUKAMP P. 2002. UV-B-type mutations and chromosomal imbalances indicate common pathways for the development of Merkel and skin squamous cell carcinomas. Int J Cancer 99: 352-360.

POPP S, WALTERING S, HOLTGREVE-GREZ H, JAUCH A, PROBY C, LEIGH IM AND BOUKAMP P. 2000. Genetic characterization of a human skin carcinoma progression model: from primary tumor to metastasis. J Invest Dermatol 115: 1095-1103.

PROBY CM, PURDIE KJ, SEXTON CJ, PURKIS P, NAVSARIA HA, STABLES JN AND LEIGH IM. 2000. Spontaneous keratinocyte cell lines representing early and advanced stages of malignant transformation of the epidermis. Exp Dermatol 9: 104-117.

PYZOCHA NK, RAN FA, HSU PD AND ZHANG F. 2014. RNA-guided genome editing of mammalian cells. Methods Mol Biol 1114: 269-277.

QUINTANILLA M, MONTERO-MONTERO L, RENART J AND MARTIN-VILLAR E. 2019. Podoplanin in Inflammation and Cancer. Int J Mol Sci 20.

RAMIREZ MI, MILLIEN G, HINDS A, CAO Y, SELDIN DC AND WILLIAMS MC. 2003. T1alpha, a lung type I cell differentiation gene, is required for normal lung cell proliferation and alveolus formation at birth. Dev Biol 256: 61-72.

RATUSHNY V, GOBER MD, HICK R, RIDKY TW AND SEYKORA JT. 2012. From keratinocyte to cancer: the pathogenesis and modeling of cutaneous squamous cell carcinoma. J Clin Invest 122: 464-472.

REINERS JJ, JR. AND SINGH KP. 1997. Susceptibility of 129/SvEv mice in two-stage carcinogenesis protocols to 12-O-tetradecanoylphorbol-13-acetate promotion. Carcinogenesis 18: 593-597.

RENART J, CARRASCO-RAMIREZ P, FERNANDEZ-MUNOZ B, MARTIN-VILLAR E, MONTERO L, YURRITA MM AND QUINTANILLA M. 2015. New insights into the role of podoplanin in epithelial-mesenchymal transition. Int Rev Cell Mol Biol 317: 185-239.

RHEINWALD JG AND BECKETT MA. 1981. Tumorigenic keratinocyte lines requiring anchorage and fibroblast support cultured from human squamous cell carcinomas. Cancer Res 41: 1657-1663.

RISHI AK, JOYCE-BRADY M, FISHER J, DOBBS LG, FLOROS J, VANDERSPEK J, BRODY JS AND WILLIAMS MC. 1995. Cloning, characterization, and development expression of a rat lung alveolar type I cell gene in embryonic endodermal and neural derivatives. Dev Biol 167: 294-306.

ROSE AM ET AL. 2018. Reduced SMAD2/3 activation independently predicts increased depth of human cutaneous squamous cell carcinoma. Oncotarget 9: 14552-14566.

RUSS WP AND ENGELMAN DM. 2000. The GxxxG motif: a framework for transmembrane helix-helix association. J Mol Biol 296: 911-919.

SAEZ E, RUTBERG SE, MUELLER E, OPPENHEIM H, SMOLUK J, YUSPA SH AND SPIEGELMAN BM. 1995. c-fos is required for malignant progression of skin tumors. Cell 82: 721-732.

SCHACHT V, DADRAS SS, JOHNSON LA, JACKSON DG, HONG YK AND DETMAR M. 2005. Up-regulation of the lymphatic marker podoplanin, a mucin-type transmembrane glycoprotein, in human squamous cell carcinomas and germ cell tumors. Am J Pathol 166: 913-921.

SCHACHT V ET AL. 2003. T1alpha/podoplanin deficiency disrupts normal lymphatic vasculature formation and causes lymphedema. EMBO J 22: 3546-3556.

SCHOLL FG, GAMALLO C AND QUINTANILLA M. 2000. Ectopic expression of PA2.26 antigen in epidermal keratinocytes leads to destabilization of adherens junctions and malignant progression. Lab Invest 80: 1749-1759.

SCHOLL FG, GAMALLO C, VILARO S AND QUINTANILLA M. 1999. Identification of PA2.26 antigen as a novel cell-surface mucin-type glycoprotein that induces plasma membrane extensions and increased motility in keratinocytes. J Cell Sci 112 (Pt 24): 4601-4613.

SCHNEIDER J 2019. Funktion des Transmembranproteins Podoplanin in der Proliferation und Nachweis der intrazellulären Signaltransduktion im kutanen Plattenepithelkarzinom.

SCHWARZ M, MUNZEL PA AND BRAEUNING A. 2013. Non-melanoma skin cancer in mouse and man. Arch Toxicol 87: 783-798.

SEKIGUCHI T, TAKEMOTO A, TAKAGI S, TAKATORI K, SATO S, TAKAMI M AND FUJITA N. 2015. Targeting a novel domain in podoplanin for inhibiting plateletmediated tumor metastasis. Oncotarget.

SIBILIA M, FLEISCHMANN A, BEHRENS A, STINGL L, CARROLL J, WATT FM, SCHLESSINGER J AND WAGNER EF. 2000. The EGF receptor provides an essential survival signal for SOS-dependent skin tumor development. Cell 102: 211-220.

SIMPSON CL, PATEL DM AND GREEN KJ. 2011. Deconstructing the skin: cytoarchitectural determinants of epidermal morphogenesis. Nat Rev Mol Cell Biol 12: 565-580.

SPADERNA S, SCHMALHOFER O, HLUBEK F, BERX G, EGER A, MERKEL S, JUNG A, KIRCHNER T AND BRABLETZ T. 2006. A transient, EMT-linked loss of basement membranes indicates metastasis and poor survival in colorectal cancer. Gastroenterology 131: 830-840.

STANLEY PL, STEINER S, HAVENS M AND TRAMPOSCH KM. 1991. Mouse skin inflammation induced by multiple topical applications of 12-O-tetradecanoylphorbol-13-acetate. Skin Pharmacol 4: 262-271.

STENMAN C, GONZALEZ H, GILLSTEDT M, DELLGREN G, HASSEUS B, HOLMBERG E, REXIUS H, OHMAN J AND PAOLI J. 2018. Degree of differentiation of cutaneous squamous cell carcinoma: a comparison between a Swedish cohort of organ transplant recipients and immunocompetent patients. Dermatol Pract Concept 8: 330-336.

STERNBERG SH, REDDING S, JINEK M, GREENE EC AND DOUDNA JA. 2014. DNA interrogation by the CRISPR RNA-guided endonuclease Cas9. Nature 507: 62-67.

SUZUKI-INOUE K, KATO Y, INOUE O, KANEKO MK, MISHIMA K, YATOMI Y, YAMAZAKI Y, NARIMATSU H AND OZAKI Y. 2007. Involvement of the snake toxin receptor CLEC-2, in podoplanin-mediated platelet activation, by cancer cells. J Biol Chem 282: 25993-26001.

SUZUKI INOUE K, INOUE O AND OZAKI Y. 2010. [Identification of the novel platelet activation receptor CLEC-2 and Its pathological and physiological roles]. Rinsho Byori 58: 1193-1202.

TAKEMOTO A, OKITAKA M, TAKAGI S, TAKAMI M, SATO S, NISHIO M, OKUMURA S AND FUJITA N. 2017. A critical role of platelet TGF-beta release in podoplanin-mediated tumour invasion and metastasis. Sci Rep 7: 42186.

TILGEN W, BOUKAMP P, BREITKREUTZ D, DZARLIEVA RT, ENGSTNER M, HAAG D AND FUSENIG NE. 1983. Preservation of morphological, functional, and karyotypic traits during long-term culture and in vivo passage of two human skin squamous cell carcinomas. Cancer Res 43: 5995-6011.

TOLL A ET AL. 2012. D2-40 immunohistochemical overexpression in cutaneous squamous cell carcinomas: a marker of metastatic risk. J Am Acad Dermatol 67: 1310-1318.

TOLL A ET AL. 2013. Epithelial to mesenchymal transition markers are associated with an increased metastatic risk in primary cutaneous squamous cell carcinomas but are attenuated in lymph node metastases. J Dermatol Sci 72: 93-102.

TOTSUKAWA G, WU Y, SASAKI Y, HARTSHORNE DJ, YAMAKITA Y, YAMASHIRO S AND MATSUMURA F. 2004. Distinct roles of MLCK and ROCK in the regulation of membrane protrusions and focal adhesion dynamics during cell migration of fibroblasts. J Cell Biol 164: 427-439.

TSUNEKI M, YAMAZAKI M, MARUYAMA S, CHENG J AND SAKU T. 2013. Podoplanin-mediated cell adhesion through extracellular matrix in oral squamous cell carcinoma. Lab Invest 93: 921-932.

VAN KRANEN HJ AND DE GRUIJL FR. 1999. Mutations in cancer genes of UV-induced skin tumors of hairless mice. J Epidemiol 9: S58-65.

VAN KRANEN HJ, DE GRUIJL FR, DE VRIES A, SONTAG Y, WESTER PW, SENDEN HC, ROZEMULLER E AND VAN KREIJL CF. 1995. Frequent p53 alterations but low incidence of ras mutations in UV-B-induced skin tumors of hairless mice. Carcinogenesis 16: 1141-1147.

VINICIUS DE LV, SCAPULATEMPO C, PERPETUO NM, MOHAMED F, DE CARVALHO TS, DE OLIVEIRA AT, SEGALLA JG AND CARVALHO AL. 2011. Prognostic and risk factors in patients with locally advanced cutaneous squamous cell carcinoma of the trunk and extremities. J Skin Cancer 2011: 420796.

WALDMAN A AND SCHMULTS C. 2019. Cutaneous Squamous Cell Carcinoma. Hematol Oncol Clin North Am 33: 1-12.

WATT FM. 2014. Mammalian skin cell biology: at the interface between laboratory and clinic. Science 346: 937-940.

WATT FM AND FUJIWARA H. 2011. Cell-extracellular matrix interactions in normal and diseased skin. Cold Spring Harb Perspect Biol 3.

WETTERWALD A, HOFFSTETTER W, CECCHINI MG, LANSKE B, WAGNER C, FLEISCH H AND ATKINSON M. 1996. Characterization and cloning of the E11 antigen, a marker expressed by rat osteoblasts and osteocytes. Bone 18: 125-132.

WICKI A AND CHRISTOFORI G. 2007. The potential role of podoplanin in tumour invasion. Br J Cancer 96: 1-5.

WICKI A, LEHEMBRE F, WICK N, HANTUSCH B, KERJASCHKI D AND CHRISTOFORI G. 2006. Tumor invasion in the absence of epithelial-mesenchymal transition: podoplanin-mediated remodeling of the actin cytoskeleton. Cancer Cell 9: 261-272.

WOJCIECHOWSKA-ZDROJOWY M, SZEPIETOWSKI JC, MATUSIAK L, DZIEGIEL P AND PULA B. 2016. Expression of Podoplanin in Non-melanoma Skin Cancers and Actinic Keratosis. Anticancer Res 36: 1591-1597.

WOLF K, ALEXANDER S, SCHACHT V, COUSSENS LM, VON ANDRIAN UH, VAN RHEENEN J, DERYUGINA E AND FRIEDL P. 2009. Collagen-based cell migration models in vitro and in vivo. Semin Cell Dev Biol 20: 931-941.

WYCKOFF JB, PINNER SE, GSCHMEISSNER S, CONDEELIS JS AND SAHAI E. 2006. ROCK- and myosin-dependent matrix deformation enables protease-independent tumor-cell invasion in vivo. Curr Biol 16: 1515-1523.

YAMAKAGE K, OMORI Y, ZAIDAN-DAGLI ML, CROS MP AND YAMASAKI H. 2000. Induction of skin papillomas, carcinomas, and sarcomas in mice in which the connexin 43 gene is heterologously deleted. J Invest Dermatol 114: 289-294.

YONEMURA S, HIRAO M, DOI Y, TAKAHASHI N, KONDO T, TSUKITA S AND TSUKITA S. 1998. Ezrin/radixin/moesin (ERM) proteins bind to a positively charged amino acid cluster in the juxta-membrane cytoplasmic domain of CD44, CD43, and ICAM-2. J Cell Biol 140: 885-895.

YURRITA MM, FERNANDEZ-MUNOZ B, DEL CASTILLO G, MARTIN-VILLAR E, RENART J AND QUINTANILLA M. 2014. Podoplanin is a substrate of presenilin-1/gamma-secretase. Int J Biochem Cell Biol 46: 68-75.

6 SUPPLEMENTS

6 SUPPLEMENTS

6.1 Declaration

I hereby declare that except where specific reference is made to the work of others, the contents of this dissertation are original and based on results of my own investigations. This dissertation has not been submitted for consideration for any other degree or qualification.

Heidelberg, September 2019

Melanie Schwab

6.2 Acknowledgements

This journey has come to an end – I think I will need a while until I have realized that now a new chapter is beginning. The time of my PhD was incredible and I am very grateful to many amazing people who accompanied me through this busy time with long working days and a lot of ups and downs. We had many great and also hilarious moments which I will never forget.

First, I kindly like to thank **Peter Angel** for giving me the chance to work in his lab. Your supervision and guidance gave me the opportunity to further develop scientifically as well as personally. Moreover, you supported me to explore my skills also outside of the lab for which I am really thankful.

I would like to thank **Michael Boutros** who agreed to be my second examiner of the thesis.

Many thanks to **Jonathan Sleeman** and **Viktor Umansky** for being referees in my disputation.

Moreover, I would like to acknowledge **Iris Augustin** and **Joy Burchell** for being supportive members of my TAC committee.

I am really grateful that I had so many great lab members. My biggest gratitude goes to the **Podoplaninis**. **Tanja** and **Barbara**, from the beginning on I really appreciated your advice and your team spirit. In between, I could not imagine that “our” protein is resulting in a phenotype. But you helped me to continue and to overcome the lows by your pleasant and humorous manner. Further, I would like to acknowledge all other **A100 members**. **Doris**, **Jule**, **Te**, **Macrina**, **Saskia**, **Ekatarina** and **Sören**, thank you all for scientific and technical support as well as for sharing the precious slots at the slidescanner. Many thanks for your help **Sabrina**, **Melanie**, **Betty**, **Sybille**, **Kathrin**, **Lena** and **Alina**. You always solved my technical questions and helped with a second pair of hands when needed. **Sabrina**, **Angelika** and **Angela** – thank you for your help with all the histological samples. You all together created such a nice working atmosphere and a positive distraction during our lunch and coffee breaks as well as during our social activities. Thank you all!

Moreover, many thanks to the **RTG2099** for generating an interactive platform for the exchange with scientists of all academic levels as well as for the financial support.

I would like to thank for the advisory and technical support given by **the DKFZ Core Facilities**, especially the **animal caretakers**, the facility of **flow cytometry**, **Manuela Brom** and **Damir Krunic** from the light microscopy facility and for statistical advice by **Tim**

Holland-Letz and **Thomas Hielscher**. Furthermore, many thanks to **Doris Helbig** for providing tissue samples and also to **Cyrill Géraud** for help with histological analysis.

Besides all the advisory and technical support concerning the lab work, many others outside of the lab contributed to accomplish this project.

I am so grateful to my fabulous **Schwabenheimer**! Some of you accompany me for more than 10 years. Thank you all, **Haiko**, **Maggy**, **Tom**, **Clarissa**, **Flo**, **Anni**, **Moritz**, **Anja** and **Robin** for having great BBQ evenings with “Swabian breakouts” and dance sessions, for being the best travel companions and for sharing your greatest moments.

My lovely Sparkling ladies, **Jule**, **Laura**, **Sara** and **Lina**! Thank you girls for always being there! Together we endured this time by sharing our frustrations but also having so many great and amazing situations!

Thank you, **Katharina**, for being such a supportive friend! I really enjoyed and appreciated our almost endless scientific discussions. I am very grateful for your support and your friendship.

Selbstverständlich gilt mein größter Dank meiner **Familie**. Ohne eure Unterstützung würde ich diese Zeilen hier nicht schreiben können.
Ich möchte mich bei meinen **Eltern** und meinem **Bruder** dafür bedanken, dass ihr immer für mich da gewesen seid und größtes Verständnis gezeigt habt! Ihr habt immer an mich geglaubt und mich motiviert. Ihr habt mir die Kraft gegeben, an mich selbst zu glauben. Vielen Dank!!!
Schließlich möchte ich mich von Herzen bei dir bedanken, **Haiko**! Du hast mir den nötigen Halt gegeben und mich motiviert, immer weiter zu machen, wenn es am schwierigsten war. Wir haben zusammen viele schöne Momente erlebt, die mir zum Teil gezeigt haben, meine Arbeit aus einem anderen Blickwinkel zu betrachten. Diese Zeit ist nun vorbei und ich freue mich sehr, viele weitere neue Abenteuer mit dir zu erleben.